Synthesis of photochemically active complexes for DNA recognition and binding

by

Jingwei Luo

A thesis submitted to the Department of Chemistry

In conformity with the requirements for

the degree of Master of Science

Queen's University

Kingston, Ontario, Canada

(August, 2009)

Abstract

The objective of this thesis is to synthesize and examine the photophysical and structural properties of 3-(pyridin-2-yl)imidazo[1,5-a]pyridine (P) and 3-(pyridin-2-yl)imidazo [1,5-a]pyridine (IQ) based cations and their potential use as DNA binding agents. The P ligand was aimed to compare with the IQ ligand as they have similar structures. Two series of compounds were synthesized; one series comprising organic cations, including PC_2, PC_3, PC_4, IQC_2 and IQC_3. The other one contains ruthenium complexes $Ru(bpy)_2P$, $Ru(bpy)_2IQ$ and $Ru(P)_3$). Compounds were prepared as Cl^-, Br^- and/or PF_6^- salts. All compounds were characterized by NMR, UV-vis, luminescescence and electrochemistry, when applicable. The results show that P and IQ based organic cations have similar electrochemical properties, and may be candidates for guanine photo-oxidation. However, $[Ru(bpy)_2P](PF_6)_2$, $[Ru(bpy)_2IQ](PF_6)_2$ and $[Ru(P)_3](PF_6)_2$ do not seem to have reduction potentials in the excited states that are appropriate for nucleic base photo-oxidation.

Acknowledgements

I would like to express my gratitude to my supervisor, Prof. Anne Petitjean, for her kind support, encouragement, consideration and the remarkable patience. This thesis would not have been completed without the educational and enjoyable discussions we have had regarding this thesis. Without her help I would not able to think like a chemist. Her great advices will benefit me for my whole life.

I would also like to thank my supervisory committee members, Dr. Wang and Dr. Macartney, for their advice at the mid-point of this project. I am thankful to the many wonderful professors and staff at Queen's University who taught me courses during my graduate studies and who were always available and supported me both academically and personally, especially Dr. Crudden. Also thanks to Dr. RuiYao Wang for his help with X-ray crystallography, Dr. Francoise Sauriol for her help with NMR, Dr. Lina Yuan for her help with Mass Spectrometry. I wish to acknowledge the financial support of the Canadian Institute for Health Research, Queen's University and the Faculty of Graduate Studies.

The teamwork of the Petitjean Group has facilitated many aspects of experimentation, so I would like to thank Arnaud Mignatelli, Dr. Gayatri Swaroop, Dr. Isabelle Nasso, Dr. Ganga Bhagavathy; special thank to my lab mate and who is also one of my best friends Xue Li. I also would like to express my appreciation to all of my friends at Queen's University, especially thanks to Dr. Ruibing Wang for his great help to me; my life will definitely be harder without his help.

Finally my deepest gratitude goes to my parents, whose love and support have been with me all my life.

Table of Contents

List of Figures

List of Tables

List of Symbols and Abbreviations

Bpy	bypiridine
c	concentration
Calcd	calculated
cm	centimetres
CD	circular dichroism
COSY	correlation spectroscopy
CV	cyclic voltametry
d	doublet
dd	doublet of doublets
ddd	doublet of doublet of doublets
dppz	dipyrido-[3,2-a:2',3'-c]phenazine
DMSO	dimethylsulfoxide
DNA	deoxyribonucleic acid
EtOAc	Ethyl acetate
Hz	hertz
IQ	3-(pyridin-2-yl)imidazo[1,5-a]pyridine
HOMO	highest occupied molecular orbital
J	coupling constant
K	kelvin
L	liter
LMCT	ligand to metal charge transfer
LUMO	lowest unoccupied molecular orbital
m	meter, multiplet

M	molar
MC	metal centred
mg	milligram
mL	millilitre
MLCT	metal to ligand charge transfer
^{3}MLCT	triplet metal to ligand charge transfer
mmol	millimole
mol	mole
m.p.	melting point
nm	nanometers
NMR	nuclear magnetic resonance
P	3-(pyridin-2-yl)imidazo[1,5-a]pyridine
PC	personal computer
Py	pyridine
Rt	room temperature
s	seconds
S_0	singlet ground state
S_1	singlet excited state
t	triplet
T_1	triplet excited state
TFA	trifluoroacetic acid
TLC	thin layer chromatography
UV	ultraviolet
UV-Vis	ultraviolet-visible
V	volts

δ	chemical shift
λ	wavelength
τ	lifetime

Chapter 1 Introduction:

Deoxyribonucleic acid (DNA) contains all the information needed for the creation of life. By the end of 2001, scientists finished sequencing the human genome.[1] Great effort has been made to explore DNA primary sequence, but the advanced 3D structure of DNA has not been revealed much so far. Some basic types of DNA structures have been found, including A-DNA, B-DNA, Z-DNA and triple and multi helical DNA, but when the cells are in their activated state, they undergo replication and transcription, and the structures change a lot, differing much from the original stacked supercoiled DNA. In addition, there are also very probably many different shapes currently not known to us. For example, damaged DNA may adopt special conformations.[2] In 2007, 7.1 millions of people died from cancer in the world. Cancer is the number one killer in the world, and can be related with DNA structure changes.[3] Many other fatal diseases are also intimately related to abnormal DNA sequences.

DNA being a polymer, it has many binding sites where different biologically active molecules and artificial agents can bind.[4,5] Binding may lead to changes in its structure and functions, and the biological activity of cells may finally be altered. As a result, more and more chemistry, as well as drug design research, are mainly focused on developing chemicals that target these binding sites.

When a cancer cell stays in G_0 state, which means it stops dividing and is in a resting state, the DNA of the cell stays in a supercoiled duplex form and ancillary proteins make it very stable. At this stage, current chemical therapies and sequence targeting drugs cannot detect the abnormal sequences. Only when the cell starts to duplicate will the DNA become loose and separate into single stands. At this stage, cells with pathological changes will show their abnormal activities. Most of anticancer drugs have side effects; they will affect all types of cell,[3] but due to cancer

cells' high metabolic activity, they are more sensitive to drugs than normal cells. After the activated cancer cells are killed, patients may stop taking drugs, but the potential cancer cells which are in their G_0 state still probably survive and not be detected, after a while these cells will start replicating, so new cancer cells appear, that is why cancer cells are hard to kill completely.[6] In order to decrease the side effects and kill G_0 sequence abnormal cells, we must find new ways to target the specific shapes of those abnormal parts, so the design, synthesis and testing of targeting molecular agents are one of the most pursued research areas. These targeting molecular agents may be aromatic small molecules, with particular sizes and shapes as well as specific electronic properties. Intercalators can insert in the space between adjacent base pairs.[2] Groove binders can bind into the DNA grooves through electrostatic attraction and van der Waals interactions;[4] some successful anticancer drugs (e.g. quinolinium quaternary salts, Chromomycin A_3 [2]) are synthesized based on those motives.

1.1 DNA interaction modes

The first DNA intercalating agents were discovered by Dr. Lerman in the early 1960s. Those were the acridines which were found to intercalate into DNA [7] (Figure 1.1). Since then, DNA targeting research has been one of the hottest biochemistry research areas.

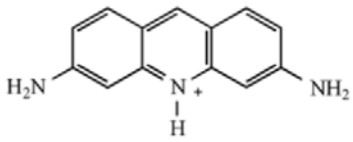

Figure 1.1 Early acridine intercalator[8]

1.1.1 DNA intercalation

1.1.1.1 Definitions and general properties

Generally speaking, intercalation refers to the "reversible insertion of a guest molecule into a lamellar host structure".[3] In the context of DNA binding, the small molecule (or "intercalator")

reversibly inserts between two base pairs (the base pairs are the analog of a lamellar structure). The guest intercalator usually is a molecule with a planar aromatic ring system which intercalates between two adjacent DNA base pairs through electrostatic, dipole-dipole and dispersive interactions as well as π stacking.[3, 5] The intercalation unit may be the whole molecule or only a part of a larger architecture. Depending on their electronic nature, intercalators may be divided into two categories: organic intercalators and metal coordination complexes (also called "metallointercalators").[5]

1.1.1.2 Organic intercalators

Organic intercalators are important DNA binding agents. Small organic intercalators may carry a positive charge as organic cations (e.g. ethidium, daunorubicin, doxorubicin (Figure 1.2)) so that there is an attraction with negatively charged double stranded DNA, while others may not require such a charge. One example is naphthalene diimide, e.g. N-[2-(2-hydroxyethoxy)ethyl]-N'-[2-(N,N-dimethylamino)-ethyl]-1,4,5,8-naphthalene tetracarboxylic diimide (Figure 1.2), for which the main driving force of intercalation is the hydrophobic effect. They are, however, most often accompanied by positive charges which provide water solubility and increase the binding constant to DNA.[8]

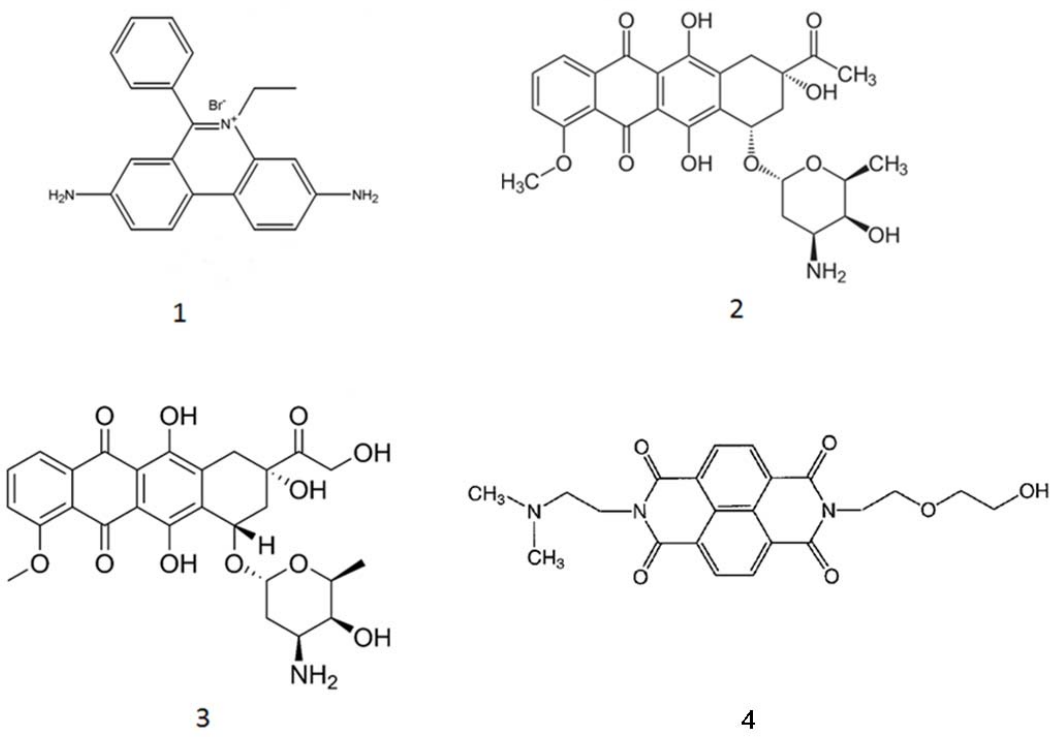

Figure 1.2 Ethidium (1), daunorubicin (2), Doxorubicin (3) and NDI intercalator (4)

Several organic intercalators have been approved by the FDA as anticancer drugs (e.g. Mitoxantrone and Doxorubicin).[3] Doxorubicin is a natural product produced by the bacterium *Strephomyces peucetius* Car. *Caesius.* It is the best known biosynthetic antitumor anthracycline, and has good anticancer activity against different kinds of tumors. Its interaction with DNA has been well characterized, as illustrated by the X-ray structure showing its intercalation between the C and N of 5'-GCN-3'sequences. [9, 10]

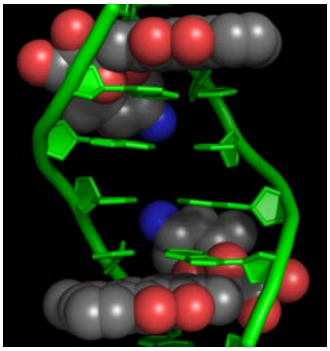

Figure 1.3 Two doxorubicin molecules intercalating into double-stranded DNA.[10]

As a consequence of doxorubicin's interaction with DNA, macromolecular biosynthesis is inhibited.[11] More exactly, the biological function of topoisomerase II, whose role is to break DNA double strand for transcription, is inhibited. Doxorubicin stabilizes the topoisomerase II-DNA complex after the DNA chain breaks. As a result, the double strand still "sticks together", and replication is terminated. In addition, the presence of intercalated doxodubicin also disrupts DNA repair processes.[12] Mitoxantrone is another anticancer drug and it is widely use as a conjugation drug together with other anticancer drugs for the treatment of acute nonlymphocytic leukaemia, metastatic breast cancer, acute myeloid leukemia, and non-Hodgkin's lymphoma.[3] It is also a topoisomerase II targeting drug, and has similar functions as doxorubicin.[13] There are some other anticancer drugs[3] whose purpose is to stop the replication and disrupt DNA synthesis.

1.1.1.3 Metallointercalators

Some of the organic intercalators can chelate transition metal ions to form metallointercalators. In metallointercalators, at least one of the ligands of the metal behaves like the organic intercalators seen above, and inserts between DNA base-pairs. Compared with organic intercalators, metallointercalators have many advantages. First, they combine intercalation with additional functions coming from the transition metals. For instance, most transition metal complexes, such as complexes of ruthenium(II) and rhodium(II), have good

solubility in aqueous solutions, are stable and have low toxicity.[14] Second, metallointercalators have special spectroscopic and electrochemical properties, so they can provide enriched information for the local binding sites (see below). Third, they can combine with more than two ligands with different functions, and this gives researchers more choices on function selection. All of these properties make metallointercalators a widely usable model, not only for DNA intercalators but also as fluorescence probes[15] and DNA foot-printing agents.[16]

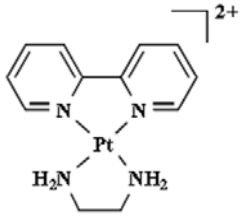

Figure 1.4 Square planar intercalator

One important property of transition metals is their coordination geometry. Depending on their different coordination geometries, metallointercalators can be defined as square planar or octahedral metallointercalators. Square planar metallointercalators involve transition metals with a d^8 configuration, and all the chelating sites are in one plane. Platinum(II) complexes[17] are the most popular choices (Figure 1.4). They show strong binding affinity to 5'-GpC sites which have a higher dipole moment. The binding constants of platinum complexes with DNA are in the order of 10^4 M^{-1}.[3,18] Square planar complexes can interact with DNA from either major or minor grooves as well as partially intercalate into DNA.

Octahedral complexes often involve transition metals with a d^6 configuration. Early studies of octahedral complexes are mainly focused on zinc, cobalt and ruthenium complexes.[19] The interaction of these complexes with DNA can be analyzed in three ways,

1. Incomplete or partial intercalation of one of the chelating ligand between the base pairs by means of π-stacking.

2. Electrostatic interactions between the positively charged metallointercalators with the negatively charged DNA double strand.

3. Minor groove binding.

$[Ru(bpy)_2(dppz)]^{2+}$ (Figure 1.5) is one of the most studied octahedral complexes, as it has two ancillary bpy ligands and one dppz ligand (see Fig 1.9 for chemical structures) which has an extended aromatic surface which can easily intercalate into DNA.[20, 21]

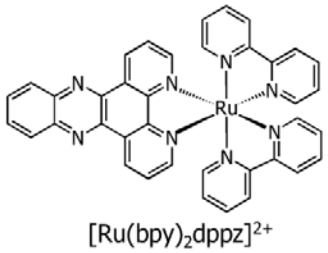

Figure 1.5 Structure of $[Ru(bpy)_2(dppz)]^{2+}$

Octahedral complexes with chelating ligands are chiral. In this context, the two enantiomers are labeled as Δ and Λ(Figure 1.6).[19] Research indicates that the right handed B-form of DNA is more likely to bind with the Δ isomers.[22, 14]

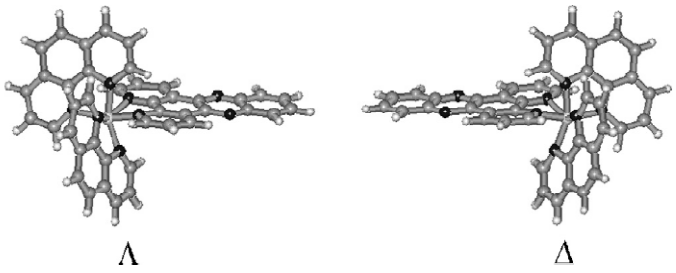

Figure 1.6 Λ-$[Ru(phen)_2(dppz)]^{2+}$ and Δ-$[Ru(phen)_2(dppz)]^{2+}$ isomers

1.1.1.4 Influence of intercalation on DNA conformation

Intercalators can induce distortion in the DNA double helix conformation. Firstly, in order for the intercalation process to be complete, the space of the intercalation point is enlarged. This leads to an angle change of the DNA strand. Secondly, the DNA strand becomes 3.4 Å longer than before,

for each intercalated unit. This is concomitant with DNA double strand unwinding, as well as with a change in the conformation of the sugars which connect with phosphates.[23, 24] Thirdly, once the intercalation process is complete, the neighbouring binding sites are not able to accept a second intercalator. This is due to the fact that the local DNA structure has been changed by the first intercalation process, so the conformation of neighbouring binding sites also changes accordingly, as it will not be as fit as before for another intercalator.[25] This is called the "neighbour exclusion principle".[26]

1.1.1.5 Photophysical properties of ruthenium-based metallointercalators: the "light switch" effect

Luminescence is the light emitted by an electronic transition between an excited state and the ground state. For instance, $[Ru(bpy)_2(dppz)]^{2+}$ (Figure 1.5) is luminescent in organic solutions such as acetonitrile (the emission wavelength is 620 nm).[27] On the other hand, when dissolved in water or an aqueous buffer, $[Ru(bpy)_2(dppz)]^{2+}$ and related complexes show very weak luminescence. However, upon addition of double-stranded DNA, the luminescence increases dramatically. This is called the "light switch" effect (Figure 1.7).[14, 28, 29]

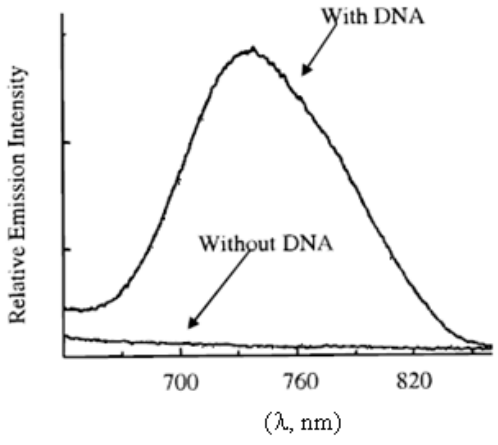

Figure 1.7 Demonstration of the light switch effect on complex luminescence.

One of the proposed mechanisms indicates that after excitation the complex reaches the ^{1}MLCT state and lowers its energy by transitioning to the ^{3}MLCT state. The molecules in this state are sensitive to the polarity of the surrounding solvent environment, and water is a very good energy acceptor. As a result, the ^{3}MLCT state complex will transfer the energy to water molecules and fall back to the ground state within a very short time (250 ps; "non-radiative decay" in Figure 1.8).[29]

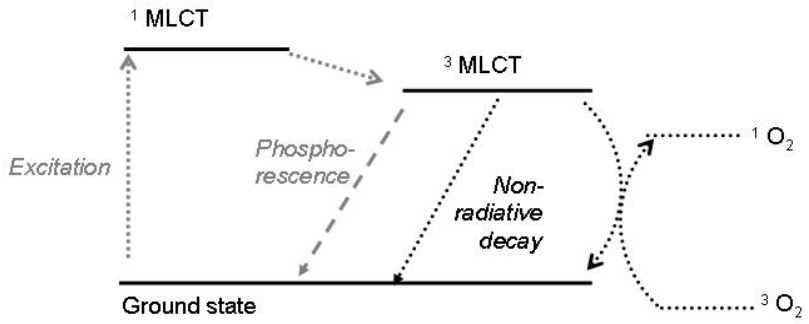

Figure 1.8 Optical transitions in ruthenium complexes equipped with bipyridine-type ligands.

In organic solvents or in the presence of DNA (which effectively shields the luminophore from water molecules), the polarity is much smaller than in aqueous conditions and the energy transfer process is prolonged due to the poor energy acceptor ability of the surrounding. In this situation, the energy is emitted as light with a longer decay (100 ns).[30] This special property can be utilized as a DNA binding indicator when testing a newly designed polypyridyl light switch complex.

This is not always true as in some cases, e.g. $[Ru(phen)_2(PHEHAT)]^{2+}$,[30] the complexes only show a slight increase in luminescence, while in other cases a decrease is even observed (see Figure 1.9 for ligand names and structures).

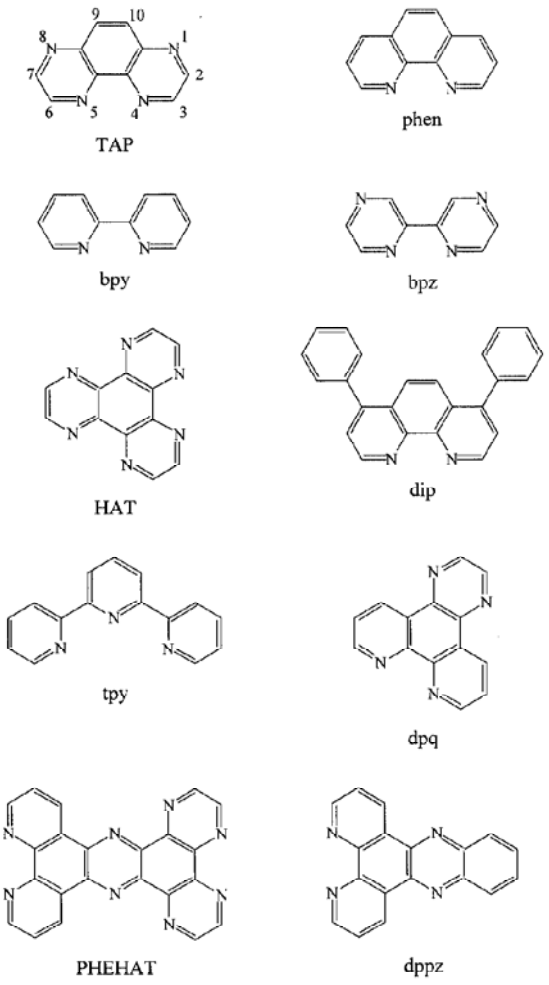

Figure 1.9 Popular ligands for DNA-binding metallo-intercalators[30]

Another function of the light switch effect is the indication of enantiomer preference for DNA. As mentioned above, polypyridyl ruthenium complexes may have two enantiomers, each possibly having a different binding affinity towards DNA. For the right handed double strand B form of DNA, most of the Δ enantiomers give higher binding affinities. This can be indicated by the light switching experiment, when testing the two enantiomers with DNA, as they will give different luminescence values.

1.1.1.6 Photochemical Properties of some ruthenium complexes: Singlet oxygen sensitization

In addition to luminescence, singlet oxygen sensitization may also be effected by ruthenium complexes substituted with bipyridines and analogues. When such ruthenium complexes are excited by UV-light (Figure 1.8), they can also transfer their energy to the nearby $^3O_2$ oxygen molecules leading to $^1O_2$ singlet oxygen (Figure 1.8, right-hand side). $^1O_2$ is highly reactive towards organic molecules. As a result, the bound nucleic acids are readily attacked if they are in close proximity to the generated $^1O_2$. For instance, guanines are readily oxidized, which may lead to subsequent strand cleavage.[31]

1.1.1.7 Photochemical Properties of some ruthenium complexes: Photo-electron transfer agents

Some ruthenium complexes, for example $[Ru(HAT)_3]^{2+}$ and $[Ru(TAP)_3]^{2+}$, have higher reduction potentials in the excited state[32] (Table 1-1) than GMP (guanosine-5'-monophosphate) whose oxidation potential is about +1.25V vs SCE,[33,34]so that when $[Ru(HAT)_3]^{2+}$ and $[Ru(TAP)_3]^{2+}$ are excited by UV-vis light to their ^{3}MLCT state, a photo-electron transfer occurs from guanine in GMP to the complexes in their ^{3}MLCT excited state. This electron transfer leads to the formation of reduced Ru complexes with one positive charge and oxidized guanine. The reduced site on the complex is the HAT or TAP ligand and it may then combine with the oxidized guanine to form photo adducts.[32] In this type of adduct, the metal center keeps its coordination sphere, and the link between complex and GMP is covalent (Figure 1.10).[35]

Complex	E_{red} (V/SCE)	$\lambda_{em,max,MeCN,nm}$	E^*_{red} (V/SCE)
Oxidising complexes			
$[Ru(HAT)_3]^{2+}$ [29]	−0.62	587	+1.49
$[Ru(TAP)_3]^{2+}$ [30]	−0.75	604	+1.30

Table 1-1 Redox properties and emission wavelengths of $[Ru(HAT)_3]^{2+}$ and $[Ru(TAP)_3]^{2+}$.[32]

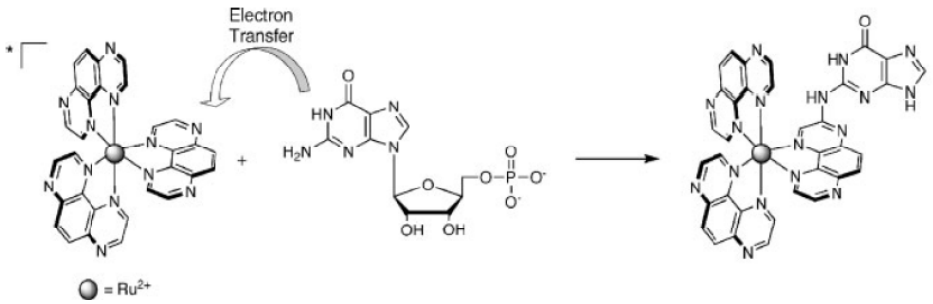

Figure 1.10 Photo-adduct formation between $[Ru(TAP)_3]^{2+}$ and GMP after hydrolysis to remove the sugar-phosphate unit.[35]

1.1.2 DNA groove binding

Double stranded DNA has two different grooves which differ in size. One is 22 Å wide and it is called the "major groove". The other one is 12 Å wide and it is called the "minor groove".[35] Both of them are potential binding sites for molecular binding agents. Large molecules such as proteins are likely to bind in the major groove, while the smaller molecules prefer the minor groove.[5] DNA groove binders are another type of DNA binders (Figure 1.11).

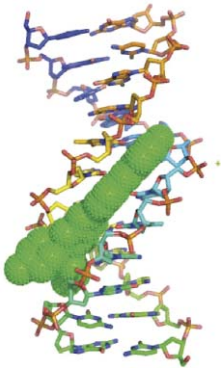

Figure 1.11 Groove binding of Hoescht 33258 to the minor groove of DNA[23]

Compared with intercalators, groove binders do not change the DNA conformation too much. The binding is stabilized by a combination of surface hydrogen bonding, van der Waals interactions and the hydrophobic effect, and they have higher binding constants than intercalators (around 10^{11} M^{-1}).[23] Groove binders also show sequence specificity, as they usually contain at

least two aromatic rings and maintain a crescent shape to fit the DNA grooves, as exemplified by netropsin (NTR, 1), distamycin A (DA, 2), and mitomycin (Figure 1.12). Many groove binders are proven to have high potential for clinical use.[23]

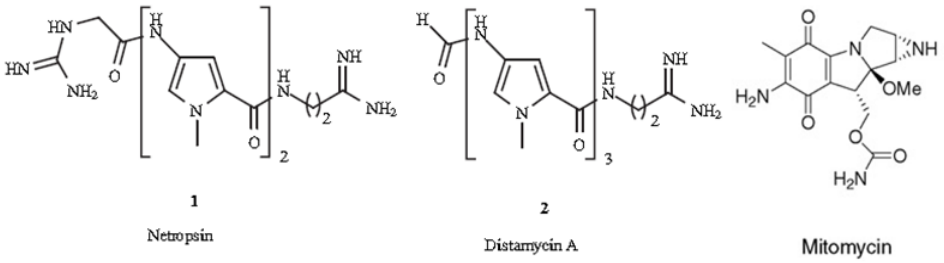

Figure 1.12 Examples of DNA minor groove binders [4,23]

DNA binding research mainly focuses on sequence specificity. Although there are thousands of natural DNA binders (e.g. distamycin A (Figure 1.12)), researchers are trying to design binders whose aim is to target particular 3D structures based on X-ray structural and NMR spectroscopic analyzes, combined with computer modeling.[36] Chromomycin A_3, an antitumor drug, is one of these examples.[37] Its Xray structure was obtained by binding the complex with a 5'-d(TTGGCCAA)-3' double strand DNA.[2]

1.2 Molecular agents that target specific sites in DNA

1.2.1 General comments

As mentioned above, not all intercalators and groove binders are sequence-specific. For instance, ethidium bromide (EtBr) (Figure 1.2 (1)) is a type of organic dye that intercalates into DNA through the minor groove, but it does not choose a specific DNA sequence to intercalate.[23] Some other agents show only weak selectivity. Researchers are aiming to design highly DNA specific targeting agents for therapeutic use.

The design for recognition of sequence can be based on different strategies, such as on the particular conformation of a DNA sequence,[38] and on the unique local electronic environment

produced by a DNA sequence.[39] These molecules will recognize DNA by reading the H-bond functionalities displayed by the bases in the grooves, for sequence recognition.

An example of the former strategy comes from the recognition of junctions. The most common DNA conformation is the right handed B-form DNA, while some other forms include A and Z form DNA as well as triplex and quadruplex DNA. A three-way junction is a special DNA conformation. It consists of three double helical strands which are all connected in a junction point and some of the bases on these strands cannot form base pairs.[2, 40] Figure 1.13 shows how an artificial agent may recognize this particular conformation based on the fit between the space that is made available by the strands, and the volume of the artificial agent.[23]

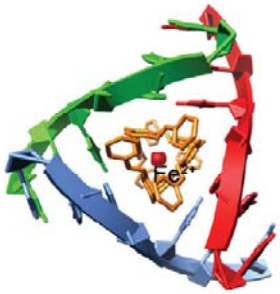

Figure 1.13 DNA three way junction with the $[Fe_2(C_{25}H_{20}N_4)_3]^{4+}$ helicate[6, 41, 42]

We will focus in this section on a couple of examples highlighting the recognition of DNA in its most common double stranded B form.

1.2.2 Sequence selective DNA duplex recognition

One of the most impressive examples of an artificial agent capable of very selectively addressing specific sequences has been developed by Prof Peter Dervan and consists of well-defined amide oligomers based on heterocyclic motifs.[43] The inspiration behind these binders comes from the natural Distamycin A binder illustrated in Figure 1.12.

Dervan et al. introduced a “reading code” which allows tailoring the design of a particular oligoamide to bind very specifically to a sequence of interest. This is the result of the direct

reading of the hydrogen-bonding pattern displayed by the base-pair by the heterocycles and amide functions. Basically, the 'reading code' (Figure 1.14)[44] is a series of programmable polyamide chains. The polyamides are composed of different types of heterocycles such as imidazole (Im), pyrrole (Py) and hydroxypyrrole (Hp), and each heterocycle is selected based on the sequence of interest. In order to recognize a specific DNA sequence, Dr. Dervan's group looked at the exact sequence and how all the hydrogen bond donors and acceptors are distributed in the DNA minor groove. Then, they designed the polyamide chain, as all the four types of base have different hydrogen bond distributions, and specific amides can recognize this information, so each one or two amides are in charge of recognizing one base. This polyamide chain will recognize a specific DNA sequence, and it can even distinguish between T:A and A:T.[47]

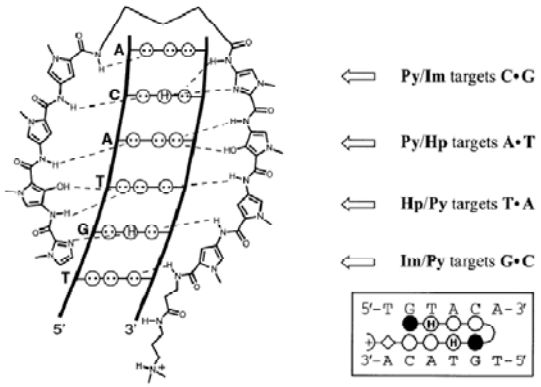

Figure 1.14 Reading the minor groove of DNA (hydrogen bonding patterns of Watson-Crick base-pairs: circles with dots represent lone pairs of N(3) and O(2) of pyrimidines, and circles containing an H represent the 2-amino group of guanine. Binding model for the complex formed between ImHpPyPy-g-ImHpPyPy-b-Dp and a 50-TGTACA-30 sequence. Hydrogen bonds are shown as dashed lines. Im is black circles, Py is open circle and Hp is open circle with H).

One exciting application of such technology is the control of gene regulation. Genes are fragments of DNA single strands which are transcribed to mRNAs. mRNAs are then translated to produce different proteins. While the genes cannot express by themselves, protein transcription

factors (TF) are needed to find the promoter region of each gene and initiate transcription. The polyamide oligomers can also be used to bind the promoter region and compete with TF binding and activate or deactivate a specific gene. Figure 1.15 shows the inhibition of gene transcription by polyamides. The top picture shows RNA polymerase II activators leading to the initiation of gene transcription while the bottom picture shows the addition of polyamides targeted to the promoter region and the inhibition of the binding of activators. As a consequence, transcription of the gene does not take place.[47]

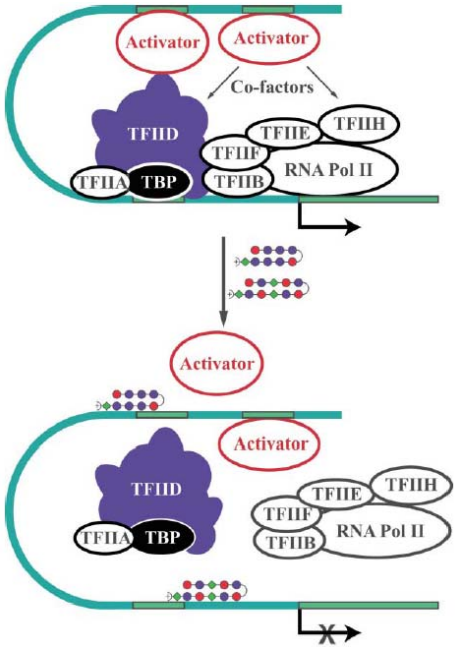

Figure 1.15: Polyamide inhibiting gene expression[44]

1.2.3 Mismatched DNA recognition

In addition to reading a DNA sequence through the electronic information of the substituents of the bases (e.g. H or lone pair, as described above), another attracting handle on DNA recognition is through its dynamic shape. In this context, DNA mismatch recognition deserves to be considered here.

DNA bases in the double helix should match each other to make a hydrogen bond interaction according to Watson-Crick base pairing rules. Among the four DNA bases, adenine (A) matches thymine (T), and guanine (G) matches cytosine (C). Mismatched DNA corresponds to all those cases which differ from the A-T and C-G base pairs, and may occur upon error in replication,[45] recombination,[46] ionizing radiation and reaction with mutagenic chemicals.[47] As illustrated in Figure 1.16, different modes of self-assembly between the bases are possible, depending on the exact nature of the bases.[48]

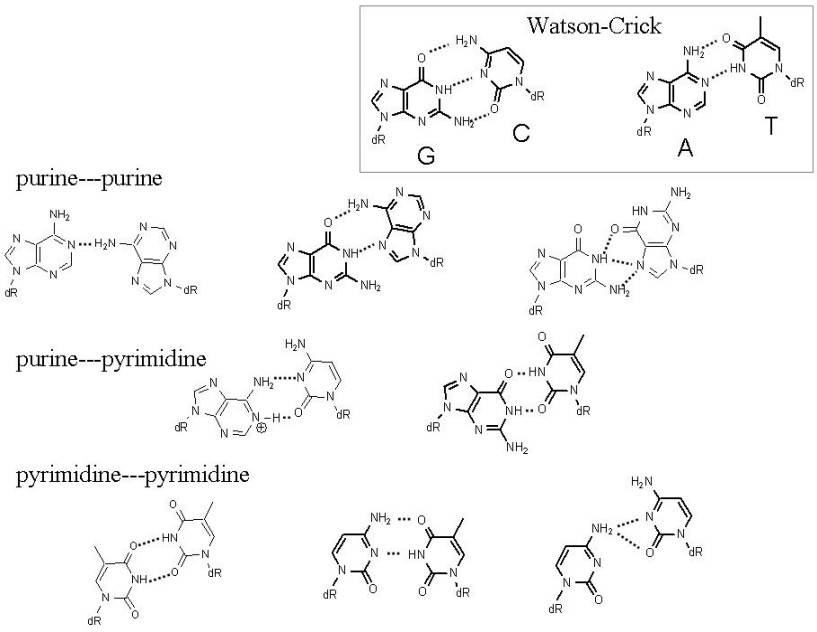

Figure 1.16 Different modes of hydrogen-bonding between mismatched bases[48]

Similarly, a mismatch may affect the actual structure and stability of duplex DNA to a different extent, depending on the actual nature of the mismatch. In simple terms, the larger bases (e.g. GG mismatches) have less of a destabilizing effect on the duplex structure (compared to Watson-Crick duplexes) than smaller bases (e.g. CC), as evidenced by melting temperature (Tm) studies. Indeed, the temperature at which 50% of the duplex is denatured to two single strands upon heating (Tm) for XY-containing duplexes in the AXT/TYA context shows the following

trend (Table 1-2): GC>GG>AA>TT>CC (note that the stability of mismatched duplex is also affected by the nearest neighbours to the mismatch).[49]

DNA base-pair	GC	AT	GG	CC	AA	TT
Tm (± 0.4°C)	83.2	79.1	74.7	67.0	70.2	70.5

Table 1-2 Comparative melting temperatures (Tm) of a family of DNA duplexes with and without mismatched base pairs, at 1 M [Na^+].[49]

In terms of structure, the presence of a mismatch may also lead to variable effects on the structure, but overall, only little distortion of B-DNA is observed. To illustrate this point, a G:A mismatch in a synthetic dodecamer (d(C-G-C-G-A-A-T-T-A-G-C-G)$_2$) was found to give very little perturbation in the local and overall conformation of the duplex (Figure 1.17).[50]

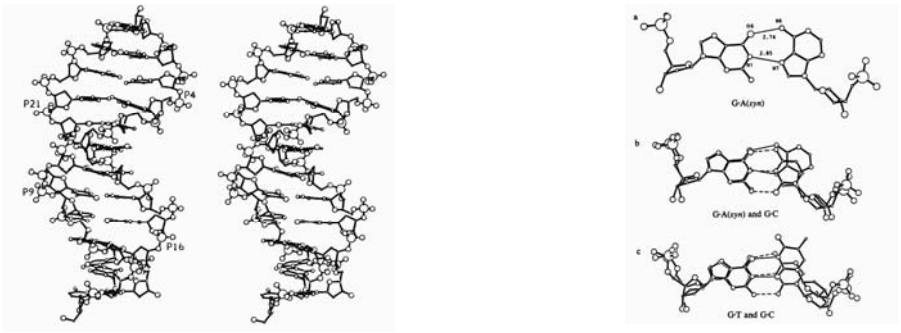

Figure 1.17 Overall (left) and local (right) effect of a GA mismatch. Left: stereoview of the mismatch dodecamer d(C-G-C-G-A-A-T-T-A-G-C-G)$_2$, with GA mismatches at G^4-A^{21} and A^6-G^{19}. Right: comparison of G-A(syn) base pair and the G-T wobble base pair with a Watson-Crick base pair.[50]

The major difference with Watson-Crick base-paired duplexes is not so much the static stability and structure of the duplex, but more importantly the local dynamics around the mismatch with base-pair opening an easier groove widening is often observed around mismatches,[51] a feature which has been taken advantage in order to develop general mismatch-specific metallointercalators (Figure 1.18).

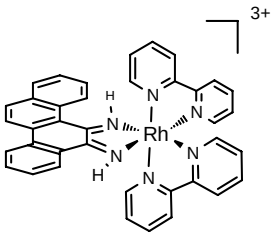

Figure 1.18 Structure of $[Rh(chrysi)(bpy)_2]3^+$ showing the 4-ring chrysi unit which is too wide to fit in Watson-Crick DNA duplex.[52]

Metallointercalators with a large chrysene-based intercalating platform (Figure 1.18) are indeed able to insert between mismatched base-pair connected DNA strands, but their insertion between Watson-Crick based paired duplex is prevented by a more "robust" duplex. This approach is very attractive since the increased dynamics around mismatches may be considered as a "universal" feature, and allows a single molecular agent to detect nearly all sorts of mismatches.[53]

Alternatively, other mismatch-recognition agents are able to read the electronic information displayed by individual bases involved directly or indirectly in mismatches. For example, it has been showed that aminonaphthyridines are complementary to the guanine Watson-Crick face. As a result, guanines that are not involved in the (strong) Watson-Crick GC base-pairs may be accessed by artificial naphthyridine agents, a feature which has been used to directly target directly GG mismatches.[54]

1.3 Combining intercalators and distortion targeting

1.3.1 Ruthenium metallo-intercalators and distortion targeting

As introduced above, ruthenium metallointercalators have many special properties on the one hand (e.g. "light switch" effect, $^1O_2$ sensitization and photo-induced electron transfer), and, on the other hand, designed DNA binders are able to target specific DNA structures (e.g. mismatched DNA). These two aspects are equally important for research in nucleic acids. So far different research groups have mainly focused on one of those two aspects (Dr. Barton on the

mismatch and Dr. Kirsch on photophysical properties of ruthenium complexes). Here, we propose to combine both the selective DNA recognition properties of metallointercalators and their inherent reactivity.

In my project, I mainly focused on one kind of ruthenium-based metallointercalator and the intercalating part is the targeting ligand which was initially designed and synthesized by my supervisor Dr. Petitjean (Figure 1.19). It derives initially from an isoquinoline molecule, and will therefore be abbreviated "IQ" in the remaining of the manuscript. Once chelated to a metal center (such as a ruthenium ion), the shape of this intercalating ligand binder is not exactly flat, contrary to most intercalating ligands (Figure 1.19).

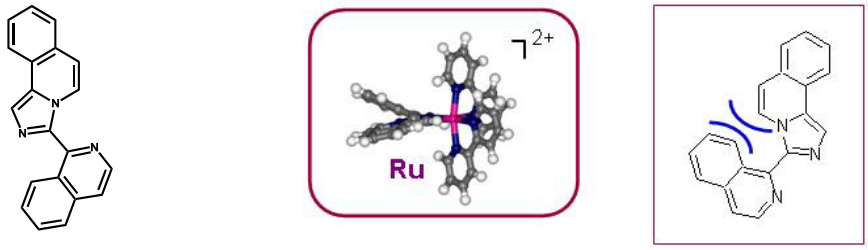

Figure 1.19 left: Molecular structure of the "IQ" intercalating ligand; right: shape of the intercalating ligand once included in a metal complex $[Ru(IQ)(Bpy)_2]^{2+}$. The steric clash preventing planarity is highlighted on the right).

This targeting ligand is specially designed to intercalate into the space between two base pairs of "twisted" DNA (Figure 1.20), a conformation which NMR studies have shown is adopted by the $d(TGGAATGGAA)_2$ sequence.[55] Interestingly, this sequence is found in human centromeres, and would therefore be an interesting target to disrupt cancer cell division. As we know, the centromere is the point where the two chromatids touch (Figure 1.20). When mitosis takes place, the two chromatids separate,[55,56] so it would be interesting to cancer researchers to have a drug towards this specific region of DNA.

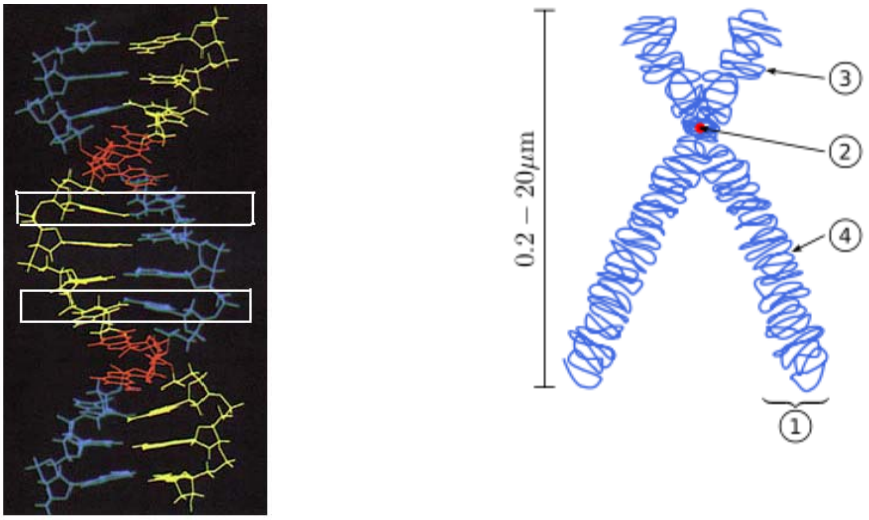

Figure 1.20 Left: staggered conformation of the d(TGGAATGGAA)$_2$. The squares show the unpaired, sheared GA base pairs.[56] Right: Chromosomal components (1) Chromatid, (2) Centromere, (3) Short arm and (4) Long arm

The synthesis of the IQ ligand has previously been worked out by Dr Petitjean, and its ruthenium complex [Ru(IQ)(bpy)$_2$]Cl$_2$) been synthesized, although maybe not in its purest form. Preliminary DNA binding properties were performed on a CC mismatched duplex and compared to a CG Watson-Crick base-paired duplex.[57] Figure 1.21 reports the most interesting findings:

- Fluorescence experiments show that a more intense "light switch effect" is provided by binding to the CC duplex vs the CG duplex. This may be a sign of preferential mismatch binding and signaling;

- Photoirradiation reactions (laser beam at 442nm) initially run to induce guanine oxidation through $^1O_2$ sensitization revealed that such complexes lead to covalent adduct formation (slow moving band on Figure 1.21 right). This is reminiscent of the behavior of the HAT and TAP based ruthenium complexes mentioned above.

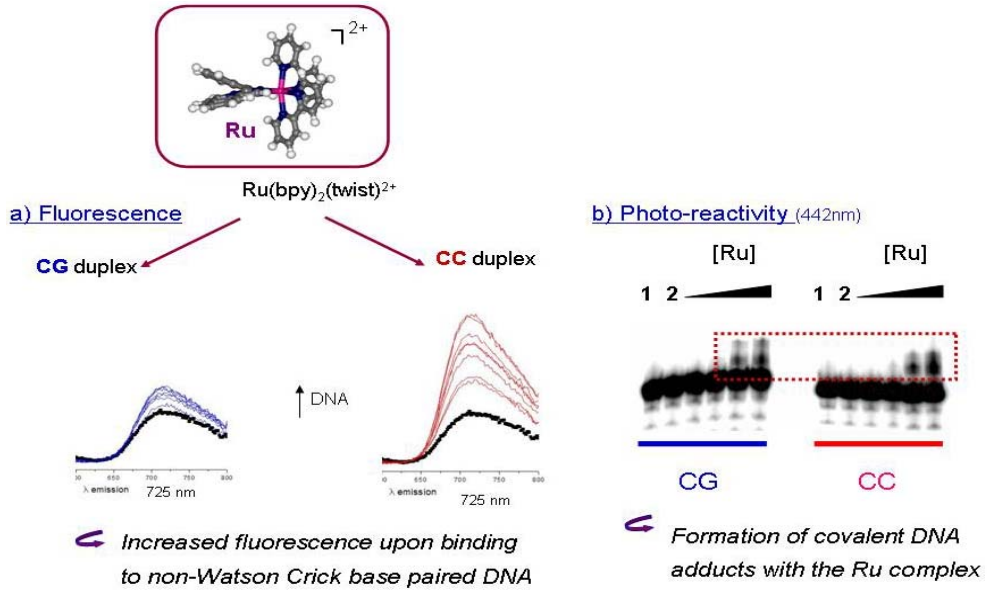

Figure 1.21 Preliminary results on a ruthenium complex based on the IQ ligand. The CC and CG duplexes are made of synthetic dodecamers.[57]

In this particular context, my role when I took over was to:

(i) synthesize and purify all forms of IQ based ruthenium complexes, i.e. $[Ru(IQ)(bpy)_2]^{2+}$, $[Ru(IQ)_2(bpy)]^{2+}$ and $[Ru(IQ)_3]^{2+}$,

(ii) determine their optical (UV-vis and fluorescence) properties, and

(iii) determine their electrochemical properties.

Indeed, as we have seen above, the knowledge of both the emission properties and of the redox properties of a ruthenium complex allow to access an estimate of the "oxidative power" of such DNA binders. Ruthenium complexes with a high E_{red}^* with HAT and TAP ligands (Table 1) are good candidates to form DNA adducts. We would like to know how IQ based complexes compare.

In order to simplify the study and to have a point of comparison, it was also envisaged to work on simpler ligands and complexes. We therefore also focused on the "P" ligand (Figure 1.22), which is a simplified IQ ligand in the sense that it does not offer a similar "twist" (no steric

hindrance) but still conserves an "internal nitrogen" (and, therefore, interesting electrochemical properties).

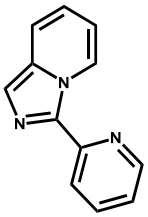

Figure 1.22 Structure of P ligand

Finally we are also interested in separating the enantiomers of the ruthenium complexes to refine the DNA binding studies.

1.3.2 Organic twist binder analogues

In addition to chelating to a metal, the IQ ligand may also be included in organic cations for DNA binding. The IQ based cations result from the bis-alkylation of IQ with biselectrophiles such as 1.2-dibromoethane (giving $[IQC_2]^{2+}$), 1,3-dibromopropane (giving $[IQC_3]^{2+}$) and 1,4-dibromobutane (giving $[IQC_4]^{2+}$), as illustrated in Figure 1.23.

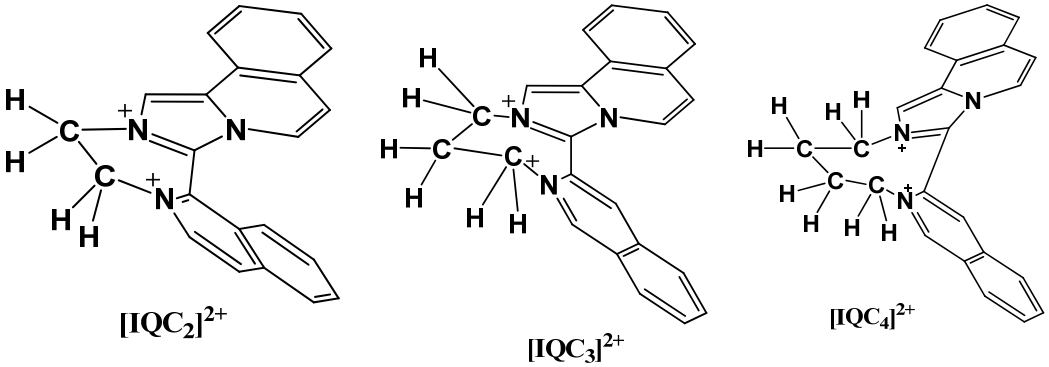

Figure 1.23 Structure of organic IQ-based cations (Br^-, PF_6^- and/or Cl^- counter ion)

Reports show that organic binders have enhanced affinities compared to metallo-intercalators and distinct binding selectivity.[58, 18]

In this specific context, the interest in those organic cationic intercalators lies in the fact that the twist angle probably depends on the nature of the alkyl spacer between the two alkylated nitrogen atoms. It is anticipated that the twist angle between the two aromatic planes of the IQ ligands will increase from $[IQC_2]^{2+}$ to $[IQC_4]^{2+}$.

Once again, simpler cationic intercalators may be obtained starting from the "P" molecules. It is therefore envisaged to synthesize and study the P-derived cations indicated in Figure 1.24.

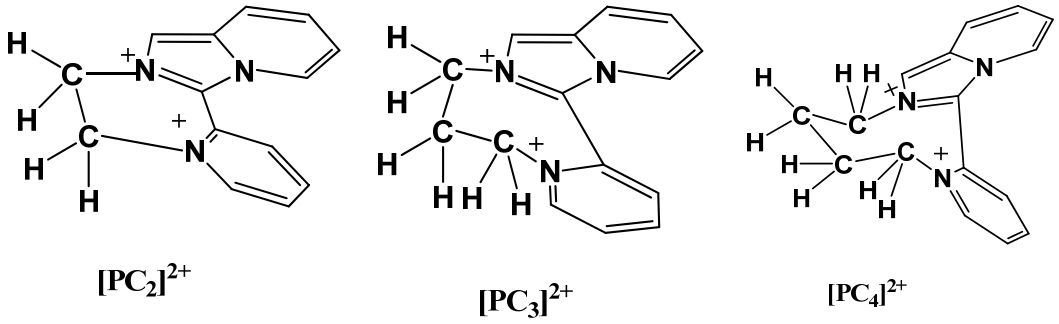

Figure 1.24 Structure of organic cations derived from the "P" molecule

Once synthesized, the optical (UV-vis and fluorescence) and electrochemical properties of those cations will be studied, with the goal in mind of testing their DNA binding properties and photochemical reactivity.

1.3.3 Plan of the thesis

The thesis will be divided in four additional chapters:

Chapter 2: Synthesis and characterizations of P, IQ ligands, their ruthenium complexes and organic cations

2.1 Synthesis of P and IQ ligand (2.1.1 P, 2.1.2: IQ)

2.2 Synthesis of organic cations (2.2.1 P, 2.2.2: IQ)

2.3 Synthesis of ruthenium complexes (2.3.1 P based complexes, 2.3.2: IQ based complexes, 2.3.3: Attempts at resolving enantiomers)

Chapter 3: Optical and electrochemical properties of the ruthenium complexes and organic cations

3.1. Optical properties (UV-vis and fluorescence): 3.1.1: P, 3.1.2: IQ, 3.1.3: $[RuPn]^{2+}$, 3.1.4: $[Ru(IQ)n]^{2+}$

3.2: Electrochemical properties: 3.2.1: P, 3.2.2: IQ, 3.2.3: $[RuPn]^{2+}$, 3.2.4: $[Ru(IQ)n]^{2+}$

3.3: Assessing the oxidative power of P and IQ based potential DNA binders

3.3.1: P based; 3.3.2: IQ based

Chapter 4: Conclusion

Chapter 5: Experimental section

5.1: General methods

5.2: P, organic cations and ruthenium complexes

5.3: IQ, organic cations and ruthenium complexes

Chapter 2

Synthesis and characterizations of P, IQ ligands, their ruthenium complexes and organic cations

2.1 General introduction

My research plan includes synthesizing a series of organic compounds and ruthenium complexes. These molecules are to be used for future DNA binding tests.

2.1.1 Synthesis of P series molecules

The synthesis starts with 3-(pyridin-2-yl)imidazo[1,5-a]pyridine (P) ligand, and involves the following steps (retrosynthesis in Fig. 2.1).

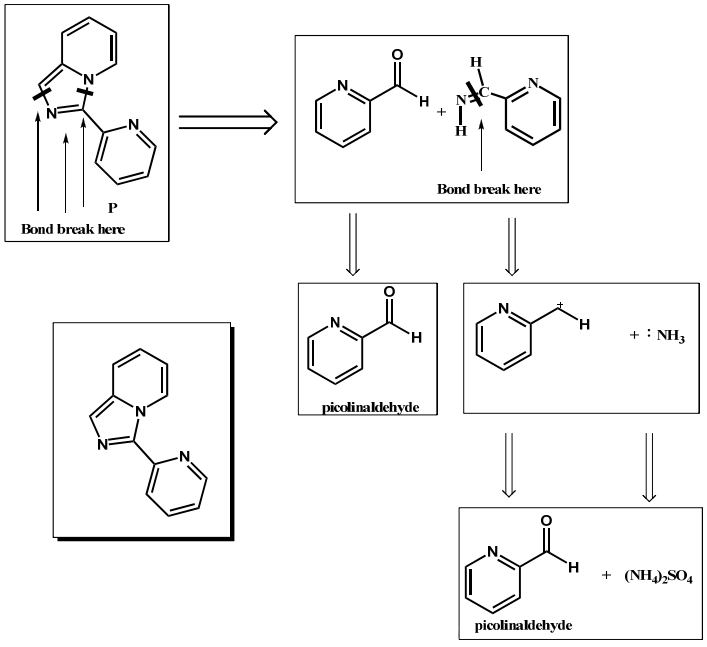

Figure 2.1 Retrosynthetic analysis of the synthesis of P

The following organic cations were synthesized, including $[PC_2]Br_2$, $[PC_3]Br_2$, $[PC_4]Br_2$, and ruthenium complexes $[RuP_3]Cl_2$, $[Ru(bpy)_2P]Cl_2$ were synthesized.

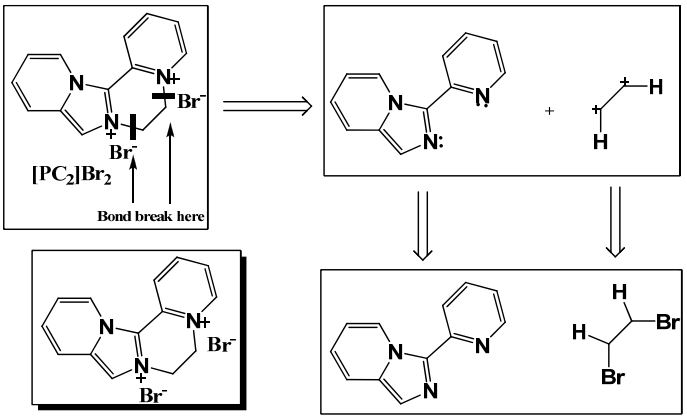

Figure 2.2 Retrosynthetic analysis of $[PC_2]Br_2$

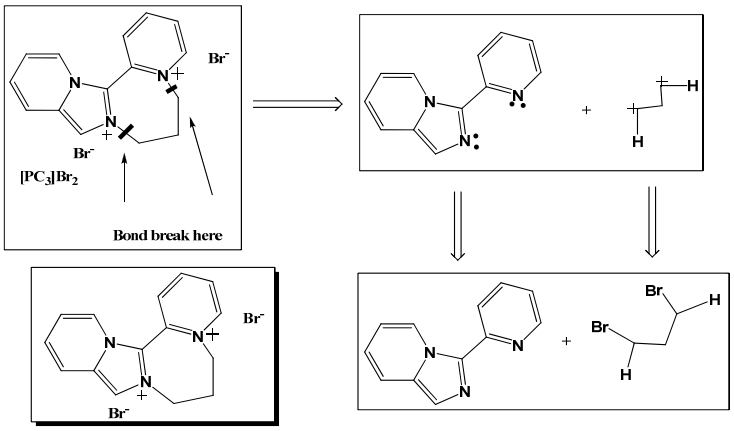

Figure 2.3 Retrosynthetic analysis $[PC_3]Br_2$

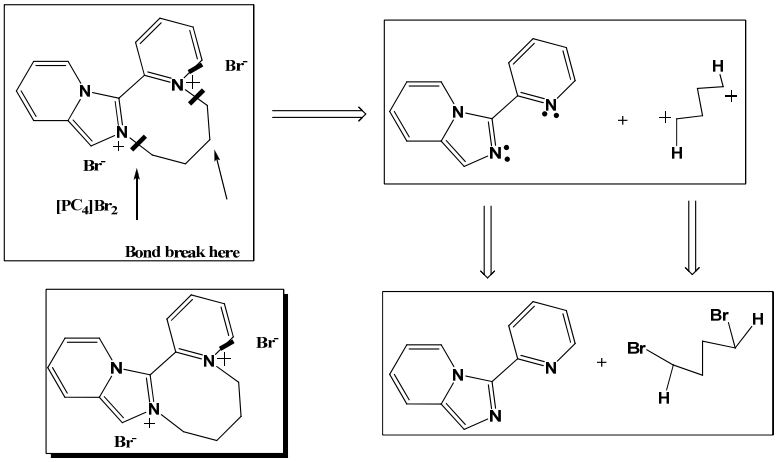

Figure 2.4 Retrosynthetic analysis $[PC_4]Br_2$

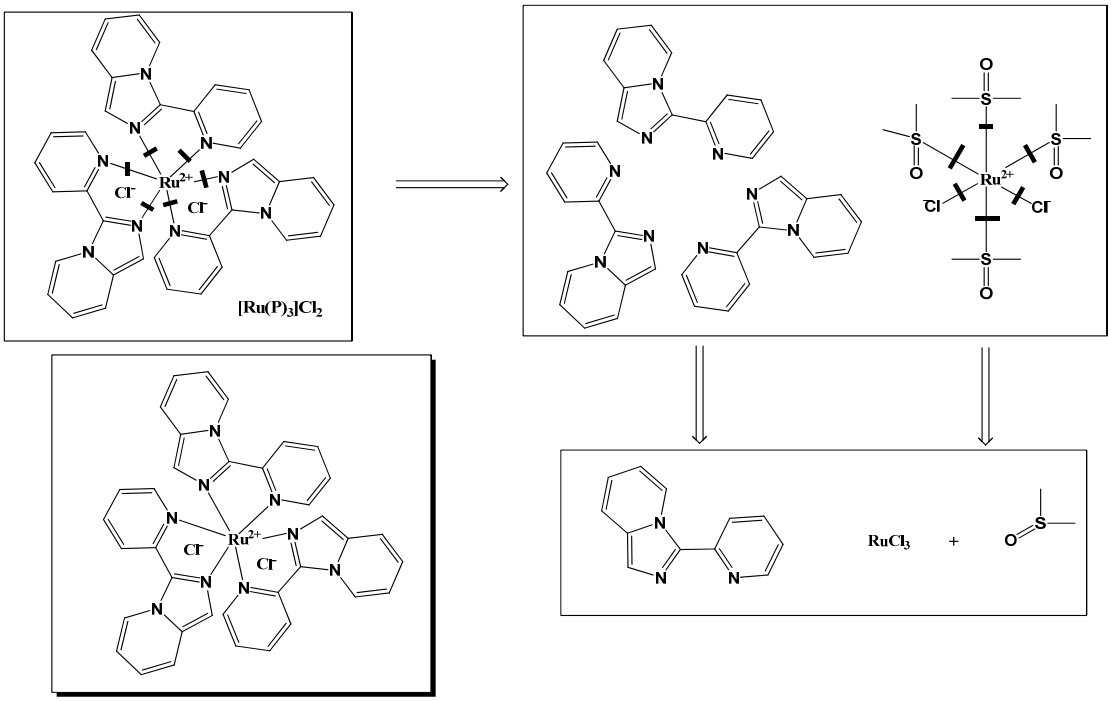

Figure 2.5 Retrosynthetic analysis of $[Ru(P)_3]Cl_2$

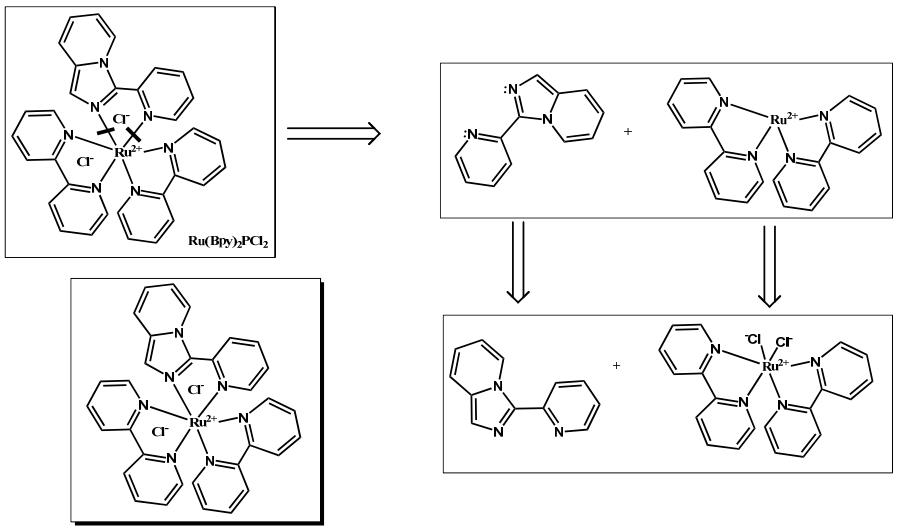

Figure 2.6 Retrosynthetic analysis of $[Ru(bpy)_2P]Cl_2$

2.1.2 Synthesis of IQ series molecules

The synthesis starts with 3-(isoquinolin-1-yl)imidazo[5,1-a]isoquinoline (IQ).

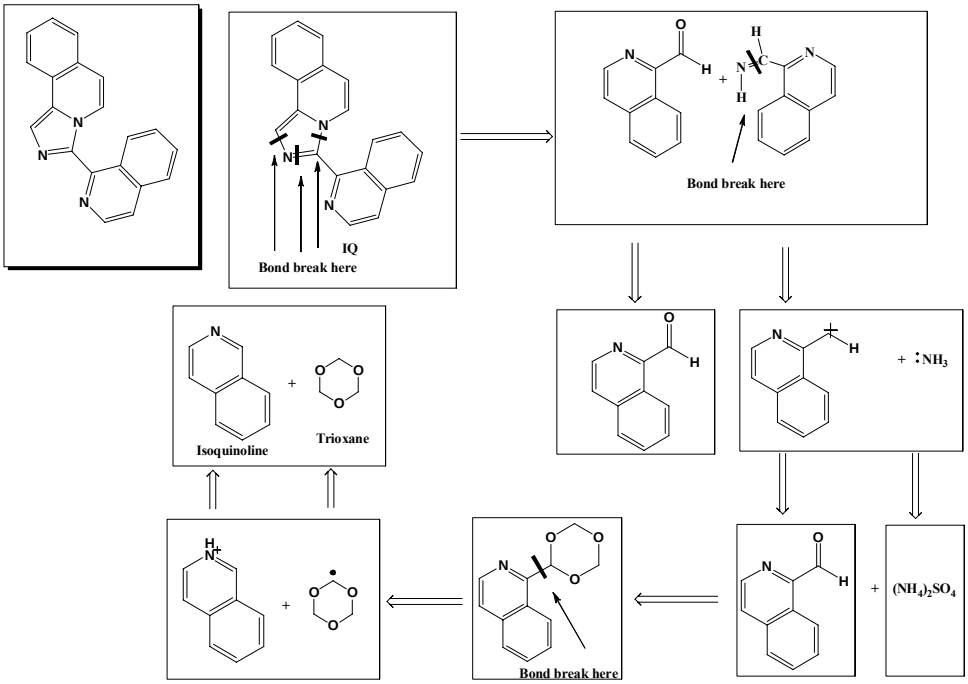

Figure 2.7 Retrosynthetic analysis for the synthesis of IQ

From IQ ligand, the following organic cations were synthesized, including $[\mathbf{IQ_2}]\mathbf{Br_2}$, $[\mathbf{IQ_3}]\mathbf{Br_2}$ and ruthenium complexes $[Ru(bpy)_2IQ]Cl_2$ were synthesized.

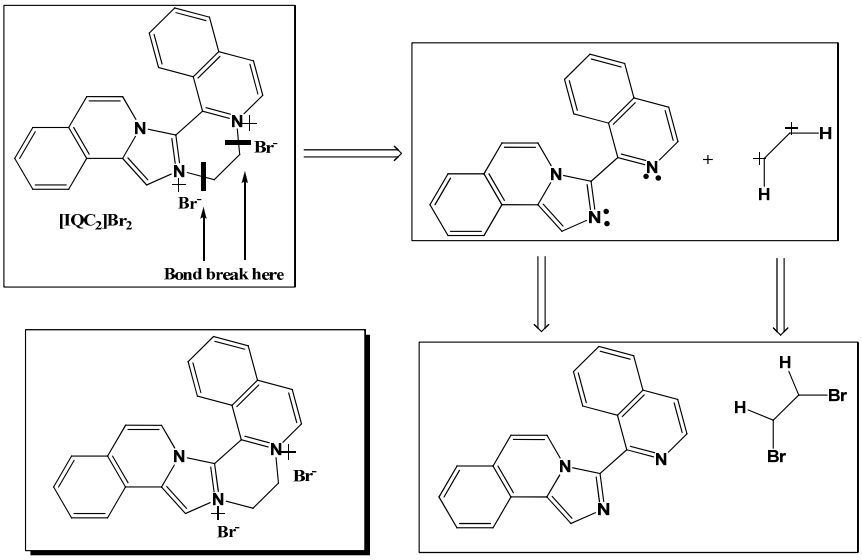

Figure 2.8 Retrosynthetic analysis of $[IQC_2]Br_2$

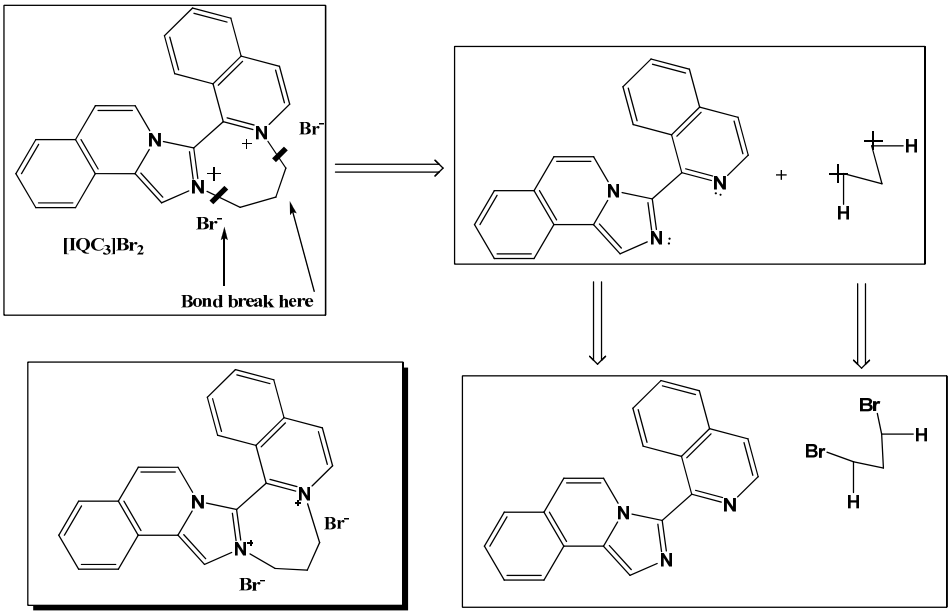

Figure 2.9 Retrosynthetic analysis of $[IQC_3]Br_2$

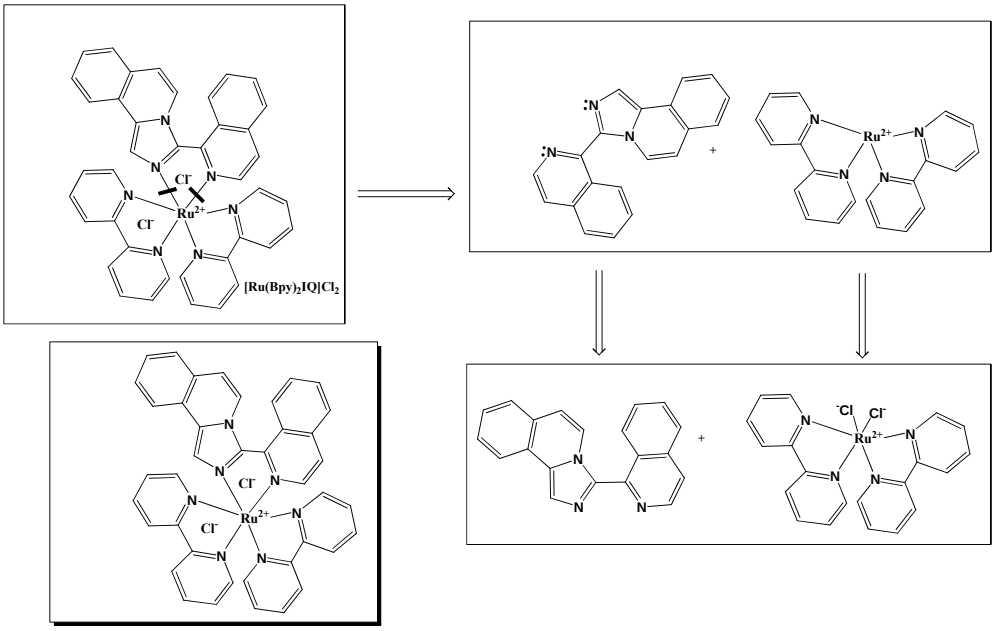

Figure 2.10 Retrosynthetic analysis $[Ru(bpy)_2IQ]Cl_2$

2.2 Synthesis of P and IQ ligand

2.2.1 Synthesis of 3-(pyridin-2-yl)imidazo[1,5-a]pyridine (P) ligand

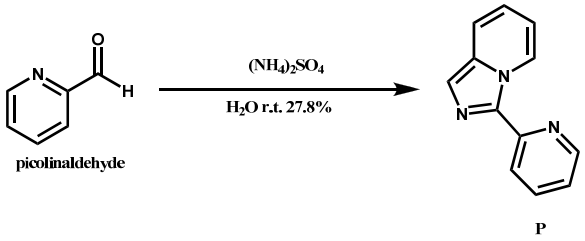

Figure 2.11 Synthesis of P ligand

The synthesis of P ligand starts from picolinaldehyde. This is a published product,[59] and it is used for checking IQ complex system. The reaction of 2.46 equivalents of picolinaldehyde with one equivalent of ammonium sulphate in water solution yields the P ligand which precipitates out of water. The precipitate was filtered, washed with water and then DCM, and finally sublimed

under vacuum. The yellow transparent needle shape crystals are characterized by NMR. The yield is average 28%. The yield reported in paper is 30%, so my yield is acceptable.

2.2.2 Synthesis of 3-(pyridin-2-yl)imidazo[1,5-a]pyridine (IQ) ligand

The synthesis of IQ starts from isoquinoline. Three steps are needed. The first step is to synthesize 1-(1,3,5-trioxan-2-yl)isoquinoline as shown in Figure 2.12.[60] It requires one equivalent of TFA and isoquinoline, and 85.5 equivalents of trioxane, 0.039 equivalent of ferrous sulphate as well as 4.86 equivalents of t-BuOOH. This is a radical reaction and ferrous sulphate acts as a catalyst.

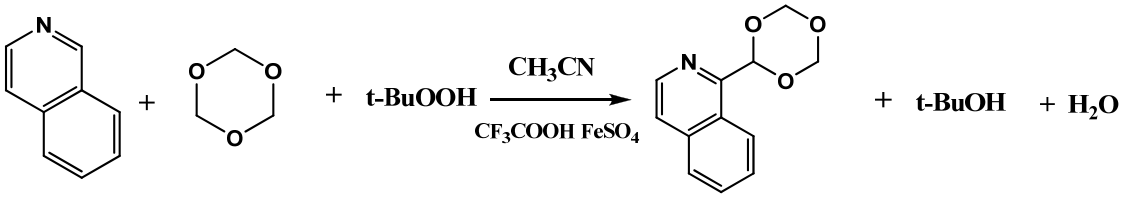

Figure 2.12 Synthesis of 1-(1,3,5-trioxan-2-yl)isoquinoline

The second step is the hydrolysis of 1-(1,3,5-trioxan-2-yl)isoquinoline as shown below in Figure 2.13. one equivalent of 1-(1,3,5-trioxan-2-yl)isoquinoline react with 7.6 equivalents of HCl. Flash column chromatography was used for purification. The yield for these two steps ranges from 36% to 51.5%. The target molecule was characterized by NMR spectroscopy.

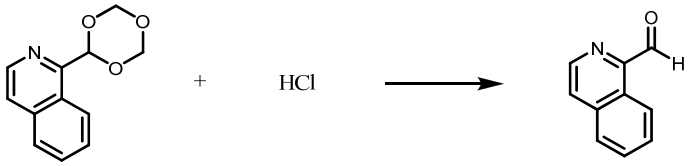

Figure 2.13 Synthesis of isoquinoline-1-carbaldehyde

The last step is the synthesis from isoquinoline-1-carbaldehyde to IQ as shown in Figure 2.14. This is the same type of reaction as the synthesis of P ligand. One equivalent of isoquinoline-1-carbaldehyde react with 0.426 equivalent of ammonium sulphate in water solution

yields IQ ligand, which precipitates out from water. The precipitate was filtered, submitted to flash column chromatography and recrystallized from hot ethanol once and acetonitrile once. The yield is 18.8% from the previous step. The successful synthesis of this compound is shown by NMR spectroscopy.

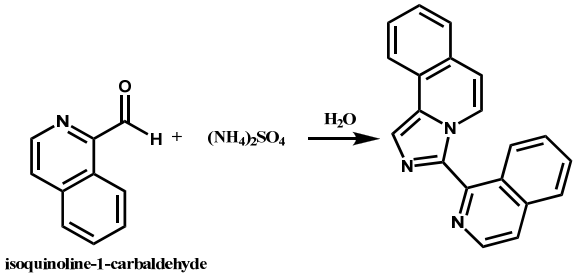

Figure 2.14 Synthesis of IQ

Another method was also tried in order to improve the yield.[61] In this reaction, ammonium sulphate is replaced by 9.36 equivalents of ammonium acetate, and the solvent was switched to acetic acid.

After reaction, the compound was purified by recrystallization. TLC analysis shows that there always is more than one spot and they are very close to each other. In these conditions, it would be difficult to separate them by column chromatography, so this attempt to improve the synthesis did not work as well as anticipated. The molecule was identified by 1D and 2D NMR spectroscopy.

2.3 Synthesis of Organic cations

2.3.1 Synthesis of P related cations

2.3.1.1 Synthesis of $[PC_2]^{2+}$ cations

In this reaction,[62] one equivalent of the P ligand reacts with 119.5 equivalent of 1,2-dibromoethane used as a reactant and solvent. $[PC_2]Br_2$ was isolated by filtration and washed with

ether. NMR and MS spectra were used to characterize the product. The yield is 80.1%. The Br^- was exchanged for a PF_6^- and Cl^- for future use. The PF_6^- salt was obtained by adding $NH_4PF_6^-$ to the aqueous solution of $[PC_2]Br_2$. The target molecule precipitated immediately; it was then filtered, and washed with water and ether. $[PC_2]Cl_2$ was obtained by using an ion exchange column.

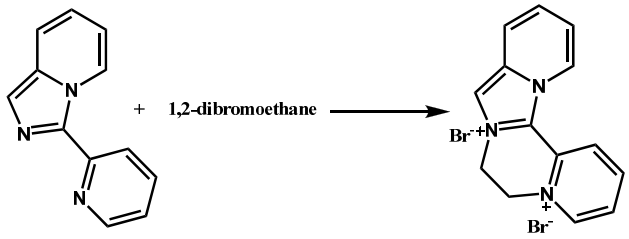

Figure 2.15 $[PC_2]Br_2$

2.3.1.2 Synthesis of $[PC_3]^{2+}$ cations

In this reaction,[63] one equivalent of the P ligand reacts with 70.5 equivalents of 1,3-dibromopropane as reactant and solution. The yield is 88.5%. The procedures were the same as with the PC_2 cations.

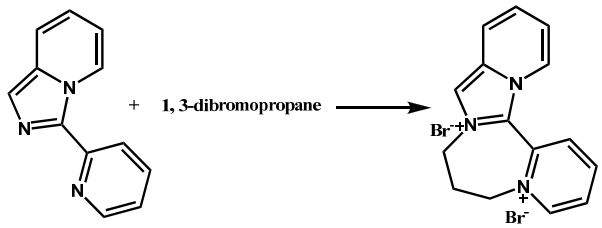

Figure 2.16 Synthesis of $[PC_3]Br_2$

2.3.1.3 Synthesis of $[PC_4]^{2+}$ cations

In this reaction,[63] one equivalent of the P ligand reacts with 66 equivalents of 1,4-dibromobutane as a reactant and solvent. The yield ranges from 12.3 to 24.7%**.** The procedures were the same as with the $[PC_2]^{2+}$ cations.

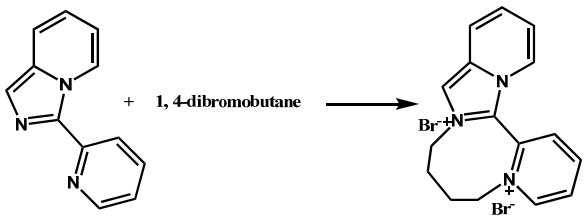

Figure 2.17 Synthesis of $[PC_4]Br_2$

Note: All of the NH_4PF_6 solution should be introduced into the $[PC_4]Br_2$ in one time, as if another aliquot of NH_4PF_6 solution was introduced, the $[PC_4]$ $(PF_6)_2$ precipitate will disappear.

2.3.2 Synthesis of P related cations

2.3.2.1 Synthesis of $[IQC_2]^{2+}$ cations

In this reaction,[62] one equivalent of the IQ ligand reacts with 136.7 equivalents of 1,2-dibromoethane as a reactant and solvent. The yield is 85.1%. The procedures were the same as for the $[PC_n]^{2+}$ cations.

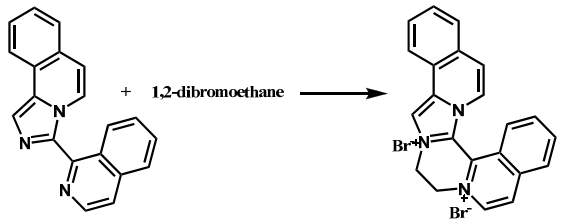

Figure 2.18 Synthesis of $[IQC_2]Br_2$

2.3.2.2 Synthesis of $[IQC_3]^{2+}$ cations

In this reaction,[63] one equivalent of IQ ligand reacts with 70.5 equivalents of 1,3-dibromopropane as a reactant and solvent. The yield is 51.2%. The procedures were the same as the for $[PC_n]^{2+}$ cations.

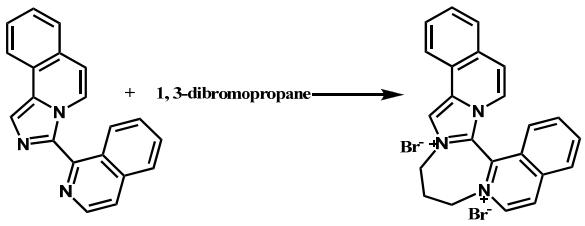

Figure 2.19 Synthesis of $[IQC_3]Br_2$

2.4 Synthesis of ruthenium complexes

2.4.1 P based complexes

2.4.1.1 Synthesis of $[Ru(bpy)_2P]^{2+}$ complex

In this reaction,[64] one equivalent of $Ru(bpy)_2Cl_2$[65] reacted with 1.1 equivalent of the P ligand in an ethanol and water mixture solution. The solution was heated to reflux and protected by Ar and aluminum foil. The $[Ru(bpy)_2P](PF_6)_2$ was precipitated by addition of NH_4PF_6 and filtered. Purification was performed by recrystallization, by adding diethyl ether to the top of solution of product in dichloromethane. Single crystals of $[Ru(bpy)_2P](PF_6)_2$ were generated. NMR spectroscopy Xray diffraction are used to characterized the target product. The yield of the final product is 68.1%. $[Ru(bpy)_2P]Cl_2$ was produced by cation exchange for future studies.

The X-ray crystal structure of $[Ru(bpy)_2P](PF_6)_2$ is represented in **Figure 2.20**. The complex crystallizes in a monoclinic P2(1)/c space group. With inversion being one of the symmetry elements of this space group, both enantiomers co-exist in the crystal, leading to racemic crystallization.

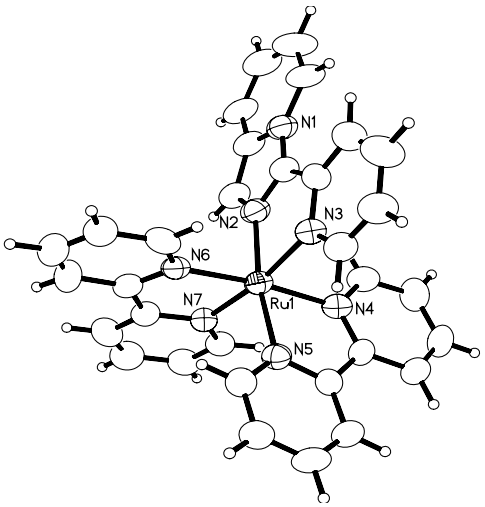

Figure 2.20 Xray crystal structure of $[Ru(bpy)_2P](PF_6)_2$ (solvents and counter ions are omitted for clarity)

2.4.1.2 Synthesis of $[Ru(P)_3]^{2+}$ complex

Two steps are needed for this reaction. The first step is the synthesis of $Ru(DMSO)_4Cl_2$.[66] One equivalent of $RuCl_3$ reacted with 24.27 equivalents of DMSO. The solution was heated to reflux and protected by Ar and aluminum foil. For this method, there was a large amount of DMSO left, so, and after the reaction, DMSO was removed first by distillation, then by washing with acetone. Diethylether was then added to precipitate the compound. The yield is 28%. IR spectroscopy was used to characterize the product. The product had the exactly the same IR absorption bands as the reported data.[67]

The second step is the reaction of one equivalent of $Ru(DMSO)_4Cl_2$ with 4.28 equivalents of the P ligand[68] with ethanol used as the solvent. The solution was heated to reflux and protected by Ar and aluminum foil. $[Ru(P)_3](PF_6)_2$ was precipitated by addition of NH_4PF_6 and filtered. Further purification was performed by interface recrystallization. The crude was dissolved in small amount of DCM and 95% ethanol was carefully added to the top of the DCM. NMR

spectroscopy was used to characterize the product. The elemental analysis, mass spectrometry and ^{1}H NMR spectrum point to the desired compound. The yield is 54.7%.

2.4.2 IQ based complexes $[Ru(bpy)_2IQ]Cl_2$

In this reaction,[64] one equivalent of $[Ru(bpy)_2]Cl_2$[65] reacts with 1.1 equivalent of the IQ ligand in an ethanol and water mixture solution. The solution was heated to reflux and protected by Ar and aluminum foil. A precipitate, obtained by addition of NH_4PF_6, was filtered. Purification was attempted in two ways: (i) interface recrystallization (the crude was dissolved in small amount of DCM and 95% ethanol was carefully added to the top of the DCM), however no precipitate came out, and using a (ii) cation exchange column. In this latter method, solutions of sodium chloride at different concentrations are used as the running eluent. Two bands were observed, with the major band running faster and byproduct running more slowly. The major band was collected from the eluted fractions and the complex was precipitated as a PF_6^- salt by addition of NH_4PF_6. The Cl^- salt was isolated by using an anion exchange column. The TLC gave two spots, indicating that the collected fraction was not pure. The cation exchange column was ran again, and this time there were still two bands, suggesting that realized the compound probably degraded on the column. Before the column work the weight of the compound was 37.3 mg, while after the column work 16.7 mg of the compound was obtained the yield is 16.2%. NMR and MS spectra were used to characterize the compounds.

2.4.3 Attempts at resolving enantiomers

In order to get enantiomerically pure $[Ru(bpy)_2IQ]^{2+}$ complexes, $[Ru(bpy)_2(Pyridine)_2]Cl_2$ was synthesized as shown in Figure 2.21,[69] $[Ru(bpy)_2(Pyridine)_2]Cl_2$ can form a Δ chiral crystal together with O,O'-dibenzoyl-D-tartrate,[69] and a Λ chiral crystal together with O,O'-dibenzoyl-L-tartrate. The resolved compounds can react with IQ to give resolved $[Ru(bpy)_2IQ]^{2+}$ complexes

(Figure 2.22). The experiment for the chiral crystallization was done by adding O,O'-dibenzoyl-L-tartrate or O,O'-dibenzoyl-D-tartrate to the $[Ru(bpy)_2(pyridine)_2]Cl_2$ solution and put it in dark place for slow evaporation. The crystals were supposed to grow slowly, however in my experiment, I failed to see any crystals form. Therefore the chiral resolution experiment could not go further.

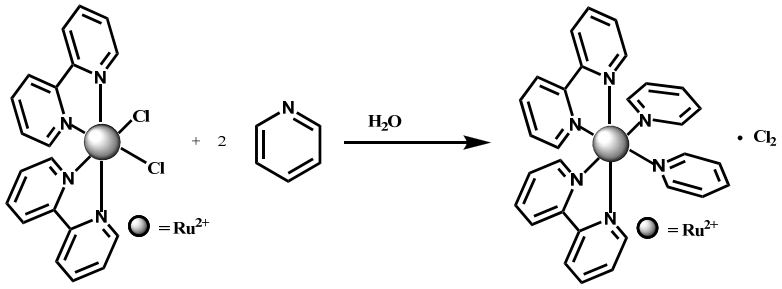

Figure 2.21 Synthesis of $[Ru(bpy)_2(Pyridine)_2]Cl_2$

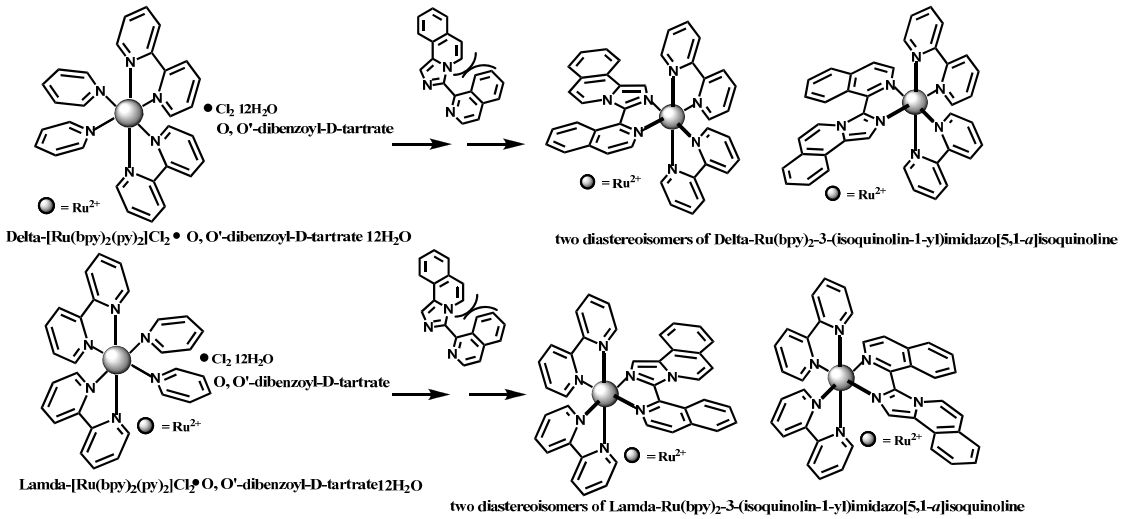

Figure 2.22 Resolving of $[Ru(bpy)_2IQ]^{2+}$ cpmplexes

2.5 Conclusion

In this chapter, I introduced all of the synthesis of my targeting molecules, organic cations and ruthenium complexes. Most compounds were successfully synthesized and purified, while the chiral separation part was found to be hard to achieve after several trials.

Column chromatography and recrystallization were the main purification methods and ^{1}H NMR was utilized as main characterization method. The NMR identification started from the P ligand and its NMR data was reported.[70] The IQ ligand was identified by 1D and 2D NMR spectroscopy and all the other molecules were identified based on these two major ligands.

Chapter 3

Optical and electrochemical properties of the ruthenium complexes and organic cations

3.1 Optical properties (UV-vis and fluorescence)

3.1.1 P and $[PC_n]^{2+}$ molecules

For the P ligand, there are three maximum absorption wavelengths, with the highest one being at 348 nm. This is confirmed with the fluorescence test where excitation at 348 nm leads to a 407 nm emission. All of the $[PC_n]^{2+}$ compounds have similar conclusions. $[PC_2]Cl_2$ has three maximum absorption wavelengths, with the highest one being at 408 nm (also an excitation wavelength), and its emission occurs at 450 nm. $[PC_2](PF_6)_2$ has three maximum absorption wavelengths, with the highest one being at 406 nm (also an excitation wavelength). It emits at 451 nm. $[PC_3]Cl_2$ has two maximum absorption wavelengths, with the higher one being at 388 nm (also an excitation wavelength), and it emits at 457 nm. $[PC_3](PF_6)_2$ has two maximum absorption wavelengths, with the higher one being at 384 nm (excitation wavelength: 385 nm), and emits at 462 nm. $[PC_4]Cl_2$ has two maximum absorption wavelengths, the higher one being at 386 nm (also an excitation wavelength), and emits at 478 nm. $[PC_4](PF_6)_2$ has two maximum absorption wavelengths, the higher one being at 366 nm. The excitation wavelength is 376 nm and there is therefore a 10 nm difference. Emission is observed at 487 nm. Another discovery is that as the number of carbons is increasing in the $[PC_n]^{2+}$, the differences between the emission and excitation wavelength are also increasing, and PF_6^- salts have bigger differences in values than Cl^- salts.

3.1.2 IQ and $[IQC_n]^{2+}$ molecules

Similar results were recorded for IQ and $[IQC_n]^{2+}$ molecules (see appendix for results). As mentioned in the introduction chapter, the P ligand was supposed to have the same electrochemical property as the IQ ligand, due to their similar structures. Here we also confirmed that the P and IQ ligands also have similar photophysical properties.

3.1.3 $[RuP_3]^{2+}$ and $[Ru(bpy)_2P]^{2+}$ molecules

For the $[RuP_3](PF_6)_2$ molecule, there are three wavelengths of maximum UV absorption, but there are four pairs of excitation and emission wavelengths. Three excitation wavelengths are the same as the UV absorption and the other one has the highest value. Similar results were observed for $[RuP_3]Cl_2$ $[Ru(bpy)_2P]$ $(PF_6)_2$ $[Ru(bpy)_2P]Cl_2$.

3.1.4 $[Ru(bpy)_2IQ]^{2+}$ molecules

For $[Ru(bpy)_2IQ]Cl_2$ and $[Ru(bpy)_2IQ]$ $(PF_6)_2$ molecules, there are three wavelength with maximum absorption, and the highest emission and excitation wavelength is different from these three.

Table 3-1 Fluorecence and UV data for organic and coordination cations based on P and IQ molecules See Appendix for UV and fluorescence spectra

	UV absorption(nm)	Excitation Wavelength	Emission Wavelength
P	226 246 348	348	407
$[PC_2]Cl_2$	246 310 408	408	450
$[PC_2]$ $(PF_6)_2$	248 312 406	406	451
$[PC_3]Cl_2$	254 386	388	457

$[PC_3]\ (PF_6)_2$	250 384	385	462
$[PC_4]Cl_2$	258 386	386	478
$[PC_4]\ (PF_6)_2$	258 366	377	487
IQ	260 374	375	435
$[IQC_2]Cl_2$	244 446	448	485
$[IQC_2]\ (PF_6)_2$	244 444	446	497
$[IQC_3]Cl_2$	242 412	415	503
$[IQC_3]\ (PF_6)_2$	242 414	416	494
$[RuP_3]Cl_2$	242 324 438		
$[RuP_3]\ (PF_6)_2$	242 324 434	350	440
$[Ru(bpy)_2P]Cl_2$	242 288 430	469	620
$[Ru(bpy)_2P]$ $(PF_6)_2$	242 288 426	469	620
$[Ru(bpy)_2IQ]Cl_2$	236 288 412 468		
$[Ru(bpy)_2IQ]$ $(PF_6)_2$	236 288 412 468	228 412 468	700

The fluorescence data for the organic cations shows a general trend as the more conjugated Q system seems to fluoresce at a longer wavelength in the neutral and alkylated compounds. This

is consistent with more extensive conjugation, decreasing the energy gap between the HOMO and the LUMO, and leading to longer emission wavelengths. Within the P family, it seems that the length of the alkyl spacer has a significant effect on fluorescence. As n increases, the $[PCn]^{2+}$ emission moves to longer wavelengths. Although many aspects may come into play, this trend may be explained by the larger conformational flexibility of a C4 spacer (compared to a C2 spacer), which may permit access to better conjugated conformers. Interestingly, this trend is not as clear for the IQ family (although this is difficult to judge with accuracy with only two alkylated IQ compounds) as in acetonitrile the emission wavelengths of $[IQC_2]^{2+}$ and $[IQC_3]^{2+}$ are fairly similar. In water, there seems to be a substantial increase.

The luminescence of the complexes deserves a few comments as well. First, the luminescence of a control complex $[Ru(bpy)_3](PF_6)_2$ was also measured (not reported in the table) to be 611 nm under these conditions, consistent with what is found in the literature. $[Ru(bpy)_2P](PF_6)_2$ and $[Ru(bpy)_2IQ](PF_6)_2$ emit in the same area (620 and 700 nm, respectively), which relates well to the data reported by Kirsch with the TAP and HAT ligands (Chapter 1, Figure 1.9) for which the $[Ru(bpy)_2L](PF_6)_2$ emission wavelengths are reported to be 679 nm and 703 nm, respectively.[32] The measured emission wavelength at 440 nm, however, is a bit more puzzling. It is known that increasing the number of heteroatoms in the ligand does indeed decrease the emission wavelength, however such a low emission wavelength (close to the highest absorption maximum) is suspicious. The emission of $[Ru(TAP)_3]^{2+}$ and $[Ru(HAT)_3]^{2+}$ are reported to occur at 604 and 587 nm,[32] respectively, which is the range of wavelengths that $[Ru(P)_3]^{2+}$ would be expected to emit in. Further investigations will have to be conducted to confirm this value.

3.2 Electrochemical properties

All of the cyclic voltammetry data can be seen below in Table 3.2. Not surprisingly, the ruthenium complexes have more redox activity than the organic binders. For the P and IQ ligands, there is only one oxidation peak.

Table 3-2 Electrochemical data for the organic and coordination cations (degassed anhydrous CH_3CN, 0.10 M nBu_4PF_6 as the supporting electrolyte, 25 ºC; "rev" stands for "reversible")

compound	Oxidation ($E_{1/2}$ (V) vs Fc^+/Fc)	Reduction ($E_{1/2}$ (V) vs Fc^+/Fc)		
IQ	~0.7 (non-rev)			
$[IQC_2](PF_6)_2$		-0.77 (rev)		
$[IQC_3](PF_6)_2$		- 0.87 (rev)		
P	~0.6 (non-rev)			
$[PC_2](PF_6)_2$		- 1.00 (rev)	- 1.64 (rev)	
$[PC_3](PF_6)_2$		- 1.10 (rev)	- 1.63 (rev)	
$[Ru(bpy)_2IQ](PF_6)_2$	0.77 (rev)	-1.64 (rev)	-1.93 (rev)	-2.17 (rev)
$[Ru(bpy)_2P](PF_6)_2$	0.77 (rev)	- 1.63 (rev)	- 1.93 (rev)	- 2.17 (rev)
$[Ru(P)_3](PF_6)_2$	0.57 (rev)	- 2.09 (rev)	- 2.28 (rev)	- 2.48 (rev)
$[Ru(bpy)_3](PF_6)_2$	0.89 (rev)	- 1.73 (rev)	- 1.92 (rev)	- 2.17 (rev)

Once again, $[Ru(bpy)_3](PF_6)_2$ was submitted to the same study under the same conditions as a test compound. As shown inTable 3-2, $[Ru(bpy)_2IQ](PF_6)_2$ and $[Ru(bpy)_2P](PF_6)_2$ show oxidation and reduction potentials in the same area, with a slightly easier reduction probably due to the presence of the internal nitrogen which makes the overall complex slightly easier to reduce. This trend is confirmed by the results obtained for $[RuP_3](PF_6)_2$, as increasing the number of P ligands renders the overall complex even more susceptible to reduction.

3.3 Assessing the oxidative power of P and IQ based potential DNA binders

In order to assessing the oxidation ability, the excited state reduction potential may be calculated according to the following equation:[71]

$E_{red}^{*} \approx E_{red} + 1241/\lambda_{em}$

where E_{red} corresponds to the first reduction wave, and λ_{em} is the emission wavelength in nm.

In order to compare with literature values, $E_{1/2}$ values are referenced against the standard SCE electrode based on the following conversion factor:

$E_{1/2\ red}$ (V, vs SCE) = $E_{1/2\ red}$ (V, vs Fc^{+}/Fc) + 0.390.[72]

Table 3-3 Estimate of the "oxidizing power" of the organic and coordination cations. See Appendix for CV spectra

	$E_{1/2\ red}$ (V, vs Fc^{+}/Fc)	$E_{1/2\ red}$ (V, vs SCE)	λ_{em} (nm)	E_{red}^{*} (V, vs SCE)
P	NA	NA	407	NA
$[PC_2](PF_6)_2$	-1.00	-0.61	451	2.14
$[PC_3](PF_6)_2$	-1.10	-0.71	462	1.98
IQ	NA	NA	435	NA
$[IQC_2](PF_6)_2$	-0.77	-0.38	497	2.12
$[IQC_3](PF_6)_2$	-0.87	-0.48	494	2.03
$[RuP_3](PF_6)_2$	-2.09	-1.7	*440*	*1.12*
$[Ru(bpy)_2P](PF_6)_2$	-1.63	-1.24	620	0.76
$[Ru(bpy)_2IQ](PF_6)_2$	-1.64	-1.25	700	0.52
$[Ru(bpy)_3](PF_6)_2$	-1.73	-1.34	611	0.69

As a first comment, let us notice that the data measured for the known $[Ru(bpy)_3](PF_6)_2$ compound are consistent with what is found in the literature. E_{red}^{*} is estimate to be 0.69 V vs SCE, and the literature reports a value of 0.65 V vs SCE,[32] which brings some confidence in our methods.

As the P ligand has no reduction peak, it has no ability to oxidize DNA base. $[PC_2](PF_6)_2$ has a larger E_{red}^* than $[PC_3](PF_6)_2$. $[IQC_2](PF_6)_2$ and $[IQC_3](PF_6)_2$ have similar E_{red}^* and they also have similar E_{red}^* to $[PC_2](PF_6)_2$ and $[PC_3](PF_6)_2$. This confirms that the P and IQ ligands have similar electrochemical properties. P is able to act as the simpler model for the IQ ligand. Those E_{red}^* values are fairly high and seem to indicate that the organic cations may be good candidates for guanine oxidation (GMP oxidation potential is 1.25 V versus SCE).

As for the ruthenium complexes, it seems that, among the three new compounds reported here, only $Ru(P)_3^{2+}$ may have a chance to be able to photo-oxidize guanine (provided the luminescence data is confirmed).

3.4 Examples of measurements

$[PC_2](PF_6)_2$ is taken as an example for organic cation to explain the measurements

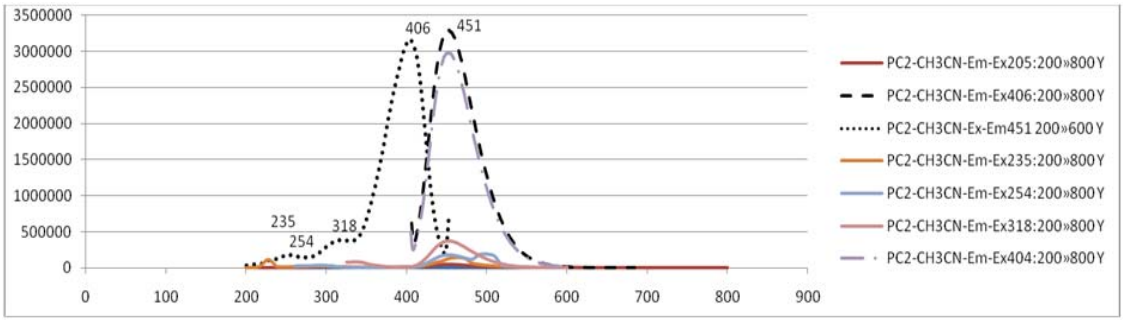

Figure 3.1 Fluorescence spectrum of $[PC_2](PF_6)_2$

The maximum excitation wavelength is the same as the UV maximum absorption wavelength. And according to the excitation wavelength, the emission wavelength is easy to obtain and this emission was used as the λ_{em} for the calculation.

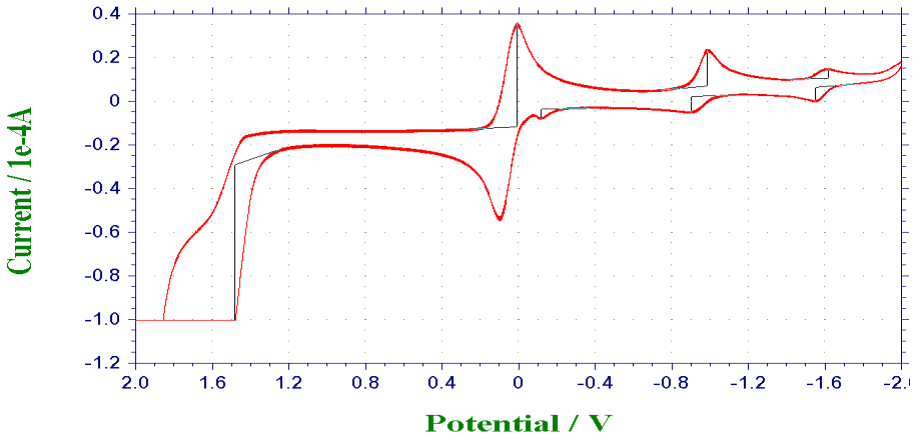

Figure 3.2 CV spectrum of $[PC_2](PF_6)_2$

In the CV spectrum, the first reduction potential was used for ground state reduction value, E_{red}.

After the E_{red} and λ_{em} are obtained, the E^* can be calculated.

$[RuP_3](PF_6)_2$ is taken as an example for ruthenium complex to explain the measurements.

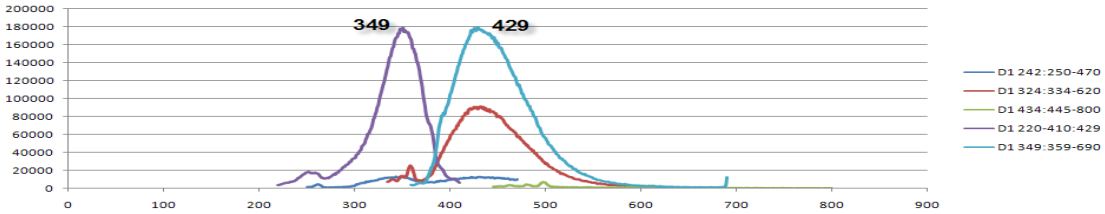

Figure 3.3 Fluorescence spectrum of $[RuP_3](PF_6)_2$

The maximum excitation wavelength is the same as the UV maximum absorption wavelength. And according to the excitation wavelength, the emission wavelength is easy to obtain and this emission was used as the λ_{em} for the calculation.

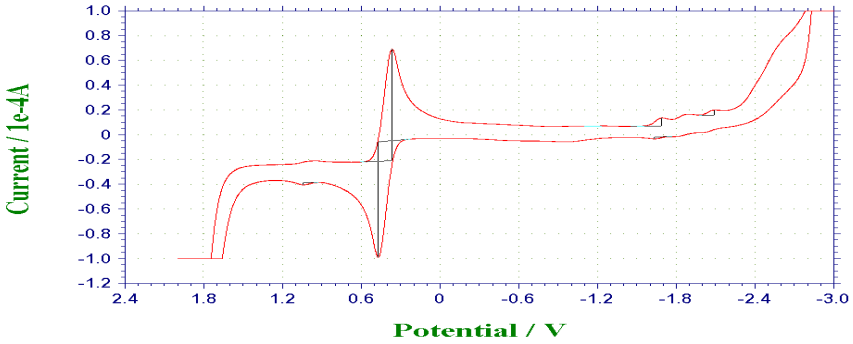

Figure 3.4 CV spectrum of $[RuP_3](PF_6)_2$

In the CV spectrum, the first reduction potential was used for ground state reduction value, E_{red}.

After the E_{red} and λ_{em} are obtained, the E^* can be calculated.

Chapter 4

Conclusion and perspectives

4.1 Summary and Conclusions

This work started with the investigation of new potential DNA binding molecules, and two basic ligands IQ and P were chosen for this aim. IQ is a potential twisted DNA binder and P is the simplified model of IQ ligand which maintains an internal nitrogen. Two series of compounds, IQ and P cations, and Ruthenium complexes were synthesized, including $[PC_2]Br_2$, $[PC_2]Cl_2$, $[PC_2](PF_6)_2$, $[PC_3]Br_2$, $[PC_3]Cl_2$, $[PC_3](PF_6)_2$, $[PC_4]Cl_2$, $[PC_4](PF_6)_2$, $[IQC_2]Br_2$, $[IQC_2]Cl_2$, $[IQC_2](PF_6)_2$, $[IQC_3]Br_2$, $[IQC_3]Cl_2$, $[IQC_3](PF_6)_2$, $[Ru(bpy)_2P](PF_6)_2$, $[Ru(bpy)_2P]Cl_2$, $[Ru(bpy)_2IQ](PF_6)_2$, $[Ru(bpy)_2IQ]Cl_2$, $[Ru(P)_3](PF_6)_2$ and $[Ru(P)_3]Cl_2$. Exploration into an improved synthetic pathway to IQ gave mixtures that proved difficult to separate. The P ligand is easy to synthesize according to published procedures. Among the organic cations, the $[PC_3]^{2+}$ compound was obtained with the highest yield among all the P ligand, indicating that the 3 carbon chain may fit the P ligand very well. $[PC_4]^{2+}$ cations were hard to synthesize (three attempts only led to 14% to 28% yields). For the ruthenium complexes, there were at least three trials to make $[Ru(bpy)P_2]^{2+}$ complexes, but there were many by-products and the interface recrystallization did not work, so new recrystallization methods or HPLC should be used to get the pure compounds. Once the $[Ru(bpy)P_2]^{2+}$ is synthesized, $[Ru(bpy)IQ_2]^{2+}$ should not be a problem. The chiral separation part was found to be hard to achieve after several trials**.**

From the electrochemical and the photophysical properties of the compounds we can prove that the P and IQ molecules are similar to each other. All of the organic cations have potential

oxidizing abilities to DNA bases, and the ruthenium complexes do not seem to be very good candidates for the photo-oxidation of bases.

4.2 Future Directions

Future direction of this work should start with the synthesis of $[Ru(bpy)P_2]^{2+}$, $[Ru(bpy)IQ_2]^{2+}$ and $[RuIQ_3]^{2+}$ complexes, as mentioned above. All the synthesis will start from the P related compounds, as the P ligand is easy to replace.

The enantiomer resolution of all the compounds needs to be done and all the compounds need future DNA electrophoresis and photochemical tests.

Also, future photophysical studies need to be done, as access to $[Ru(bpy)P_2]^{2+}$ may shine some light into the emission behaviour of $[Ru(P)_3]^{2+}$. Once the whole series of compounds are synthesized and characterized, it will be easier to identify what, in the preliminary results, gave photo-adducts with DNA, and what the chemical nature(s) of those adducts is(are).

Finally, as these compounds are potentially anticancer drugs, biochemical tests should be conducted in the future.

Chapter 5

Experimental section

5.1 General methods

All starting materials were purchased from Alfa Aesar or Aldrich and used without further purification. Solvents were used from the original bottle without further purification. Argon gas was used as an inert gas. Thin layer chromatography (TLC) was carried out on silica gel. Flash chromatography was carried out on silica (silica gel 40-63 μm). Cation exchange chromatography was performed on Sephadex SP C25, and anion exchange on Amberlite IRA-400. Melting points were recorded on a TEL-TEMP II instrument. Mass spectrometry was conducted at Queen's University Mass Spectrometry facility using electro-spray ionization. Elemental analysis was obtained by Laboratoire d'Analyse Élémentaire de l'Université de Montréal. 1D ^{1}H NMR spectra were recorded on Bruker Avance 300 MHz and 500Hz spectrometers. Chemical shifts in ^{1}H NMR were referenced according to the residual solvent signal ($CHCl_3$, CH_3CN) except for water (in D_2O, $(CH_3)_3OH$ was used as an internal reference). ^{13}C NMR spectra were recorded on a Bruker Avance 400Hz spectrometer. Excitation and emission spectra were recorded on a Photon Technologies International QuantaMaster model C-60 spectrometer. Cyclic voltammetry was performed using 610B Electrochemical Analyzer from CH Instruments, Inc, with a scan rate of 100 mV s^{-1}. The electrolytic cell used was a conventional three-compartment cell, in which a glass carbon working electrode, a Pt auxiliary electrode, and a Ag/AgCl reference electrode were employed. The CV measurements were performed at room temperature using 0.10 M tetrabutylammonium hexafluorophosphate (TBAP) as the supporting electrolyte and anhydrous

CH_3CN as the solvent. The ferrocenium/ferrocene couple was used as the internal standard (E_0 = 0.45 V SCE).

The P and IQ ligand and $[PC_2]^{2+}$, $[PC_3]^{2+}$, $[PC_4]^{2+}$, $[IQC_2]^{2+}$, $[IQC_3]^{2+}$ and $[Ru(bpy)_2P]^{2+}$, $[Ru(P)_3]^{2+}$, $[Ru(bpy)_2IQ]^{2+}$ complexes were synthesized according to literature procedures.

5.2 P, organic cations and ruthenium complexes

5.2.1 Synthesis of P ligand[59]

A solution of 5.00 g of pyridine-2-carboxaldehyde (46.7 mmol, 2.46 eq), 2.5 g of ammonium sulphate (18.95 mmol, 1.00 eq), MilliQ water (25 mL) was stirred in room temperature for 24h. The precipitate was filtered and washed with water. It was then dissolved in dichloromethane and washed with MilliQ water three times. The dichloromethane layer was dried (Na_2SO_4) and concentrated in vacuo. Purification was performed by sublimation. The experiment was run twice (yield 27.8%-28.4%). ^{1}**H** (300 MHz; $CDCl_3$) δ: 9.96 (d, J = 7.2 Hz, 1H, H_5), 8.63 (dd, J = 4.2 Hz, J = 1.2 Hz, 1H, H_{12}), 8.34 (m, 1H, H_{15}), 7.77 (td, J = 7.8 Hz, J = 1.5 Hz, 1H, H_{14}), 7.59(s, 1H, H_7), 7.53 (m, 1H, H_1), 7.18 (ddd, J = 7.2 Hz, J = 4.8 Hz, J = 1.2 Hz, 1H, H_{13}), 6.85 (ddd, J = 9.3 Hz, J = 6.3 Hz, J = 4.2 Hz, J = 1.2 Hz, 1H, H_2), 6.72 (td, J = 7.2 Hz, J = 1.2 Hz, 1H, H_6). Mp:109.0-113.0°C; R_f: 0.27 (CH_2Cl_2 2.0: EtOAc:0.5) Appendix figure A.1, A.2.

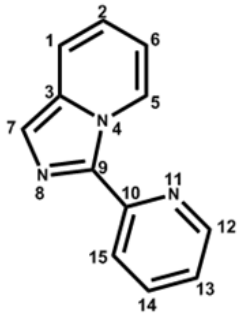

Figure 5.1 Structure of P ligand

5.2.2 Synthesis of $[PC_2]Br_2$, $[PC_2]Cl_2$ and $[PC_2](PF_6)_2$[62]

5.2.2.1 Synthesis of $[PC_2]Br_2$

47 mg of 3-(pyridin-2-yl)imidazo[1,5-a]pyridine (P ligand, 0.241 mmol, 1 eq) was introduced into 3 mL of freshly distilled 1,2-dibromoethane (34.7 mmol, 144 eq). The solution was refluxed at 130 ^{o}C for 25 hours under argon and aluminium foil. The product was filtered and washed by dichloromethane and diethylether (yield 80.1 %). ^{1}H (300 MHz; D_2O) δ: 9.18 (d, J = 6.6 Hz, 1H, H_{12}), 9.12 (d, J = 6.6 Hz, 1H, H_{15}), 8.93-8.83 (m, 2H, $H_{14,}$ H_5), 8.66 (s, H_7), 8.23-8.18 (m, 2H, H_1, H_{13}), 7.77-7.67 (m, 2H, H_2, H_6).29-5.26 (m, 4H, H_{16}, H_{17}, H_{18}, H_{19}). Appendix figure A.35. Mp >260 °C; Elemental analysis for $C_{14}H_{13}N_3Br_2$: 0.35 CH_2Cl_2, calculated: %C 41.75, %H 3.34, %N 10.18, found: %C 41.75, %H 3.36, %N 10.24. ESI-MS *m/z found*(M^{2+}:223.3) 111.3 calcd: 111.6) Appendix figure A.4 R_f: 0.45 (CH_2Cl_2 1.0: EtOAc:0.35).

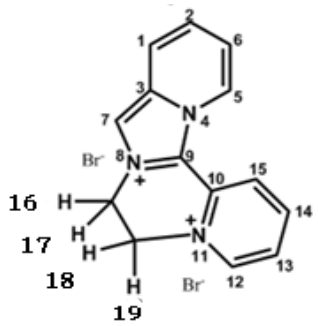

Figure 5.2 Structure of $[PC_2]Br_2$

5.2.2.2 Synthesis of $[PC_2](PF_6)_2$

10 mg of $[PC_2]Br_2$ (26.1 mmol) was dissolved in 1 mL of MilliQ water, three equivalents of ammonium hexafluorophosphate (NH_4PF_6) saturated water solution were introduced into the $[PC_2]Br_2$ solution and a yellow powder precipitated. The compound was filtered and washed with

water and diethylether (yield 71.7%). ^{1}**H** (300 MHz; CD_3CN) δ: 8.93 (d, J = 6.0 Hz, 1H, H_{12}), 8.88 (d, J = 7.2 Hz, 1H, H_{15}), 8.78 (dd, J = 8.1 Hz, J = 8.1 Hz), 8.66 (d, J = 7.5 Hz, 1H, H_5), 8.45 (s, 1H, H_7), 8.21-8.12 (m, 2H, H_1, H_{13}), 7.74-7.63 (m, 2H, H_2, H_6), 5.26 (m, 4H, H_{16}, H_{17}, H_{18}, H_{19}). Mp >260 °C**.**

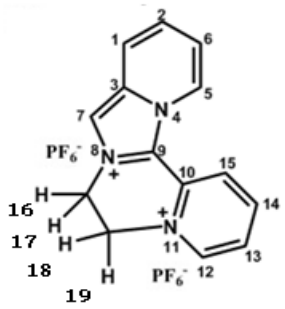

Figure 5.3 Structure of $[PC_2](PF_6)_2$

5.2.2.3 Synthesis of $[PC_2]Cl_2$

$[PC_2]Cl_2$ was prepared by using an anion exchange column conditioned with chloride anions (first wash the column with 20 mL of 1 M NaCl and then with 250 mL of MilliQ water). 37 mg of $[PC_2]Br_2$ were loaded in water and eluted with MilliQ water. The collected yellow band was frozen in liquid nitrogen for 15 minutes and lyophilized for 24 hours (yield 93 %). Mp >260 °C

5.2.3 Synthesis of $[PC_3]Br_2$, $[PC_3]Cl_2$ and $[PC_3](PF_6)_2$[63]

5.2.3.1 Synthesis of $[PC_3]Br_2$

54.3 mg of 3-(pyridin-2-yl)imidazo[1,5-a]pyridine (P ligand (0.278 mmol, 1 eq) was dissolved into 2 mL of 1,3-dibromopropane (19.6 mmol, 70.5 eq). The solution was refluxed at 120 ^{o}C for 24 hours under argon and aluminium foil. The product was filtered and washed with dichloromethane and diethylether (yield 88.5 %). Mp >260 °C**;** ESI-MS *m/z found* (M^{2+}:237.30) 118.4 calcd: 118.7 R_f: 0.46 (CH_2Cl_2 1.0: EtOAc:0.35)

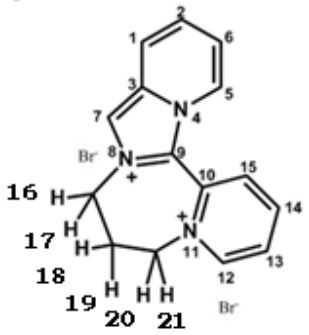

Figure 5.4 Structure of $[PC_3]Br_2$

5.2.3.2 Synthesis of $[PC_3](PF_6)_2$

14.3 mg of $[PC_3]Br_2$ (0.36 mmol) were dissolved in 1 mL of MilliQ water, 3 equivalents of NH_4PF_6 saturated water solution was introduced into the $[PC_3]Br_2$ solution; the yellow precipitate was filtered and washed with water and diethylether (yield 71.5 %). ^{1}**H** (300 MHz; acetonitrile) δ: 9.08 (d, J = 5.7 Hz, 1H, H_{12}), 8.80 (dd, J = 7.8 Hz, J = 8.1 Hz, 1H, H_{14}), 8.50 (m, 2H, H_5, H_{15}), 8.37(s, 1H, H_7), 8.37 (dd, J = 6.9 Hz, J = 7.2 Hz, H_{13}), 8.11 (d, J = 9.3 Hz, 1H, H_1), 7.62(m, 1H, H_2), 7.49 (dd, 1H, J = 6.3 Hz, J = 6.9 Hz, H_6). 4.87 (m, 2H, H_{16}, H_{17}) 4.54-4.34 (m, 2H, H_{20}, H_{21}) 2.89 (m, 2H, H_{18}, H_{19}) overlap with water peak. Mp >260 °C. Elemental analysis: $C_{15}H_{15}N_3P_2F_{12}$. 0.5 NH_4PF_6: calculated: %C 29.60, %H 2.82, %N 8.05; found: %C 29.66, %H 2.79, %N 7.91 Appendix figure A.5 , A.6.

5.2.3.3 Synthesis of $[PC_3]Cl_2$: $[PC_3]Cl_2$ was prepared by using an anion exchange column (yield 99%). Mp >260 °C.

5.2.4 Synthesis of $[PC_4]Br_2$, $[PC_4]Cl_2$ and $[PC_4](PF_6)_2$[63]

5.2.4.1 Synthesis of $[PC_4](PF_6)_2$

50.4 mg of 3-(pyridin-2-yl)imidazo[1,5-a]pyridine (P ligand, 0.256 mmol, 1 eq) was introduced into 2 mL of 1,4-dibromobutane (16.9 mmol, 66 eq). The solution was refluxed at 120

^{o}C for 40 hours under argon and aluminium foil. 5 mL of MilliQ water were added and the aqueous solution washed with dichloromethane. The water layer was isolated, and 100 mg of NH_4PF_6 were added. The precipitate was filtered and washed with MilliQ water (yield 24.7%). ^{1}**H** (300 MHz; CD_3CN) δ: 9.18 (d, J = 5.7 Hz, 1H, H_{12}), 8.81 (dd, J = 8.1 Hz, J = 7.8 Hz, 1H, H_{14}), 8.44-8.43 (m, 2H, H_{13} , H_{15}), 8.35 (s, 1H, H_7), 8.22 (d, J = 6.9 Hz, H_5), 8.07 (d, J = 9.3 Hz, 1H, H_1), 7.60 (dd, 1H, J = 9.3 Hz, J = 6.9 Hz, H_2), 7.40 (t, 1H, J = 6.9 Hz, H_6), 4.88-4.80 (m, 2H, H_{16}, H_{23}), 4.27 (dd, 1H, J = 11.1 Hz, J = 14.2 Hz, H_{17}), 4.08 (dd, 1H, J = 11.4 Hz, J = 14.2 Hz, H_{22}), 2.53-2.00 (m, 4H, H_{18}, H_{19}, H_{20}, H_{21}) overlap with water peak. Appendix figure A.7, A.8 Mp >260 °C**;** ESI-MS *m/z found*(M^{2+}:251.3) 125.4 calcd: 125.7; RF: 0.33 (CH_2Cl_2 1.0: EtOAc:0.3). Appendix figure A.9.

Note: All of the NH_4PF_6 solution should be introduced into the $[PC_4]Br_2$ in one time, as if another aliquot of NH_4PF_6 solution was introduced, the $[PC_4](PF_6)_2$ precipitate will disappear.

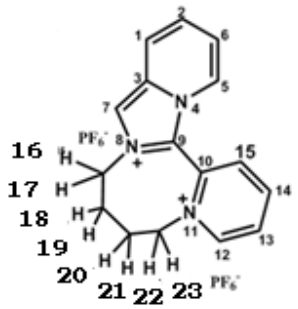

Figure 5.5 Structure of $[PC_4](PF_6)_2$

5.2.4.3 Synthesis of $[PC_4]Cl_2$:

$[PC_4]Cl_2$ was prepared by using anion exchange column (yield 88.6 %). Mp >260 °C.

5.2.5 Synthesis of $[Ru(bpy)_2P](PF_6)_2$ and $[Ru(bpy)_2P]Cl_2$[64]

5.2.5.1 Synthesis of $[Ru(bpy)_2P](PF_6)_2$

A mixture of 51 mg of $[Ru(bpy)_2]Cl_2$[65] (1 eq, 0.11 mmol) and 23.4 mg of P (1.14 eq, 0.12 mmol) was refluxed at 85 °C in 12 mL of a 3:1 95% ethanol/water mixture overnight, protected by argon. four equivalents of NH_4PF_6 were added to the solution to form the $[Ru(bpy)_2P]$ $(PF_6)_2$ precipitate. The precipitate was filtered, washed with 2 mL of MilliQ water and 3 mL of diethylether and dried under high vacuum. The compound was further purified by interface recrystallization. The compound was dissolved in 5 mL of dichloromethane in a 50 mL round bottom flask and 95% ethanol was added to the top of dichloromethane layer carefully. The flask was placed in the fridge overnight. Single crystals were obtained, filtered and dried (yield 86%). ^{1}**H** (300 MHz; CD_3CN) δ: 8.83 (d, J = 6.9 Hz, 1H), 8.52-8.44 (m, 4H), 8.32 (d, J = 8.1 Hz, 1H), 8.07-7.99 (m, 5H), 7.84-7.82 (d, J = 5.4 Hz, 2H), 7.80-7.78 (d, J = 5.4 Hz, 1H), 7.73-7.69 (t, J = 6.3 Hz, 2H), 7.65-7.62 (d, J = 8.7 Hz, 1H), 7.43-7.31 (m, 4H), 7.26-7.16 (m, 3H), 7.03 (s, 1H). For the X-ray crystal structure analysis see the appendix. Mp:184-190 °C. R_f: 0.71 (CH_3CN 2.0: H_2O 0.5:KNO_3 0.5). Appendix figure A.10, A.11.

A crystal of the compound (brown, plate-shaped, size 0.35 x 0.15 x 0.08 mm) was mounted on a glass fiber with grease and cooled to -93 °C in a stream of nitrogen gas controlled with a Cryostream Controller 700. Data collection was performed on a Bruker SMART APEX II X-ray diffractometer with graphite-monochromated Mo K_α radiation (λ = 0.71073 Å), operating at 50 kV and 30 mA over 2θ ranges of 4.82 ~ 52.00º. No significant decay was observed during the data collection. Data were processed on a PC using the Bruker AXS Crystal Structure Analysis Package:[73] Data collection: APEX2 (Bruker, 2006); cell refinement: SAINT (Bruker, 2005); data reduction: SAINT (Bruker, 2005); structure solution: XPREP (Bruker, 2005) and SHELXTL (Bruker, 2000); structure refinement: SHELXTL; molecular graphics: SHELXTL; publication materials: SHELXTL. Neutral atom scattering factors were taken from Cromer and Waber.[74] The

crystal is monoclinic space group $P2_1/c$, based on the systematic absences, E statistics and successful refinement of the structure. The structure was solved by direct methods. Full-matrix least-square refinements minimizing the function $\sum w (F_o^2 - F_c^2)^2$ were applied to the compound. All non-hydrogen atoms were refined anisotropically. All of the H atoms were placed in geometrically calculated positions, with C-H = 0.95 (aromatic) and 0.99Å (CH_2), and refined as riding atoms, with Uiso(H) =1.2 Ueq(other C). In addition to the dichloromethane molecules, difference electron density maps also revealed the presence of disordered lattice solvate molecules, which were ultimately modeled through the use of the SQUEEZE subroutine of the PLATON software suite. PLATON,[75] A46, 194. Two solvent accessible voids per lattice were found, comprising a total volume of 2 x 317 = 634 Å^3 and contributing a total of 2 x 57 = 114 electrons. The voids were thus assigned to 4 disordered ethanol molecules, which contribute 4 x 26 = 104 electrons, and occupy about 240 Å^3 in space. The larger volume of the void may be a result of the disorder. The contributions have been included in all derived crystal quantities although the precise composition of the lattice solvate is somewhat speculative. Convergence to final R_1 = 0.0705 and wR_2 = 0.1821 for 4804 (I>2σ(I)) independent reflections, and R_1 = 0.1189 and wR_2 = 0.1911 for all 8200 (R(int) = 0.0578) independent reflections, with 514 parameters, were achieved.[1] The largest residual peak and hole to be 1.010 and – 1.081 e/Å^3, respectively.

---

[1] $R_1 = \sum | |Fo| - |Fc| | / \sum |Fo|$

$wR_2 = \{\sum [w (Fo^2 - Fc^2)^2] / \sum [w(Fo^2)^2]\}^{1/2}$

($w = 1 / [\sigma^2(Fo^2) + (0.0957P)^2 + 0.526P]$, where $P = [\text{Max}(Fo^2, 0) + 2Fc^2] / 3$)

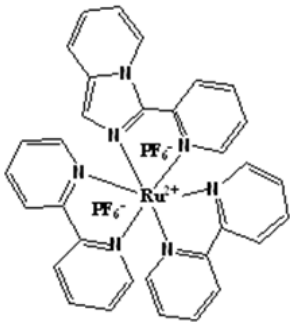

Figure 5.6 Structure of $[Ru(bpy)_2P](PF_6)_2$

5.2.5.2 Synthesis of $[Ru(bpy)_2P]Cl_2$:

$[Ru(bpy)_2P]Cl_2$ was prepared by anion exchange column (yield 96.5%). Mp >260 °C.

5.2.6 Synthesis of $[RuP_3](PF_6)_2$ and $[RuP_3]Cl_2$

5.2.6.1 Synthesis of $[RuP_3](PF_6)_2$

a) Synthesis of $Ru(DMSO)_4Cl_2$[66]

226 mg of $RuCl_3$ were dissolved in 1.88 mL of DMSO (26.4 mmol, 24.3 eq) protected by argon, refluxed for 5 minutes and concentrated to half of its original volume by heating for 15 minutes. 50 mL of acetone were introduced and the solid was filtered and washed with diethylether. The solid product was suspended again in acetone for 30 minutes and filtered again to get rid of extra DMSO (yield = 28 %). IR (KBr pellet): 1638 w; 1423 m; 1310 m; 1114 s; 1024 s; 992 s; 960 m; 936 s; 716 m; 676 m; 483 w; 426 m. Appendix figure A.28.

b) Synthesis of $[RuP_3](PF_6)_2$[68]

A mixture of 61.0 mg of $Ru(DMSO)_4Cl_2$ (0.127 mmol, 1 eq) and 106 mg of P ligand in 95% ethanol (18 mL) was refluxed for 23 h under argon and protected from light. MilliQ water was added and the solution was washed with dichloromethane three times. The water layer was isolated and 50 mg of NH_4PF_6 were added. $[RuP_3](PF_6)_2$ was filtered and washed with water and diethylether. Purification was performed by interface recrystallization (dichloromethane / 95%

ethanol, in fridge overnight). The precipitate was filtered and washed with ethanol and diethylether (yield = 25.2%). ^{1}**H** (300 MHz; CD_3CN) δ: 8.86-8.84 (m, 3H), 8.34-8.28 (m, 3H), 8.03-7.97 (m, 3H), 7.91-7.79 (m, 3H), 7.65-7.58 (m, 3H), 7.23-7.11 (m, 12H). Mp >260 °C. R_f: 0.5 (CH_3CN 2.0: H_2O 0.3:KNO_3 0.1).

5.2.5.2 Synthesis of $[RuP_3]Cl_2$

$[Ru(bpy)_2P]Cl_2$ was prepared by using an anion exchange column (yield 99.9%). Mp >260 °C. Elemental Analysis for $C_{36}H_{27}N_9Cl_2Ru$. 6.0 H_2O: calculated: %C 49.95, %H 4.54, %N 14.56; found: %C 49.91, %H 4.26, %N 14. ESI-MS *m/z found*(M^{2+}:686.7) 343.6 calcd: 343.4; Appendix figure A.12, A.13, A.14.

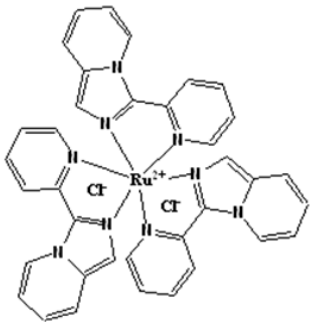

Figure 5.7 Structure of $[RuP_3]Cl_2$

5.3 IQ, organic cations and ruthenium complexes

5.3.1 Synthesis of 1-(1,3,5-trioxan-2-yl)isoquinoline (IQ ligand)

5.3.1.1 Synthesis of 1-(1,3,5-trioxan-2-yl)isoquinoline[60]

A solution of 500 mL CH_3CN, 10.23 g of isoquinoline (79.2 mmol,1.00 eq), 610 g of 1,3,5-trioxane (6.77 mol, 85.5 eq), 63.4 mL of t-BuOOH (385 mmol, 4.86 eq), 856 mg of $FeSO_4$•$7H_2O$ (3.08 mmol, 0.039 eq, 0.8% of t-BuOOH) and 6.10 mL of TFA (79.18 mmol, 1.00 eq) was heated at 110 °C under reflux for 5h20min. The solution was concentrated in vacuo, and the resulting

dark brown solid was dissolved in diethylether (50 mL) and washed with water (800 mL). The aqueous layer was further extracted with diethylether, and the combined organic layers dried with sodium sulphate and concentrated in vacuo to yield 12.4 g of a dark brown liquid. As a large amount of trioxane was left in the crude product, the yield cannot be calculated at this stage. ^{1}**H** (300 MHz; $CDCl_3$) δ: 8.89 (d, J = 7.8 Hz, 1H, H_1), 8.49 (d, J = 5.7 Hz, 1H, H_{10}), 7.84 (d, J = 4.35 Hz, 1H, H_7), 7.68 (m, 3H, H_2, H_8, H_9), 6.42 (s, 1H, H_{11}), 5.46 (J = 6.3 Hz, J_d=14.1Hz, 4H, H_{15a}, H_{15e}, H_{13a}, H_{13e}) Appendix figure A.15.

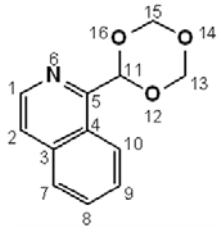

Figure 5.8 Structure of 1-(1,3,5-trioxan-2-yl)isoquinoline

5.1.2.2 Synthesis of isoquinoline-1-carbaldehyde[60]

A solution of 1-(1,3,5-trioxan-2-yl)isoquinoline 15.2g (n^{max}=79.2 mmol, 1.0 eq) was refluxed in 6N HCl (100 mL, 0.6 mol, 7.6 eq) at 110°C for 1.5h. After cooling in an ice bath, solid NaOH was slowly added (24.28 g) to adjust the pH to 7. The aqueous layer was extracted by dichloromethane (4 times), dried and concentrated. The crude was purified by flash column chromatography (SiO_2, built in dichloromethane) eluted with dichloromethane**:**EtOAc=2:0.14. The reaction was conducted twice leading to 36% and 51.5% yields. ^{1}**H** (300 MHz; $CDCl_3$) δ:10.35 (s, 1H, H_{12}), 9.32 (dd, J = 6.6 Hz, J = 3.3 Hz, 1H, H_1), 8.76 (d, J = 5.4 Hz, 1H, H_{10}), 7.91 (m, 2H, H_7, H_9), 7.76 (m, 2H, H_2, H_8). R_f: 0.36 (CH_2Cl_2 2.0: EtOAc 0.14). Appendix figure A.16.

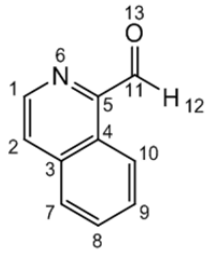

Figure 5.9 Structure of Isoquinoline-1-carbaldehyde

5.1.2.3 Synthesis of 3-(isoquinolin-1-yl)imidazo[5,1-a]isoquinoline (IQ ligand)[59]

A solution of 1.68 g of pyridine-2-carboxaldehyde (11.0 mmol, 2.38 eq), 0.61 g of $(NH_4)_2SO_4$ (4.60 mmol, 1.00 eq), MilliQ water (4 mL) and methanol (1.5 mL) was stirred for 72h at room temperature. After extraction with dichloromethane, drying and evaporation, the crude was purified by flash column chromatography (SiO_2, built in dichloromethane, eluted with dichloromethane:EtOAc=4:0.5). The experiment was conducted twice leading to yields of 24% and 25%. ^{1}**H** (300 MHz; $CDCl_3$) δ: 9.29 (d, J = 7.5 Hz, 1H, H_{16}), 9.08 (d, J = 7.5 Hz, 1H, H_6), 8.65 (d, J = 5.4 Hz, 1H, H_7), 8.17 (m, 1H, H_{22},) 8.14 (s, 1H, H_{13}), 7.89 (m, 1H, H_{10}), 7.60 (m, 6H, H_{19}, H_5, H_{20},H_{21}, H_8, H_9), 6.94 (d, J = 7.8 Hz, 1H, H_{17}). Mp:151.2-154.1°C R_f: 0.21 (CH_2Cl_2 2.0: EtOAc 0.25) Appendix figure A.17, A.18.

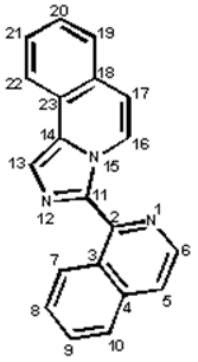

Figure 5.10 Structure of IQ

5.3.2 Synthesis of $[IQC_2]Br_2$, $[IQC_2]Cl_2$ $[IQC_2](PF_6)_2$[62]

5.3.2.1 Synthesis of $[IQC_2]Br_2$

50.0 mg of IQ ligand (0.169 mmol, 1.0 eq) was introduced into 2 mL of freshly distilled 1,2-dibromoethane (23.1 mmol, 138 eq). The solution was refluxed at 130°C for 24 hours under argon and aluminium foil. The precipitated was filtered and washed with dichloromethane and ether (yield 85.1%). Mp >260 °C. Appendix figure A.20.

5.2.2.2 Synthesis of $[IQC_2](PF_6)_2$

13.6 mg of $[IQC_2]Br_2$ was dissolved in 1 mL of MilliQ water, 3 equivalents of NH_4PF_6 saturated water solution was introduced into the $[IQC_2]Br_2$ solution. A yellow powder was filtered, washed with water and diethylether (yield 51.2%). ^{1}**H** (300 MHz; CD_3CN) δ: 9.01 (s, 1H), 8.77 (d, J = 6.9 Hz, 1H), 8.67 (d, J = 6.6 Hz, 1H), 8.55-8.52 (m, 1H), 8.49-8.47 (m, 1H), 8.40-8.32 (m, 2H), 8.19-8.10 (m, 3H), 8.01-7.93 (m, 2H), 7.80-7.78 (d, J = 7.5 Hz, 1H), 5.29-5.04 (m, 4H). Mp >260 °C; Elemental analysis for $C_{22}H_{17}N_3P_2F_{12}$. 0.2 $(C_2H_5)_2O$: calculated: %C , %H , %N ; found: %C 43.58, %H 2.43, %N 6.55. ES-MS *m/z found*(M^{2+}:323.39) 161.6 calcd: 161.7; Appendix figure A.19, A.21.

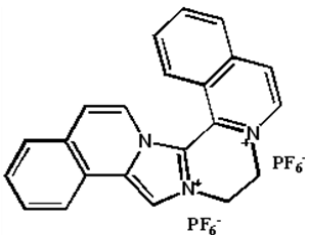

Figure 5.11 Structure of $[IQC_2](PF_6)_2$

5.2.2.3 Synthesis of $[IQC_2]Cl_2$: $[IQC_2]Cl_2$ was prepared by using an anion exchange column (yield 91.1%). Mp >260 °C.

5.3.3 Synthesis of $[IQC_3]Br_2$, $[IQC_3]Cl_2$ $[IQC_3](PF_6)_2$[63]

5.3.3.1 Synthesis of $[IQC_3]Br_2$

50.0 mg of IQ ligand (0.169 mmol, 1.0 eq) was introduced into 2 mL of freshly distilled 1,3-dibromopropane (19.6 mmol, 116 eq). The solution was refluxed at 120°C for 24 hours, protected by argon and aluminium foil. The precipitate was filtered, and washed with dichloromethane and ether (yield 92.8%). Mp >260 °C, Elemental analysis for $C_{23}H_{19}N_3Br_2$. 0.47 CH_2Cl_2: calculated: %C 52.46, %H 3.74, %N 7.82; found: %C 52.46, %H 3.87, %N 7.76. ESI-MS *m/z found*(M^{2+}:337.4) 168.0 calcd: 168.7; Appendix figure A.23, A.24.

5.2.3.2 Synthesis of $[IQC_3](PF_6)_2$

16.2 mg of $[IQC_3]Br_2$ was dissolved in 1 mL of MilliQ water, 3 equivalents of NH_4PF_6 saturated water solution were introduced into the $[IQC_3]Br_2$ solution. The yellow powder was filtered and washed with water and diethylether (yield 35.1%). ^{1}**H** (300 MHz; CD_3CN) δ: 8.96 (s, 1H), 8.88-8.82 (m, 2H), 8.54-8.51 (m, 2H), 8.39-8.34 (m, 1H), 8.12-8.04 (m, 3H), 8.01-7.90 (m, 2H), 7.84-7.82 (d, J = 7.5 Hz, 1H), 7.71-7.68 (d, J = 7.5 Hz, 1H), 5.04-4.93 (m, 2H), 4.70-4.48 (m, 2H), 3.01-2.95 (m, 2H). Mp >260 °C. Appendix figure A.22.

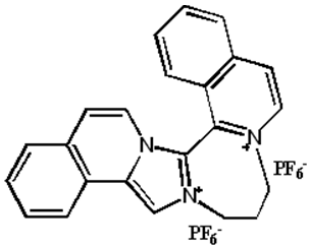

Figure 5.12 Structure of $[IQC_3](PF_6)_2$

5.2.3.3 Synthesis of $[IQC_3]Cl_2$: $[IQC_3]Cl_2$ was prepared by using anion exchange column (yield 45.3%). Mp >260 °C.

5.3.4 Synthesis of $[Ru(bpy)_2IQ](PF_6)_2$ and $[Ru(bpy)_2IQ]Cl_2$[64]

5.3.4.1 Synthesis of $[Ru(bpy)_2IQ](PF_6)_2$

A mixture of 50 mg of $Ru(bpy)_2Cl_2$ (1.0 eq, 0.103 mmol) and 33.5 mg of IQ (1.1 eq, 0.113 mmol) was refluxed at 85°C in a 3:1 mixture of 95% ethanol and water for 20 hours, protected by argon and aluminum foil. The crude product was taken up in 5 mL MilliQ water and washed with dichloromethane three times. four equivalents of NH_4PF_6 were added to the aqueous solution and the precipitate was filtered and dried under high vacuum (94%). ^{1}**H** (500 MHz; CD_3CN) δ: 8.54-8.44 (m, 4H), 8.38 (d, J = 7.5 Hz, 1H), 8.34 (d, J = 8.0 Hz, 1H), 8.13-8.04 (m, 4H), 8.00-7.88 (m, 6H), 7.82-7.80 (m, 3H), 7.72-7.66 (m, 4H), 7.54-7.53 (d, J = 6.0 Hz, 1H), 7.43-7.41 (m, 2H), 7.34 (d, J = 7.5 Hz, 1H), 7.31-7.26 (m, 2H). Mp 227-232°C, ESI-MS *m/z found*(M^{2+}:711.2) 354.2 calcd: 355.6; Appendix figure A.25, A.26.

Figure 5.13 Structure of $[Ru(bpy)_2IQ](PF_6)_2$

5.3.4.2 Synthesis of $[Ru(bpy)_2IQ]Cl_2$: $[Ru(bpy)_2IQ]Cl_2$ was prepared by using an anion exchange column (yield 44.6%). Mp 176-190 °C.

5.4 Attempts at resolving enantiomers

5.4.1 Synthesis of $[Ru(bpy)_2(pyridine)_2]Cl_2$[69]

A mixture of 200 mg of $Ru(bpy)_2Cl_2$ (0.413 mmol, 1.0 eq) and 2.3 mL of pyridine (0.45 mol, 1000 eq) was refluxed at 105 ^oC in 4.6 mL of H_2O for four hours protected by argon and aluminum foil. The mixture was filtered while hot to remove an insoluble impurity. The aqueous layer was distilled to remove an extra pyridine. The residue was dissolved in methanol and precipitated by the addition of diethylether (yield = 91.8%) NMR: ^{1}**H** (300 MHz; D_2O) δ: 9.03 (d, J = 5.1 Hz, 2H), 8.42 (d, J = 5.4 Hz, 4H), 8.38 (d, J = 5.1 Hz, 2H), 8.30 (d, J = 8.4 Hz, 2H), 8.12 (t, J = 5.1 Hz, 2H), 8.00 (d, J = 5.4 Hz, 2H), 7.90 (t, J = 7.8 Hz, 2H), 7.85 (t, J = 7.5 Hz, 2H), 7.75 (t, J = 6.6 Hz, 2H).

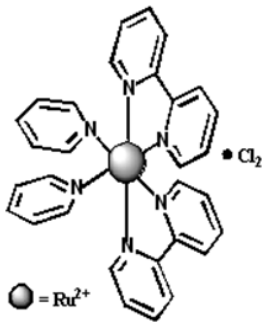

Figure 5.14 Structure of $[Ru(bpy)_2(pyridine)_2]Cl_2$

5.4.2 Chiral crystallization of Δ-$Ru(bpy)_2(pyridine)_2Cl_2$•O,O'-dibenzoyl-D-tartrate and Λ-$Ru(bpy)_2(pyridine)_2Cl_2$•O,O'-dibenzoyl-L-tartrate

In order to prepare Δ-$Ru(bpy)_2(pyridine)_2Cl_2$•O,O'-dibenzoyl-D-tartrate, O,O'-dibenzoyl-D-tartrate was prepared first. 94 mg of O,O'-dibenzoyl-D-tartaric acid (0.25 mmol, 3.21 eq) were suspended in 0.41 mL of MillQ water. 24.7 mg of NaOH were dissolved in 0.088 mL of MilliQ water, and the suspension was converted to a clear solution after introducing the NaOH solution slowly to it until the pH of the solution was set to pH 9. The solution was stirred for 2 hours and the pH changed to 6.5, and another half drop of the NaOH solution was added to get the pH back to 9. In another small vial, 50 mg of $[Ru(bpy)_2(pyridine)_2]Cl_2$ (0.078 mmol, 1.0 eq) were

dissolved in 1 mL of MilliQ water (using ultrasound for 1 minute) and filtered to get a deep red solution. The O,O'-dibenzoyl-D-tartrate solution was added to this vial carefully. The vial was covered with aluminum foil and let it evaporate slowly in a ventilated cabinet. two months later, no crystals were formed. Same result was obtained for Λ-$Ru(bpy)_2(pyridine)_2Cl_2$•O,O'-dibenzoyl-L-tartrate.

References:

(1) Lander, E. S.; Linton, L. M.; Birren, B.; Nusbaum, C.; Zody, M. C.; Baldwin. J.; Devon, K.; Dewar, K.; Doyle, M.; FitzHugh, W.; Funke, R.; Gage, D.; Harris, K.; Heaford, A.; Howland, J.; Kann, L.; Lehoczky, J.; LeVine, R.; McEwan, P.; McKernan, K.; Meldrim, J.; Mesirov, J.P.; Miranda, C.; Morris, W.; Naylor, J.; Raymond, C.; Rosetti, M.; Santos, R.; Sheridan, A.; Sougnez, C.; Stange-Thomann, N.; Stojanovic, N.; Subramanian, A.; Wyman, D.; Rogers, J.; Sulston, J.; Ainscough, R.; Beck, S.; Bentley, D.; Burton , J.; Clee, C.; Carter, N.; Coulson, A.; Deadman, R.; Deloukas, P.; Dunham ,A.; Dunham, I.; Durbin, R.; French, L.; Grafham, D.; Gregory, S.; Hubbard, T.; Humphray, S.; Hunt, A.; Jones, M.; Lloyd, C.; McMurray, A.; Matthews, L.; Mercer, S.; Milne, S.; Mullikin, J. C.; Mungall, A.; Plumb, R.; Ross, M.;Shownkeen, R.; Sims, S.; Waterston, R.H.; Wilson, R. K.; Hillier, L. W.; McPherson, J. D.; Marra, M. A.; Mardis, E. R.; Fulton, L. A.; Chinwalla, A. T.; Pepin, K. H.; Gish, W. R.; Chissoe, S. L.; Wendl, M. C.; Delehaunty, K. D.; Miner, T. L.; Delehaunty, A.; Kramer, J. B.; Cook, L.L.; Fulton, R. S.; Johnson, D. L.; Minx, P. J.; Clifton, S. W.; Hawkins, T.; Branscomb, E.; Predki, P.; Richardson, P.; Wenning, S.; Slezak, T.; Doggett, N.; Cheng, J. F.; Olsen, A.; Lucas, S.; Elkin, C.; Uberbacher, E.; Frazier, M.; Gibbs, R. A.; Muzny, D. M.; Scherer, S. E.; Bouck, J. B.; Sodergren, E. J.; Worley, K. C.; Rives, C. M.; Gorrell, J. H.; Metzker, M, L.; Naylor, S. L.; Kucherlapati, R. S.; Nelson, D. L.; Weinstock, G. M.; Sakaki, Y.; Fujiyama, A.; Hattori, M.; Yada, T.; Toyoda, A.; Itoh, T.; Kawagoe, C.; Watanabe, H.; Totoki, Y.; Taylor, T.; Weissenbach, J.; Heilig, R.; Saurin, W.; Artiguenave, F.; Brottier, P.; Bruls, T.; Pelletier, E.; Robert, C.; Wincker, P.; Smith, D. R.; Doucette-Stamm, L.; Rubenfield, M.; Weinstock, K.; Lee, H. M.; Dubois, J.; Rosenthal, A.; Platzer, M.; Nyakatura, G.; Taudien, S.; Rump, A.; Yang, H.; Yu, J.; Wang, J.; Huang, G.; Gu, J.; Hood, L.; Rowen, L.; Madan, A.; Qin, S.; Davis, R. W.; Federspiel,

N. A.; Abola, A. P.; Proctor, M. J.; Myers, R. M.; Schmutz, J.; Dickson, M.; Grimwood, J.; Cox, D. R.; Olson, M. V.; Kaul, R.; Raymond, C.; Shimizu, N.; Kawasaki, K.; Minoshima, S.; Evans, G. A.; Athanasiou, M.; Schultz, R.; Roe, B. A.; Chen, F.; Pan, H.; Ramser, J.; Lehrach, H.; Reinhardt, R.; McCombie, W. R.; de la Bastide, M.; Dedhia, N.; Blöcker, H.; Hornischer, K.; Nordsiek, G.; Agarwala, R.; Aravind, L.; Bailey, J. A.; Bateman, A.; Batzoglou, S.; Birney, E.; Bork, P.; Brown, D. G.; Burge, C. B.; Cerutti, L.; Chen, H. C.; Church, D.; Clamp, M.; Copley, R. R.; Doerks, T.; Eddy, S. R.; Eichler, E. E.; Furey, T. S.; Galagan, J.; Gilbert, J. G.; Harmon, C.; Hayashizaki, Y.; Haussler, D.; Hermjakob, H.; Hokamp, K.; Jang, W.; Johnson, L. S.; Jones, T. A.; Kasif, S.; Kaspryzk, A.; Kennedy, S.; Kent, W. J.; Kitts, P.; Koonin, E. V.; Korf, I.; Kulp, D.; Lancet, D.; Lowe, T. M.; McLysaght, A.; Mikkelsen, T.; Moran, J. V.; Mulder, N.; Pollara, V. J.; Ponting, C. P.; Schuler, G.; Schultz, J.; Slater, G.; Smit, A. F.; Stupka, E.; Szustakowski, J.; Thierry-Mieg, D.; Thierry-Mieg, J.; Wagner, L.; Wallis, J.; Wheeler, R.; Williams, A.; Wolf, Y. I.; Wolfe, K. H.; Yang, S. P.; Yeh, R. F.; Collins, F.; Guyer, M. S.; Peterson, J.; Felsenfeld, A.; Wetterstrand, K. A.; Patrinos, A.; Morgan, M. J.; de Jong, P.; Catanese, J. J.; Osoegawa, K.; Shizuya, H.; Choi, S.; Chen, Y. J. *Nature*. **2001***, 409*, 860-92.

(2) Boer, D.R.; Canals, A.; Coll, M. *Dalton Transactions*. **2009**, *3,* 399-414.

(3) Wheate, N. J.; Brodie, C. R., Collins, J. G.; Kemp, S.; Janice, R.; Wright, A. *Mini-Reviews in Medicinal Chemistry*. **2007**, *7*, 627-648.

(4) Lauria, Antonino.; Montalbano, A.; Barraja, P.; Dattolo, G.; Almerico, A. M. *Current Medicinal Chemistry.* **2007**, *14*, 2136-2160.

(5) Ihmels, H. Otto, D. *Topics in Current Chemistry*. **2005**, *258*, 161-204

(6) Alberts, B.; Johnson, A.; Lewis, J.; Raff, M.; Roberts, K.; Walter, P. *Molecular Biology of the Cell-Fourth Edition*, Garland Science, New York, US, **2002**.

(7) Lerman, L.S. *Journal of Molecular Biology.* **1961**, *3*, 18-30.

(8) Chu Y.; Sorey S.; Hoffman, D.W.; Iverson, B. L. *Journal of the American Chemical Society.* **2007**, *129*, 1304-1311.

(9) Wang, A. H.; Gao, Y. G.; Liaw, Y. C.; Li, Y. K. *Biochemistry.* **1991**, *30*, 3812-3815.

(10) Frederick, C. A.; Williams, L. D.; Ughetto, G.; van der Marel, G. A.; van Boom, J. H.; Rich, A.; Wang, A. H.J. *Biochemistry.* **1990**, *29*, 2538-2549.

(11) Momparler, R. L.; Karon, M.; Siegel, S. E.; Avila, F. *Cancer Research*. **1976**, *36*, 2891-2895.

(12) Fornari, F. A.; Randolph, J. K.; Yalowich, J. C.; Ritke, M. K. *Molecular Pharmacology*. **1994**, *45*, 649-656.

(13) Mazerski, J.; Martelli, S.; Borowski, E. *Acta Biochimica Polonica.* **1998,** *45*, 1-11.

(14) Erkkila, K. E.; Odom, D. T.; Barton, J. K. *Chemical Reviews.* **1999**, *99*, 2777-2795.

(15) Zeglis, B. M.; Barton, J. K. *Journal of the American Chemical Society.* **2006**, 128, 5654-2655.

(16) Sastri, C. V. *Physical Sciences.* **2004**, *70*, 355-365.

(17) Jamieson, E. R.; Lippard, S. J. *Chemical Reviews*. **1999**, *99*, 2467-2498.

(18) Howe-Grant, M.; Lippard, S.J. *Biochemistry,* **1979**, *18*, 5762-5769.

(19) Biver, T.; Secco, F.; Venturini, M. *Coordination Chemistry Reviews*. **2008**, *252*, 1163-1177.

(20) Friedman, A. E.; Chambron, J. C.; Sauvage, J.-P.; Turro, N. J.; Barton, J. K. *Journal of the American Chemical Society.* **1990**, *112*, 4960-4962.

(21) Coates, C. G.; McGarvey, J. J.; Callaghan, P. L.; Coletti, M.; Hamilton, J. G. *The Journal of Physical Chemistry B.* **2001**, *105*, 730 −735.

(22) Zeglis, B. V.; Pierre, V. C.; Barton, J. K.; *Chemical Communications.* **2007**, *44,* 4565-4579.

(23) Palchaudhuri, R.; Hergenrother, P. J. *Current Opinion in Biotechnology.* **2007**, *18*, 497-503.

(24) Herzyk, P.; Neidle, S.; Goodfellow, J.M. *Journal of Biomolecular Structure and Dynamics.* **1992**, *10*, 97-139.

(25) Rao, S.N.; Kollman, P.A. *Proc. Proceedings of the National Academy of Sciences. USA,* **1987**, *84*, 5735-5739.

(26) Brenno, A. D. N.; Alexandre, A. M. Lapis. *Molecules.* **2009***, 14,* 1725-1746.

(27) Choi, C.S.; Mishra, L.; Mutai, T.; Araki, K. *Bulletin of the Chemical Society of Japan.* **2000***, 73*, 2051-2058.

(28) Gao, F.; Chao, H.; Ji, L. *Chemistry & Biodiversity.* **2008**, *5*, 1962-1979.

(29)Coates, C. G.; Coletti, M.; Hamilton, J.; McGarvey, J. J. *Central Laser Facility Annual Report.* **1999/2000**, 113-115.

(30) Blasius, R.; Moucheron, C.; Kirsch-De, A. M. *European Journal of Inorganic Chemistry.* **2004**, *20,* 3971-3979.

(31) Emiliano, C.; Snyder, J. W.; Ogilby, P. R.; Gothelf, K. V. *ChemBioChem.* **2007**, *8*, 475-481.

(32) Elias, B; Kirsch-De, B. M. *Coordination Chemistry Review.* **2006,** *250*, 1627-1641.

(33) Jovanovic, S. V.; Simic, M. G.; *Biochimica et Biophysica Acta.* **1989,** *1008*, 39-44.

(34) *Kittler*, *L.*; Löber, G.; Gollmick, F.; Berg, H. *Bioelectrochemistry and Bioenergetics.* **1980**, *116*, 503-511.

(35) Herman, L.; Ghosh , S.; Defrancq, E.; Kirsch-De, A. M . *The Journal of Physical Chemistry.***2008**, *21*, 670-681.

(36) Dohm, J. A.; Hsu, M. H.; Hwu, J. R.; Huang, R. C. C.; Moudrianakis, E. N.; Lattman, E.E.; Gittis, A. G. *Journal of Molecular Biology.* **2005**, *349*, 731-744.

(37) Hou, M. H.; Lin,S.B.; Yuann, J. M.; Lin,W. C.; Wang, A. H. J.; Kan, L. S. *Nucleic Acids Research.* **2004**, *32*, 2214-2222.

(38) Keene, F. R.; Smith, J. A.; Collins, J. G. *Coordination Chemistry Reviews.* **2009**, *253*, 2021-2035.

(39) Nicholas, G. N. *Nucleic Acids Research.* **2007**, *35*, 363-370.

(40) Wu, B.; Girard, F.; van Buuren, B.; Schleucher, J.; Tessari, M.; Wijmenga, S. *Nucleic Acids Research*. **2004**, *10*, 3228-3239.

(41) Oleksi, A.; Blanco, A. G.; Boer, R.; Uson, I.; Aymami, J.; Rodger, A.; Hannon, M. J.; Coll, M. *Angewandte Chemie International Edition*. **2006**, *45*, 1227-1231.

(42) Cerasino, L.; Hannon, M. J.; Sletten, E. *Inorganic Chemistry.* **2007**, *46*, 6245-6251.

(43) Dervan, P. B.; Doss, R. M.; Marques, M. A. *Current Medicinal Chemistry - Anti-Cancer Agents.* **2005***, 5,* 373-387.

(44) Dervan, P. B. *Bioorganic & Medicinal Chemistry.* **2001**, *9*, 2215-2235.

(45) Goodman, M. F.; Creighton, S.; Bloom, L. B.; Petruska, J. *Critical Reviews in Biochemistry and Molecular Biology.* **1993**, *28*, 83-126.

(46) Bhattacharyya, A. *Journal of Molecular Biology.* **1989**, *209*, 583-597.

(47) Brown, T. *Aldrichimica Acta.* **1995**, *28*, 15-20.

(48) Hunter, W. N.; Brown, T. *Oxford Handbook of Nucleic Acid Structure*, Oxford University Press, USA, **1999**.

(49) Tikhomirova, Anna.; Beletskaya, I. V.; Chalikian, T. V. *Biochemistry*. **2006**, *45*, 10563-10571.

(50) Brown, T.; Hunter, W. N.; Kneale, G.; Kennard, O. *Proceedings of the National Academy of Sciences*. **1986**, *83*, 2402-2406.

(51) Patel, D. J.; Kozlowski, S. A.; Ikuta, S.; Itakura, K. *Federation proceedings.*. **1984**, *43*, 2663-2670.

(52) Jackson, B. A.; Barton, J. K. *Journal of the American Chemical Society.* **1997**, *119*, 12986-12987.

(53) Jackson, B. A.; Barton, J. K. *Biochemistry.* **2000**, *39,* 6176-6182.

(54) Peng, T.; Dohno, C.; Nakatani, K. *Angewandte Chemie International Edition.* **2006**, *45*, 5623-5625.

(55) Chou, S. Zhu, L.; Reid, B. R. *Journal of Molecular Biology.* **1994**, *244*, 259-268.

(56) Pluta, A. F.; Cooke, C. A.; Earnshaw, W. C. *Trends in Biochemical Sciences.* **1990**, *15*, 181-185.

(57) Dr Anne Petitjean, unpublished data

(58) Phillips, T.; Rajput, C.; Twyman, L.; Haq, I.; Thomas, J. A. *Chemical Communications*. **2005**, *34,* 4327-4329.

(59) Tomazic, A. *Tetrahedron*. **1981**, *37*, 1787-1793.

(60) Giordano, C.; Minisci, F.; Vismara, E.; Levi, S. *The Journal of Organic Chemistry.* **1986**, *51*, 536-537.

(61) Bakzewski, P.; Kieran, M.; Mallon, J.; Street, J. D.; Joule, J. A. *Journal of Chemical Society Perkin Transactions 1*. **1990**, 3193-3198.

(62) Campa, C.; Camps, J.; Font, J.; Demarch, P. *The Journal of Organic Chemistry*. **1987**, *52*, 521-525.

(63) Thummel, R. P.; Lefoulon, F.; Chirayil, S.; Goulle, V. *The Journal of Organic Chemistry*. **1988**, *53*, 4745-4747.

(64) Ioachim, E.; Medlycott, E. A.; Hanan, G. S.; Loiseau, F.; Campagna, S. *Inorganic Chimica Acta*. **2006**. *359*. 766-774.

(65) Synthesized by Dr Petitjean

(66) Canard, G.; Piguet, C. *Inorganic Chemistry*. **2007,** *46*, 3511-3522.

(67) Duliere, E.l; Devillers, M.; Marchand-Brynaert, J. *Organometallics.* **2003**, 22, 804-811

(68) Tyson, D. S.; Henbest, K. B.; Bialecki, J.; Castellano, F. N. *The Journal of Physical Chemistry A*. **2001**, *105*, 8154-8161.

(69) Morgan, O.; Wang, S.; Sung-A, B.; Morgan, R. J.; Baker, D.; Strekas, T. C.; Engel, R. J. *Journal of Chemical Society Dalton Transactions*. **1997**, 3773-3776.

(70) Ashauer, U.; Wolff, C.; Haller, R. *Archiv der Pharmazie*. **1986**, *319***,** 43-52.

(71) Herman, L.; Ghosh, S.; Defrancq, E.; Kirsch-De Mesmaeker, A. *Journal of Physical Organic Chemistry.* 2008, *21,* 670–681.

(72) Bard, A.; Faulkner, L. "Electrochemical Methods, Fundamentals and Applications", Jihn Wiley, **1980**

(73) Bruker AXS Crystal Structure Analysis Package:

Bruker (2000). SHELXTL. Version 6.14. Bruker AXS Inc., Madison, Wisconsin, USA.

Bruker (2005). XPREP. Version 2005/2. Bruker AXS Inc., Madison, Wisconsin, USA.

Bruker (2005). SAINT. Version 7.23A. Bruker AXS Inc., Madison,Wisconsin, USA.

Bruker (2006). APEX2. Version 2.0-2. Bruker AXS Inc., Madison, Wisconsin, USA.

(74) Cromer, D. T.; Waber, J. T. *International Tables for X-ray Crystallography*; Kynoch Press: Birmingham, UK, **1974**, 4, Table 2.2 A

(75) Sluis, P.; Spek, A.L.. *Acta Crystallographica*. **1990**, *46*, 194-201

Appendix

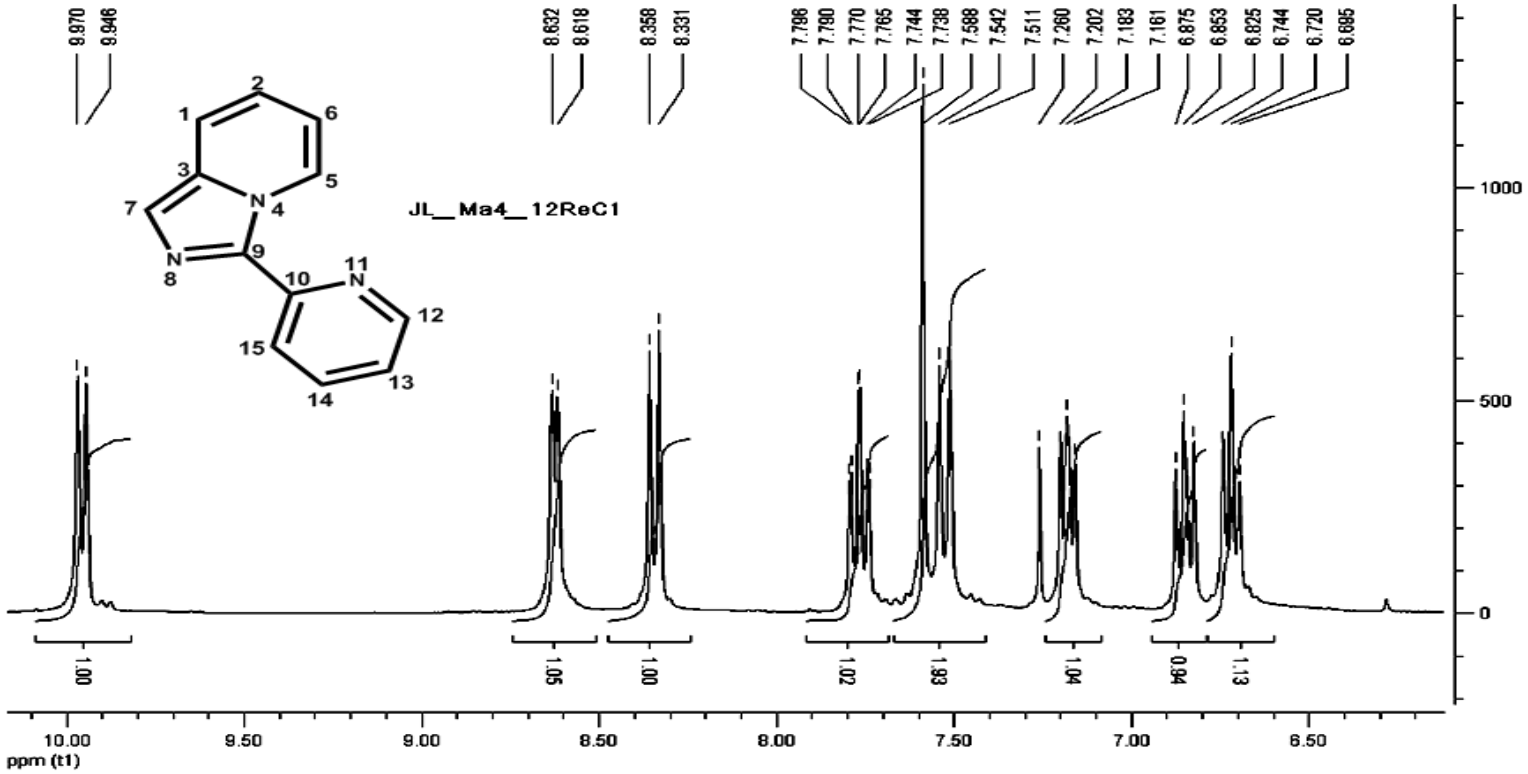

Figure A.1 ^{1}H NMR of P (300Hz, $CDCl_3$)

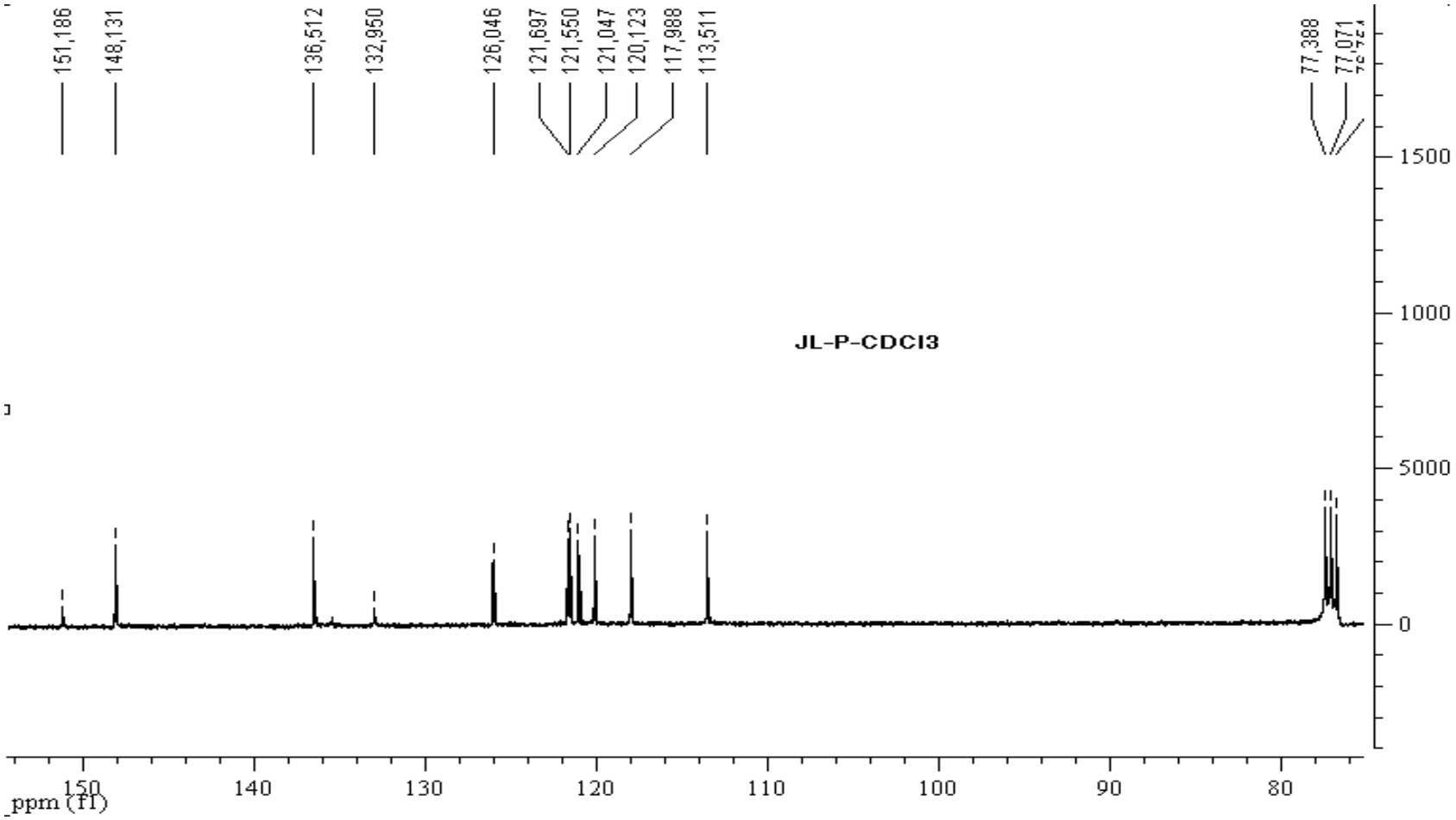

Figure A.2 ^{13}C NMR of P (400Hz, $CDCl_3$)

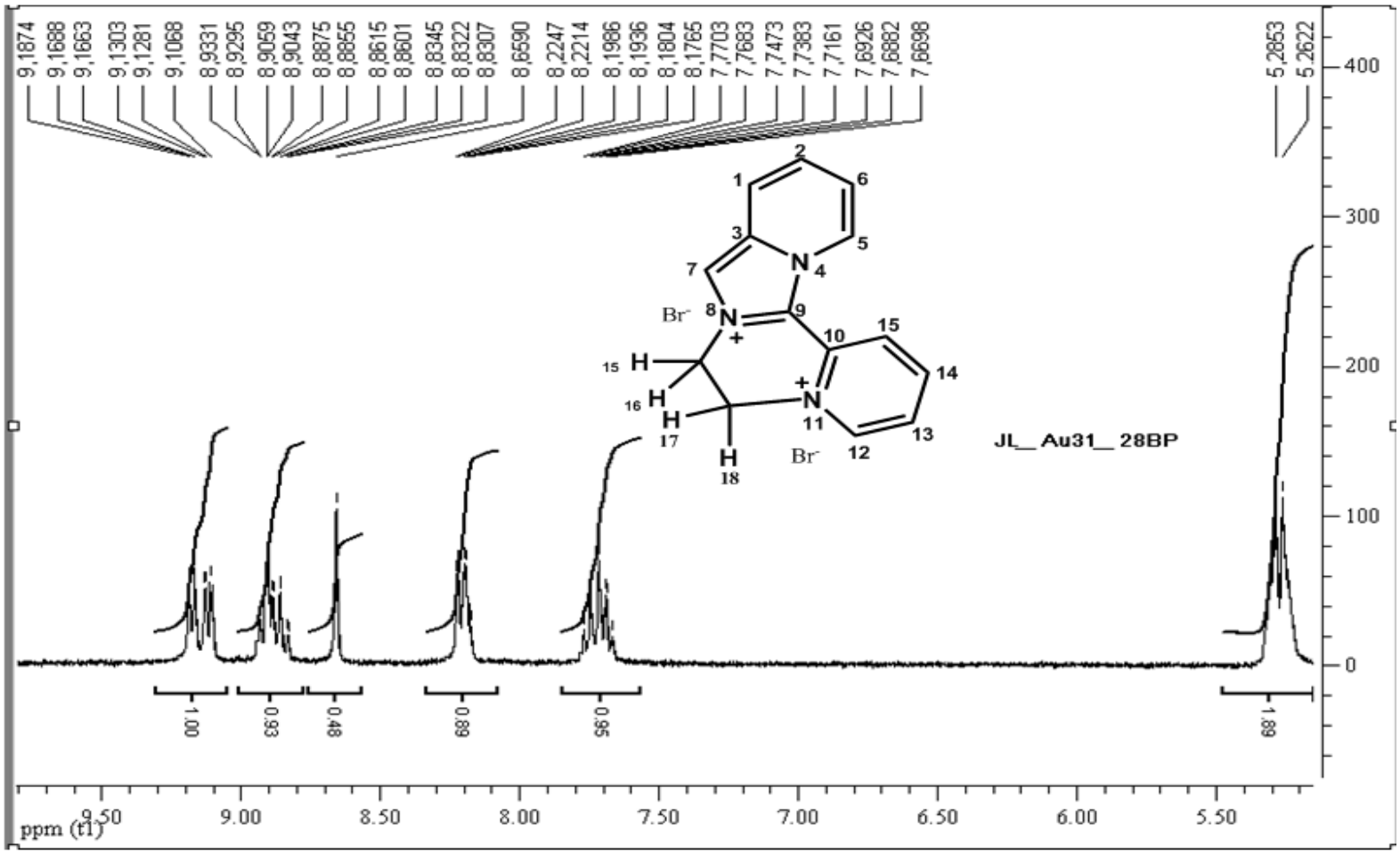

Figure A.3 ^{1}H NMR of $[PC_2]Br_2$ (300Hz, D_2O)

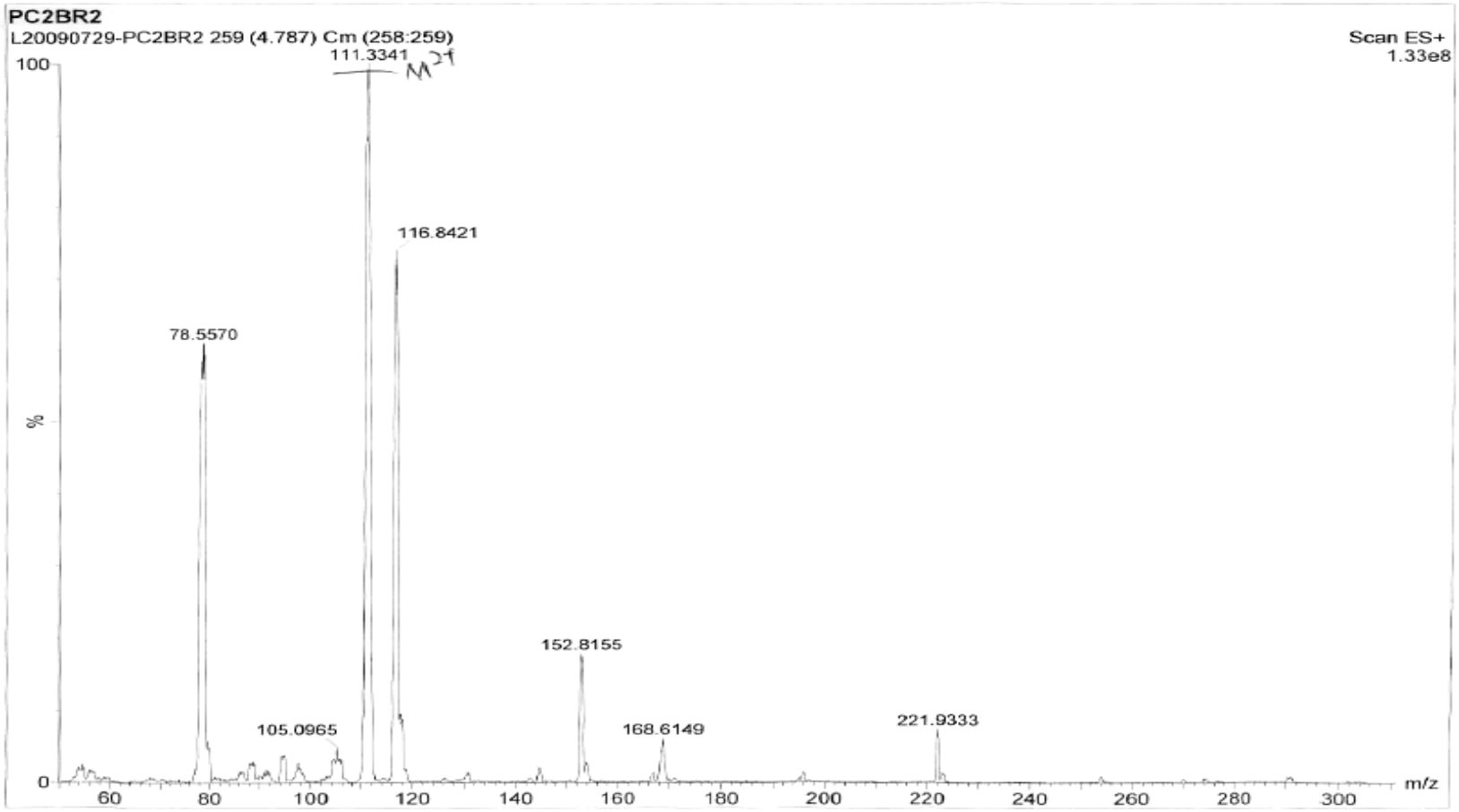

Figure A.4 MS of $[PC_2]Br_2$

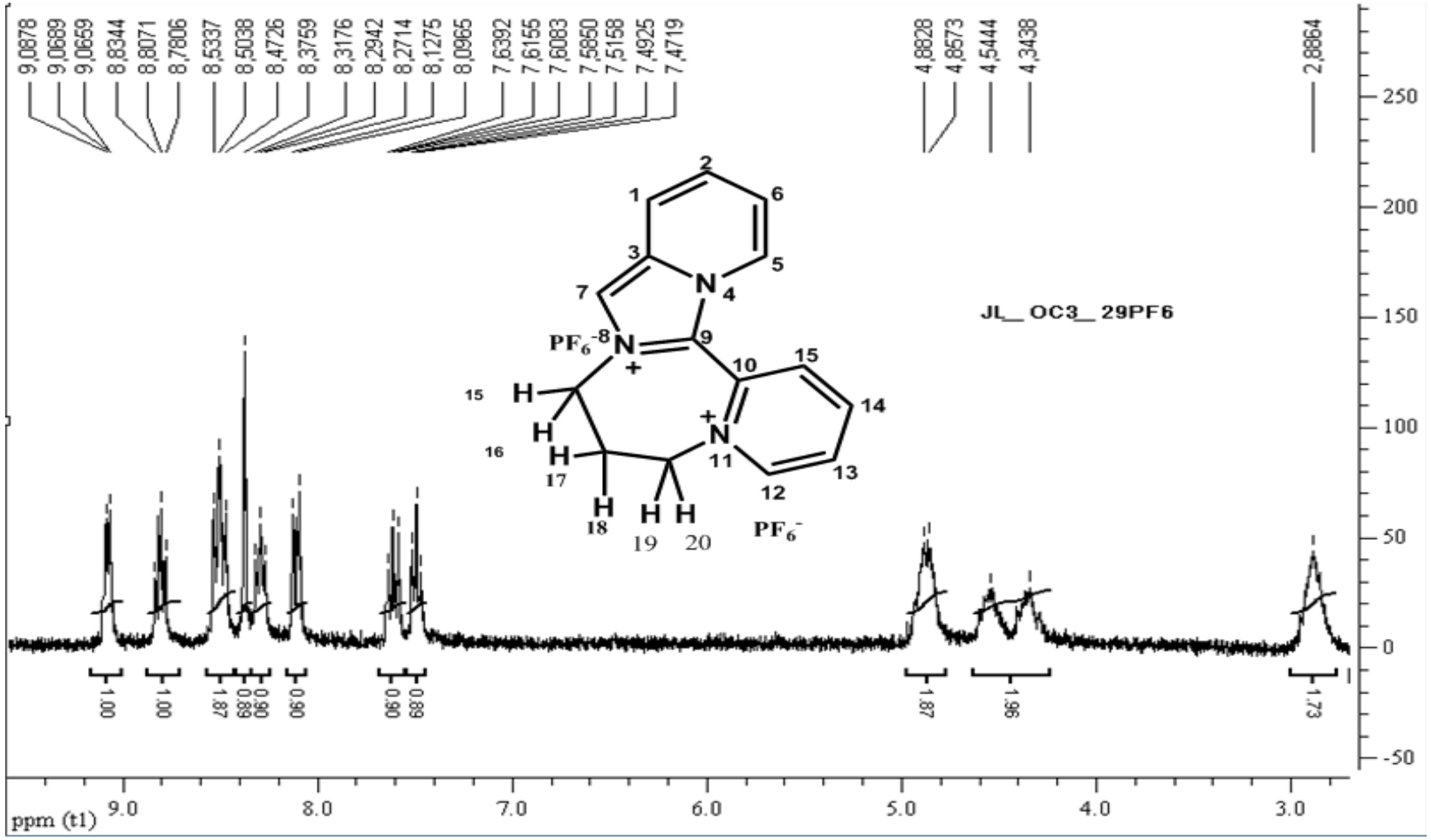

Figure A.5 ^{1}H NMR of $[PC_3]PF_6$ (300Hz, CD_3CN)

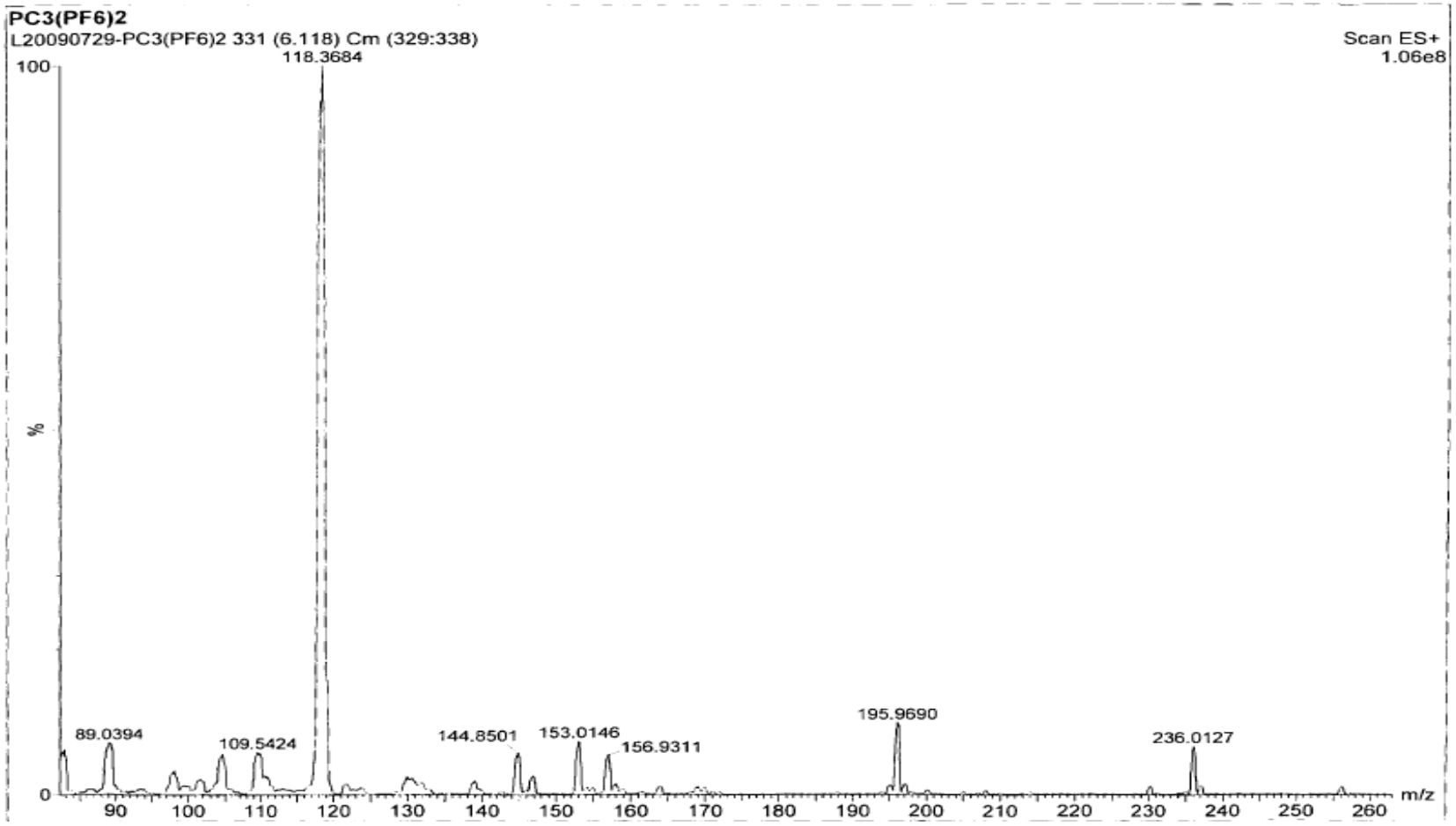

Figure A.6 MS of $[PC_3]PF_6$

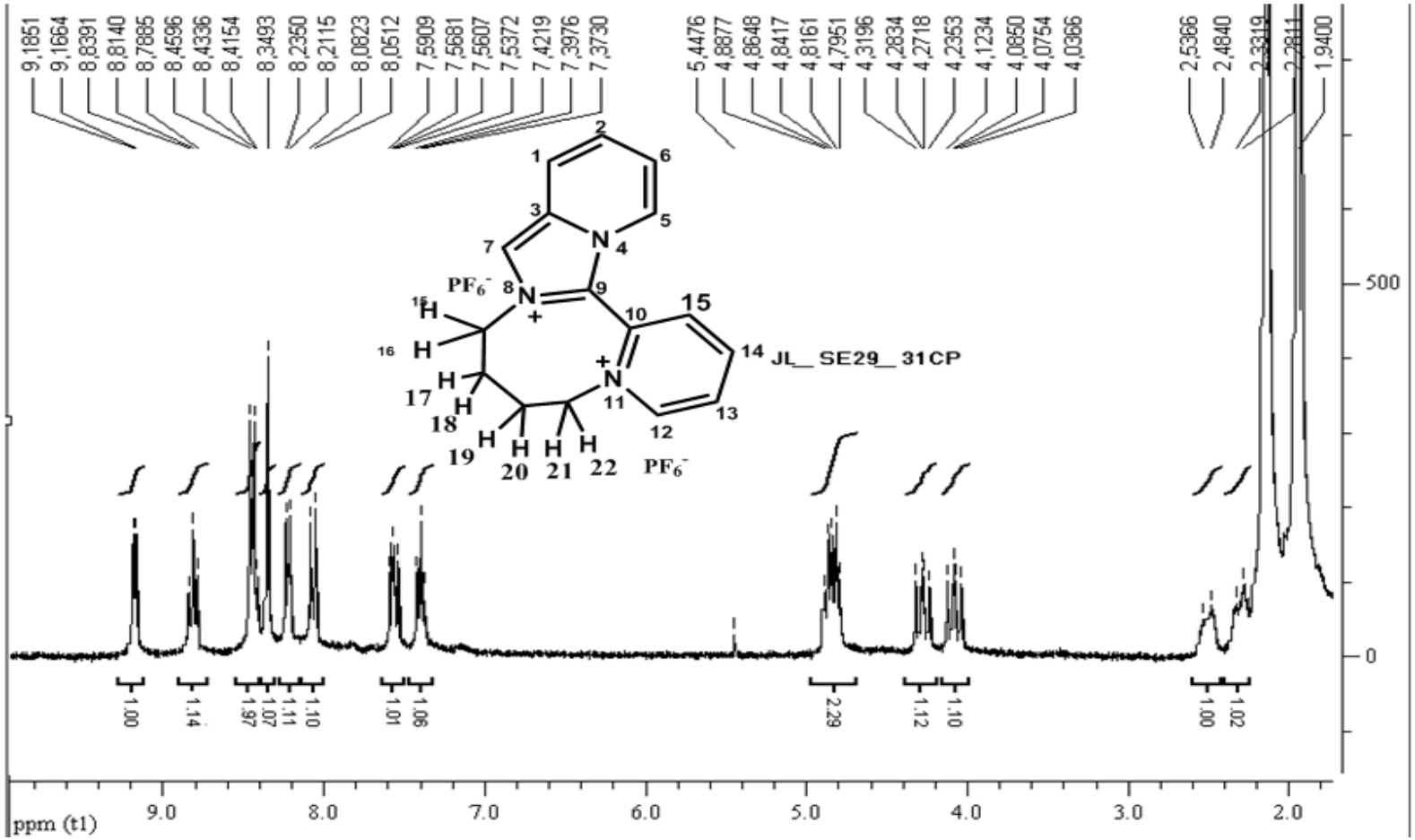

Figure A.7 ^{1}H NMR of $[PC_4]PF_6$ (300Hz, CD_3CN)

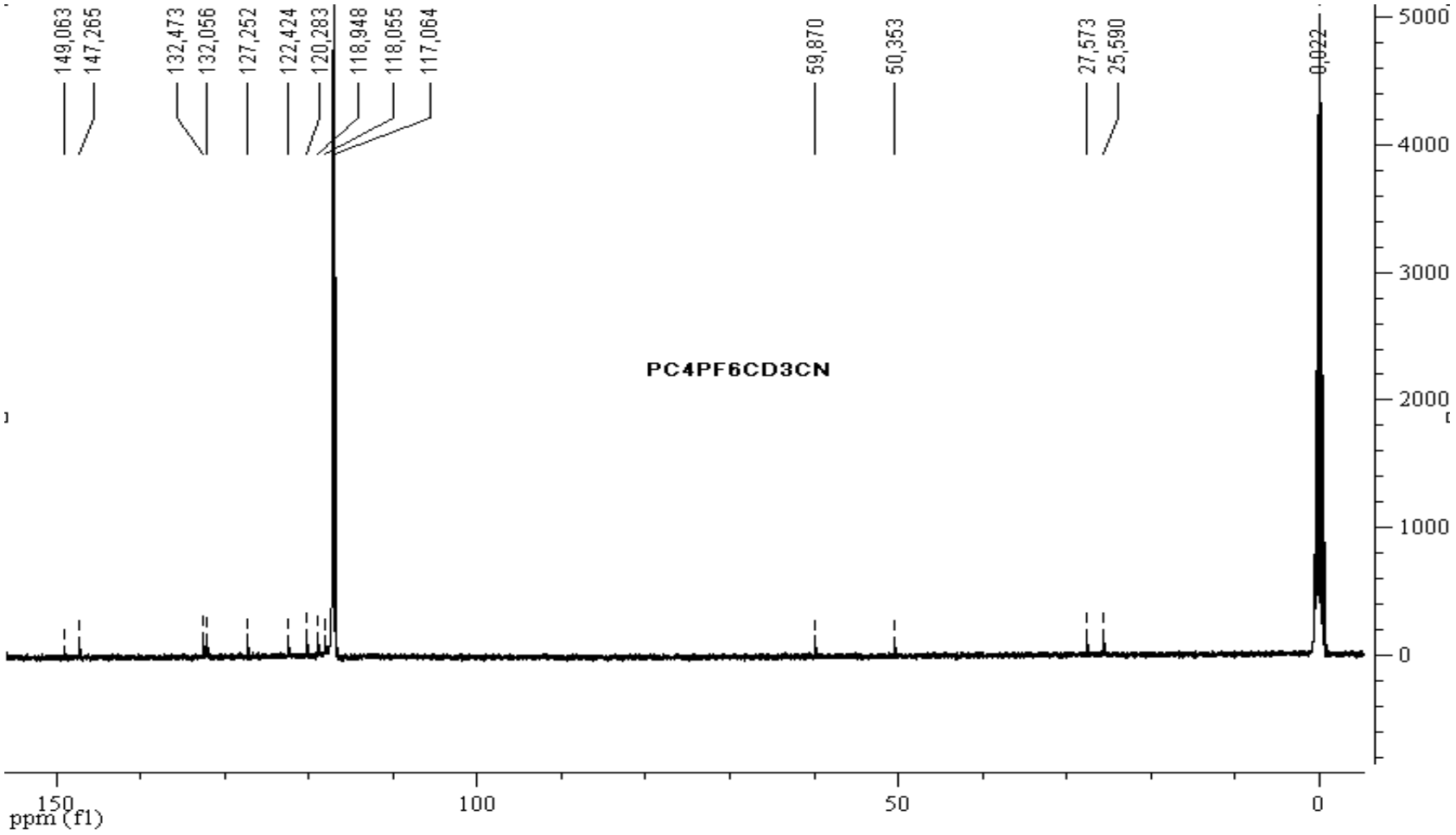

Figure A.8 ^{13}C NMR of $[PC_4]PF_6$ (400Hz, CD_3CN)

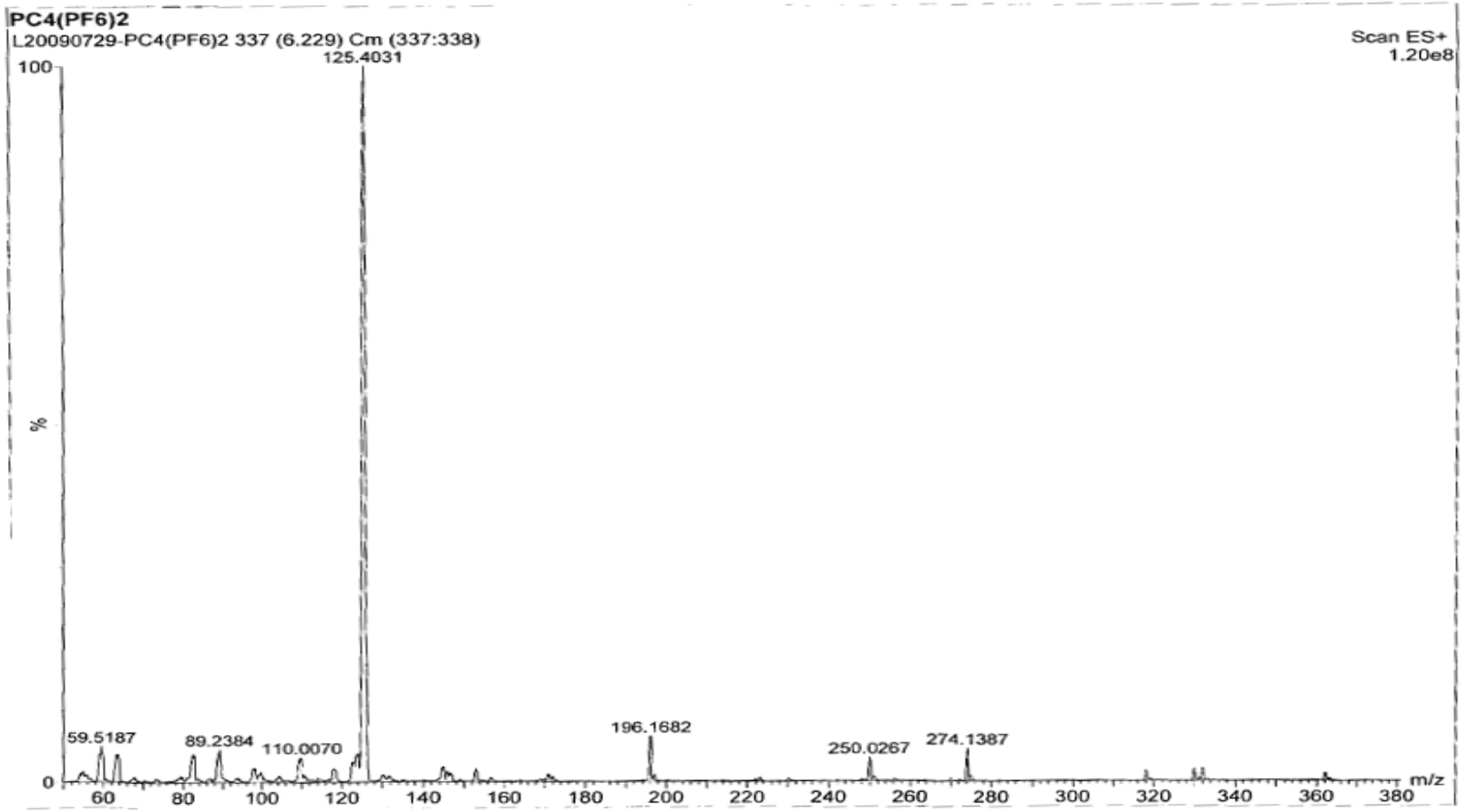

Figure A.9 MS of $[PC_4]PF_6$

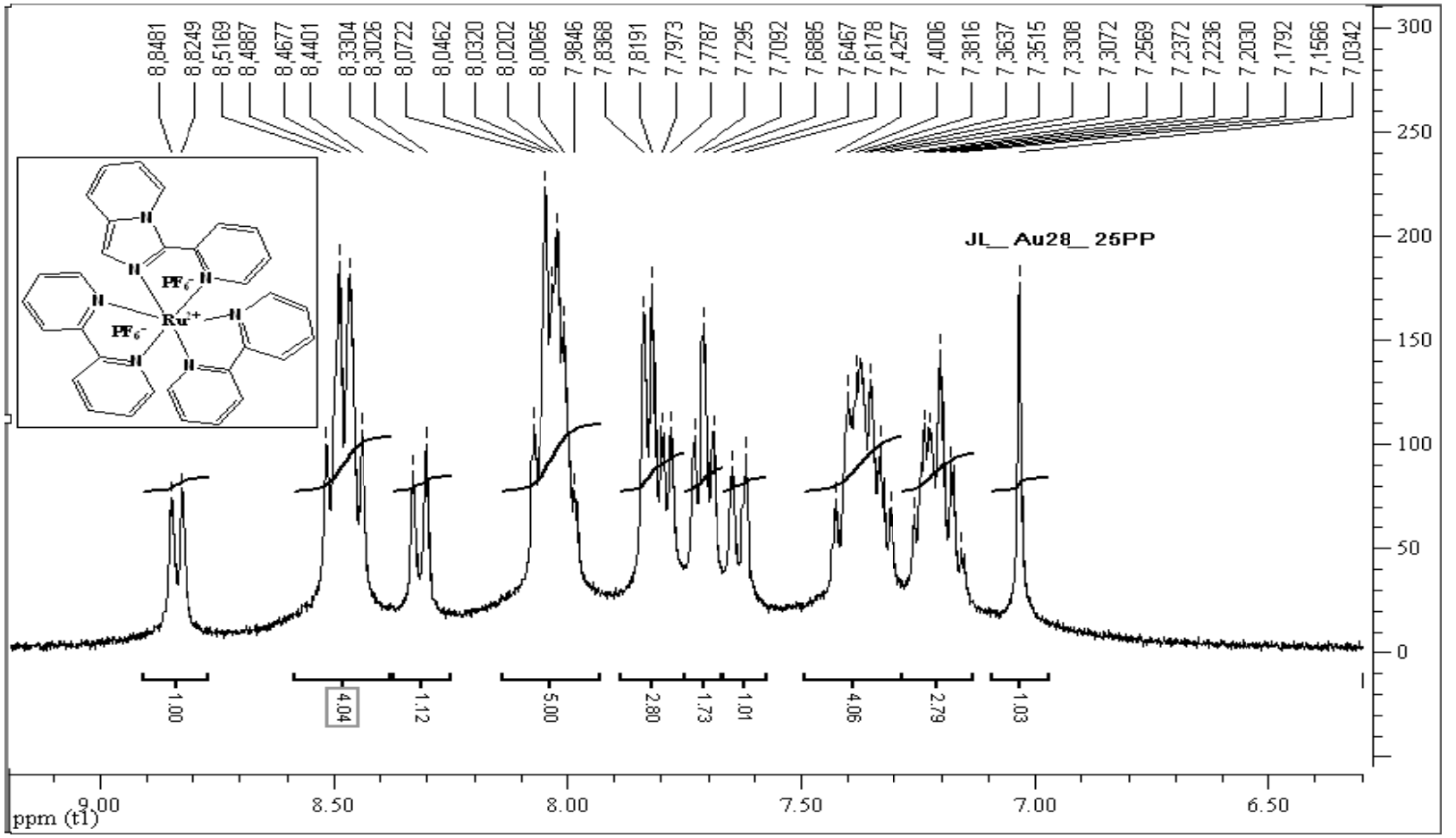

Figure A.10 ^{1}H NMR of $[Ru(bpy)_2P](PF_6)_2$ (300Hz, CD_3CN)

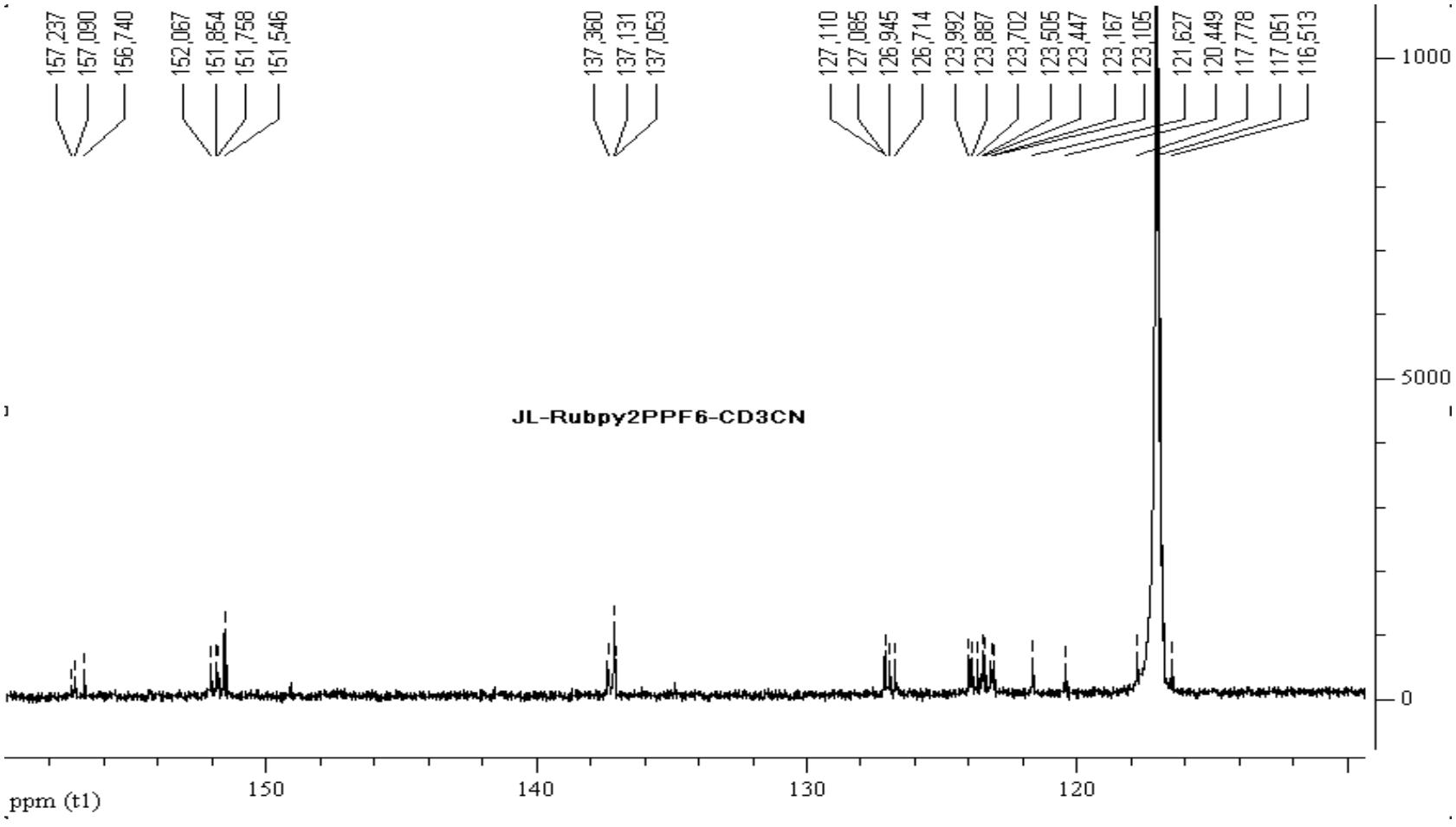

Figure A.11 ^{13}C NMR of $[Ru(bpy)_2P](PF_6)_2$ (400Hz, CD_3CN)

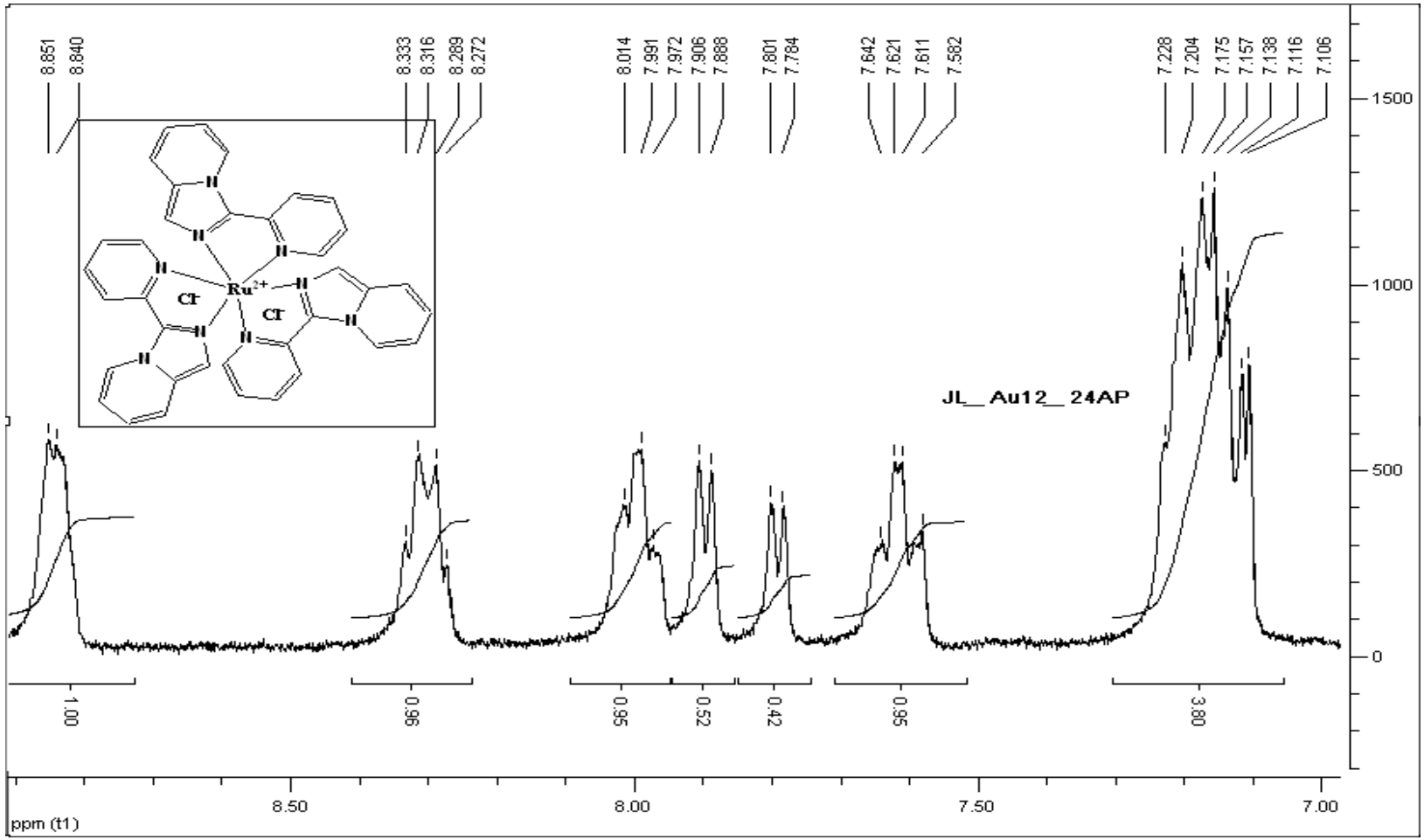

Figure A.12 ^{1}H NMR of $[Ru(P)_3]Cl_2$ (300Hz, D_2O)

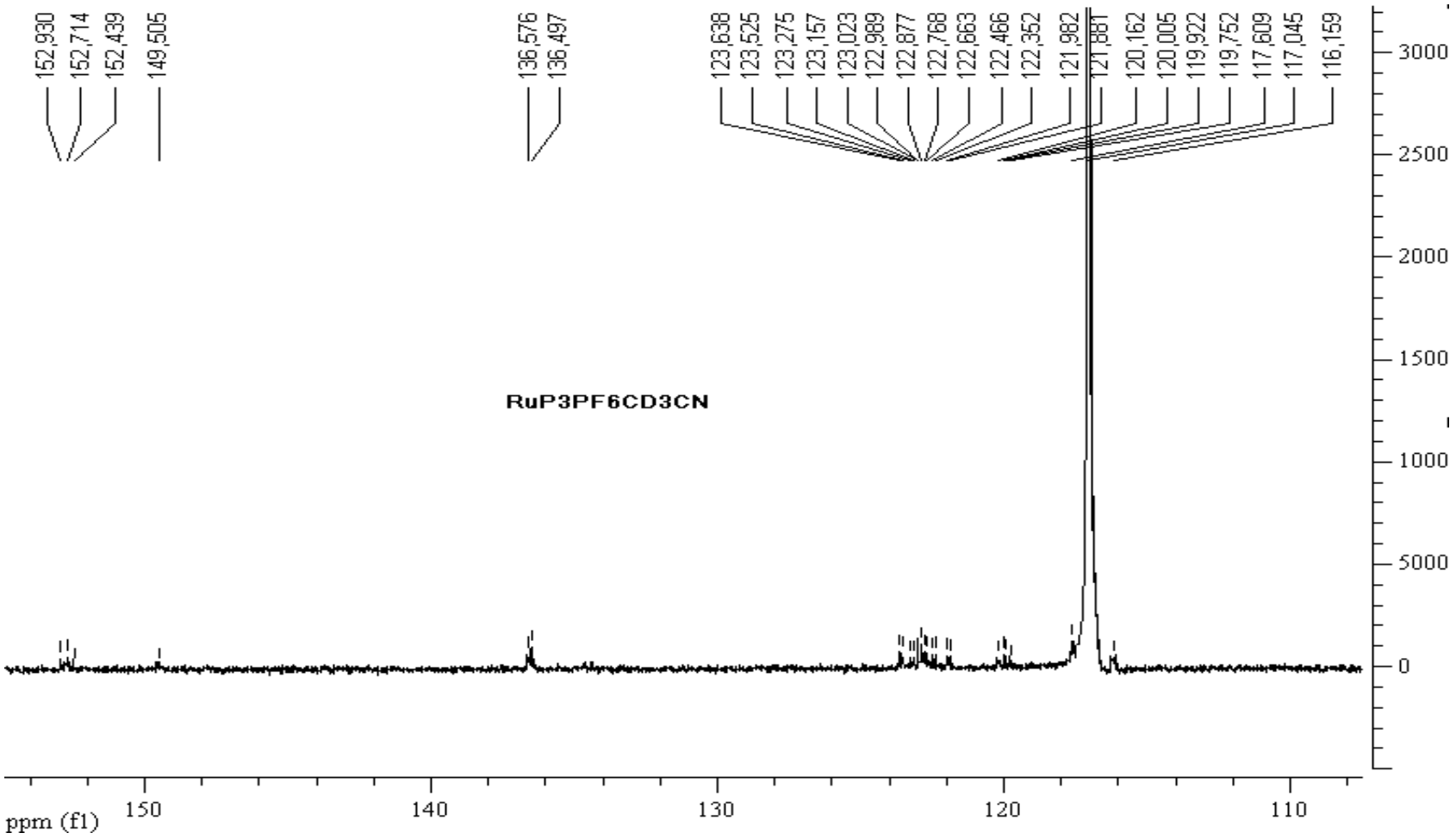

Figure A.13 ^{13}C NMR of $[Ru(P)_3](PF_6)_2$ (400Hz, D_2O)

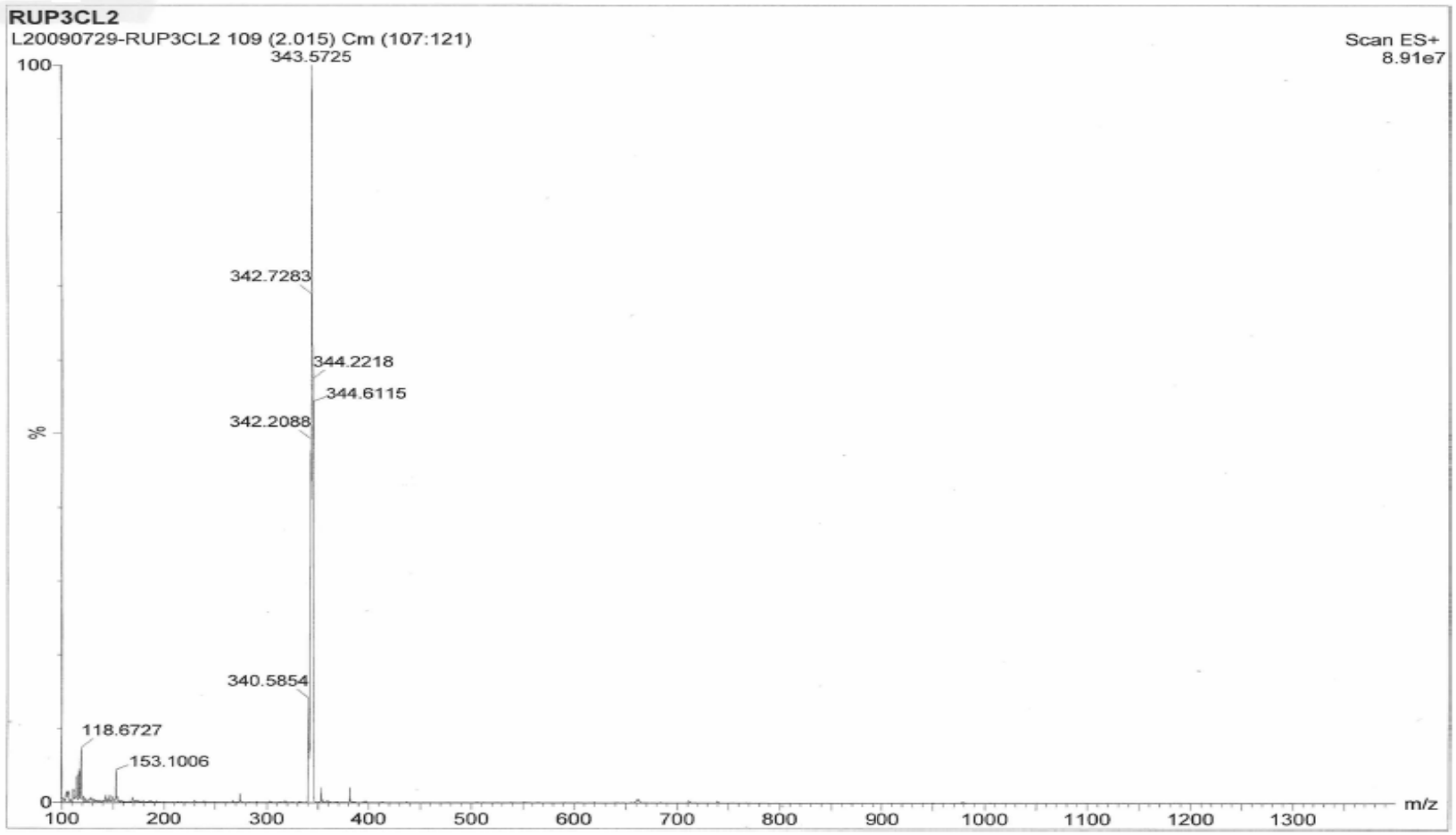

Figure A.14 MS of $[RuP_3]Cl_2$

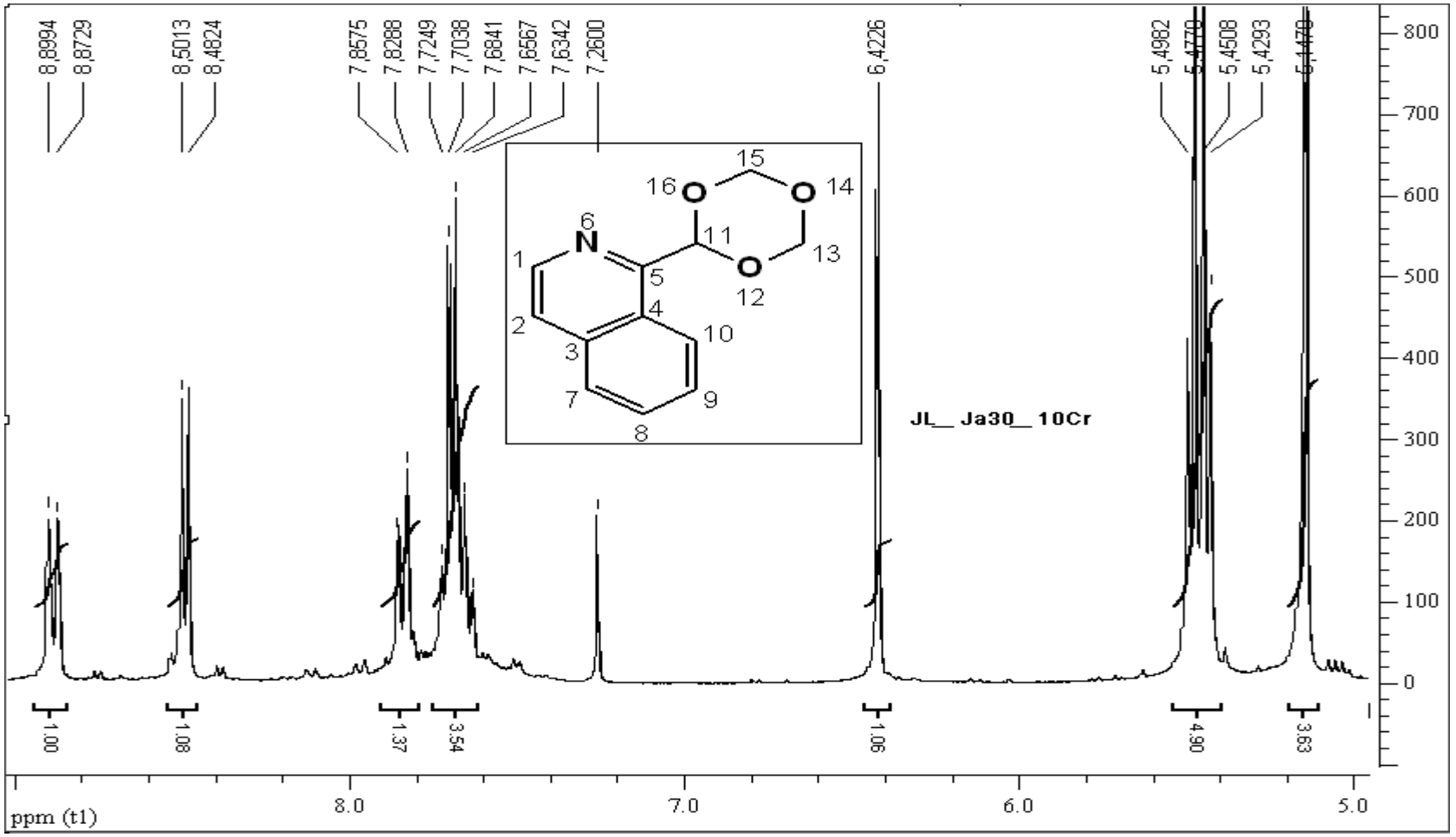

Figure A.15 ^{1}H NMR of 1-(1,3,5-trioxan-2-yl)isoquinoline (300Hz, $CDCl_3$)

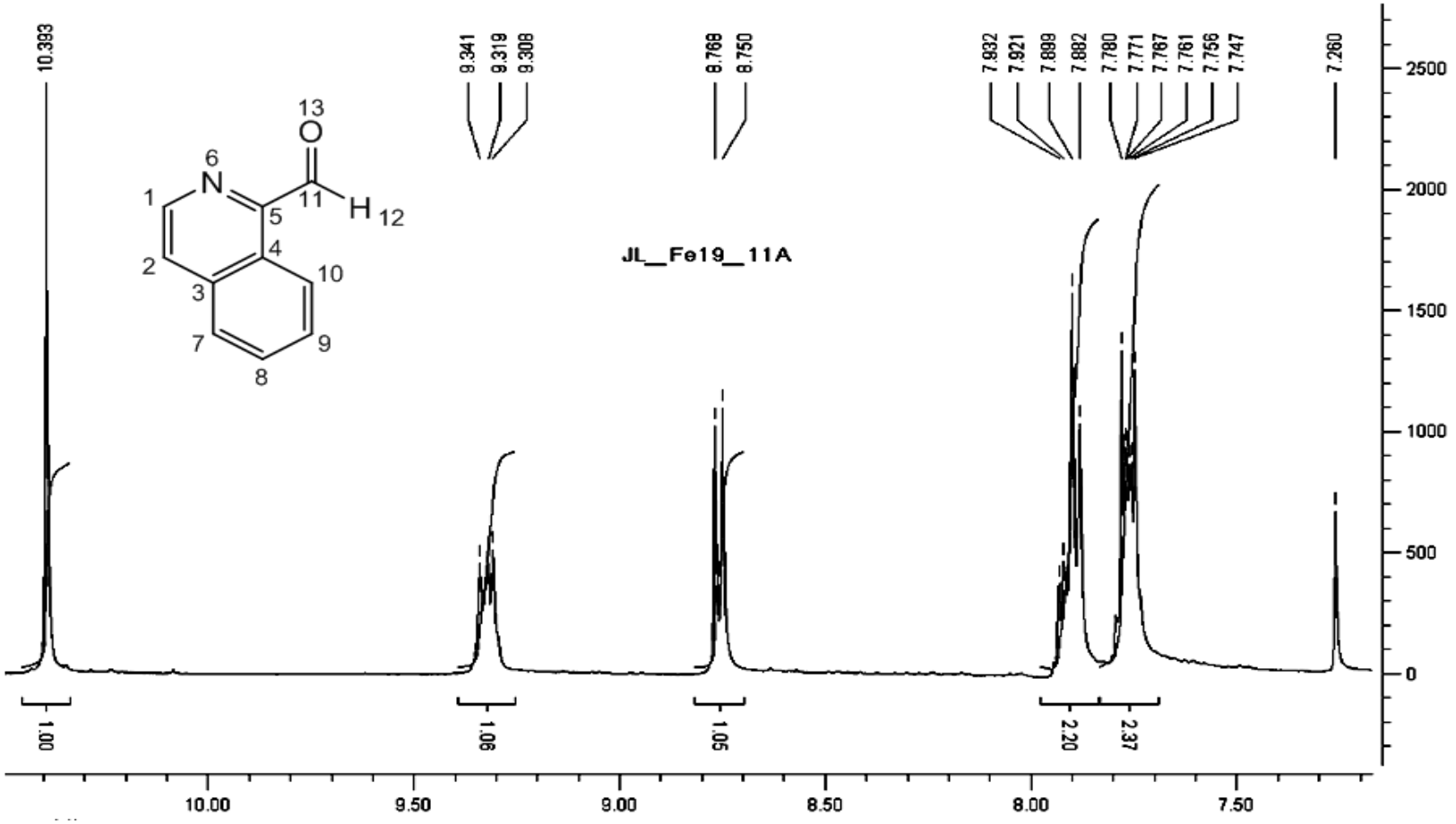

Figure A.16 ^{1}H NMR of isoquinoline-1-carbaldehyde (300Hz, $CDCl_3$)

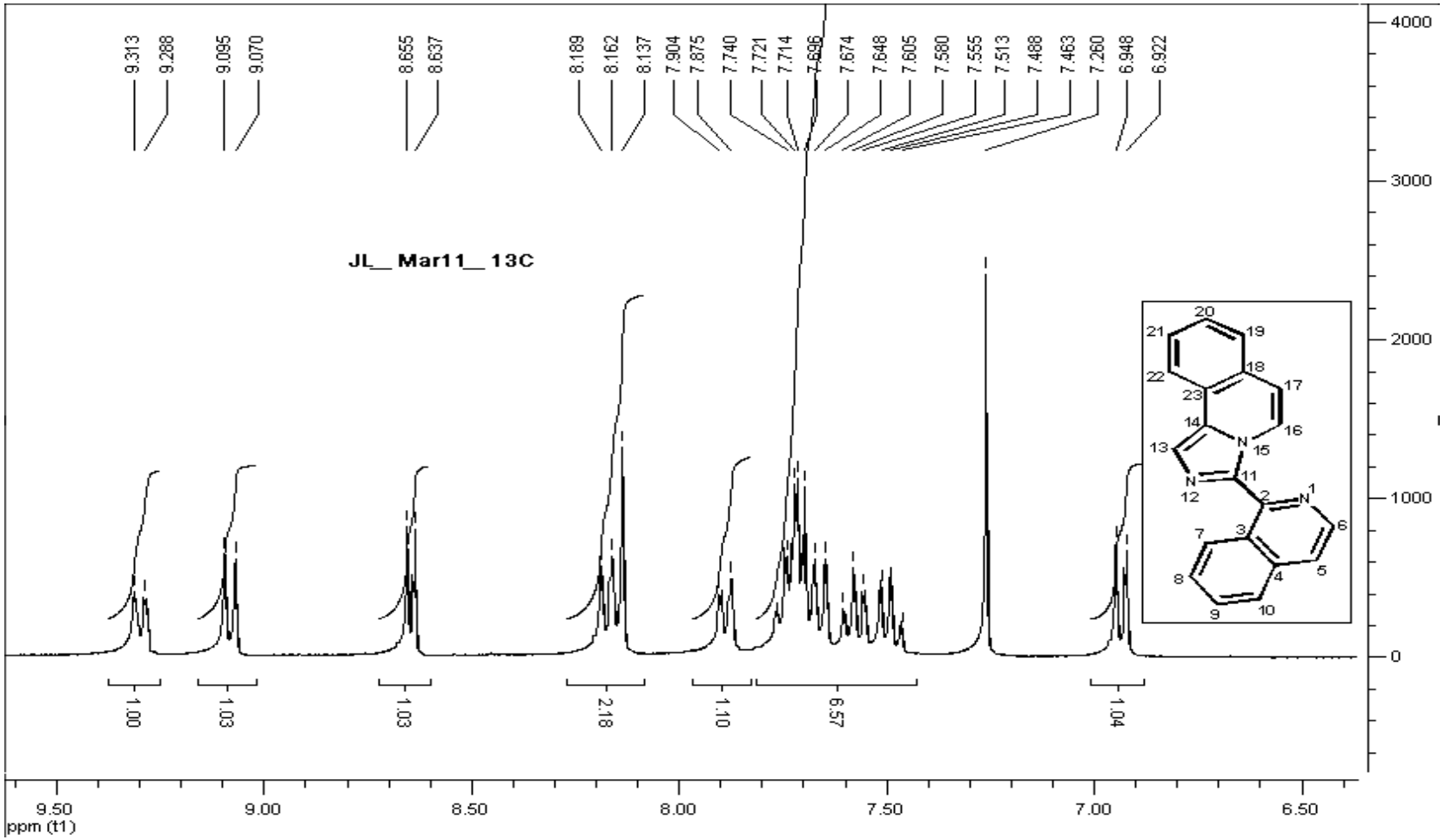

Figure A.17 ^{1}H NMR of IQ (300Hz, $CDCl_3$)

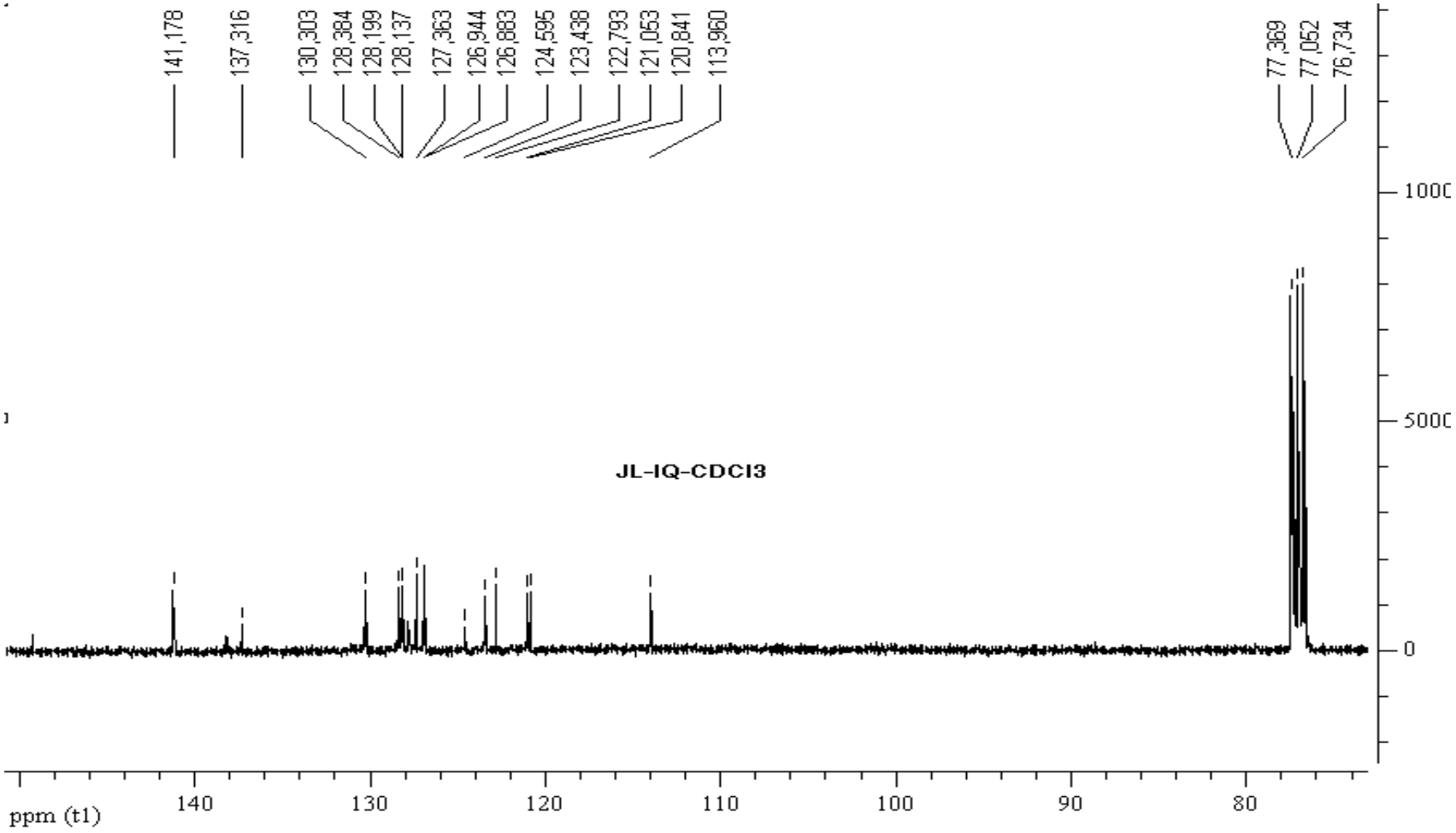

Figure A.18 ^{13}C NMR of IQ (400Hz, $CDCl_3$)

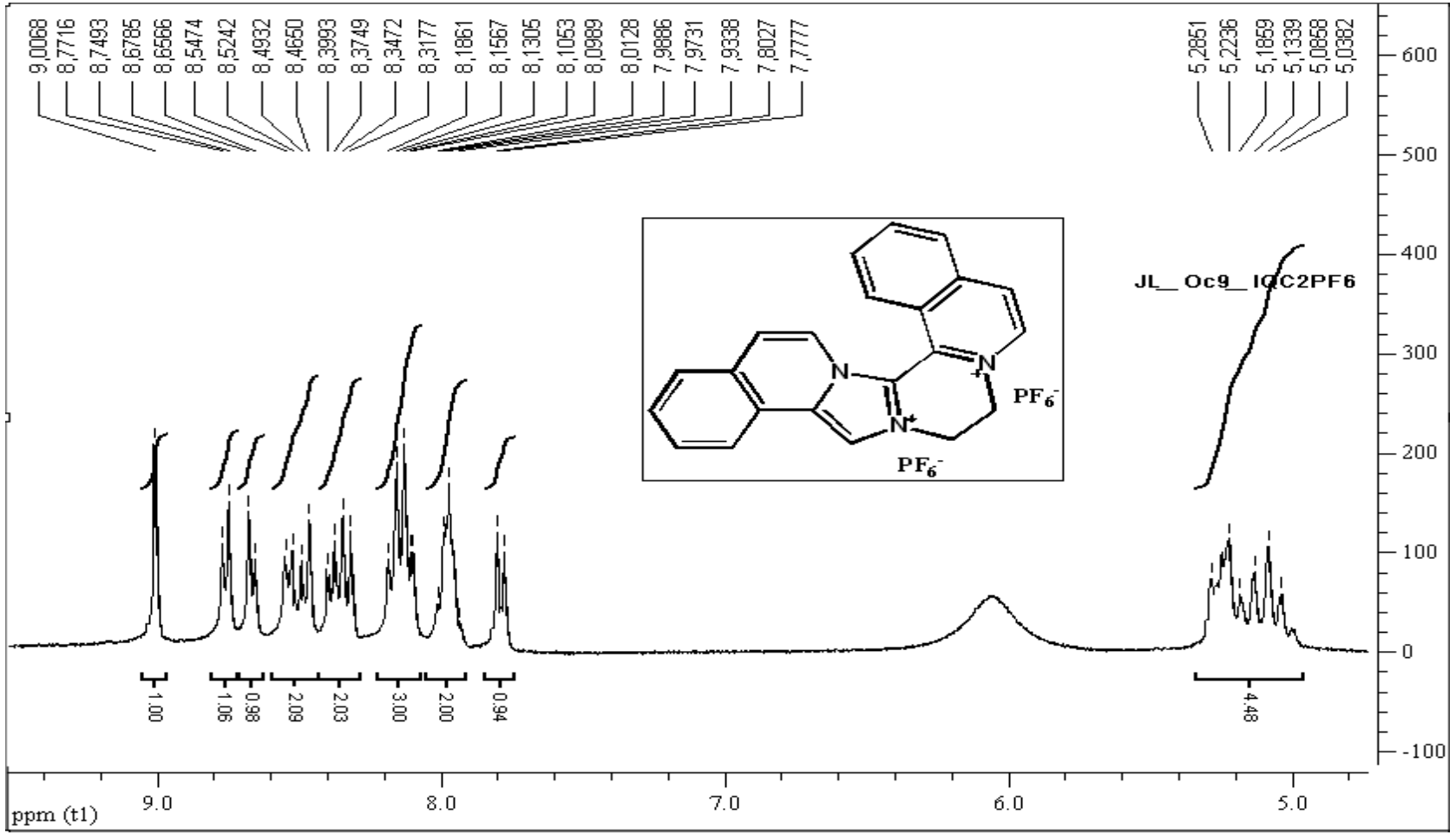

Figure A.19 ^{1}H NMR of $[IQC_2](PF6)_2$ (300Hz, CD3CN)

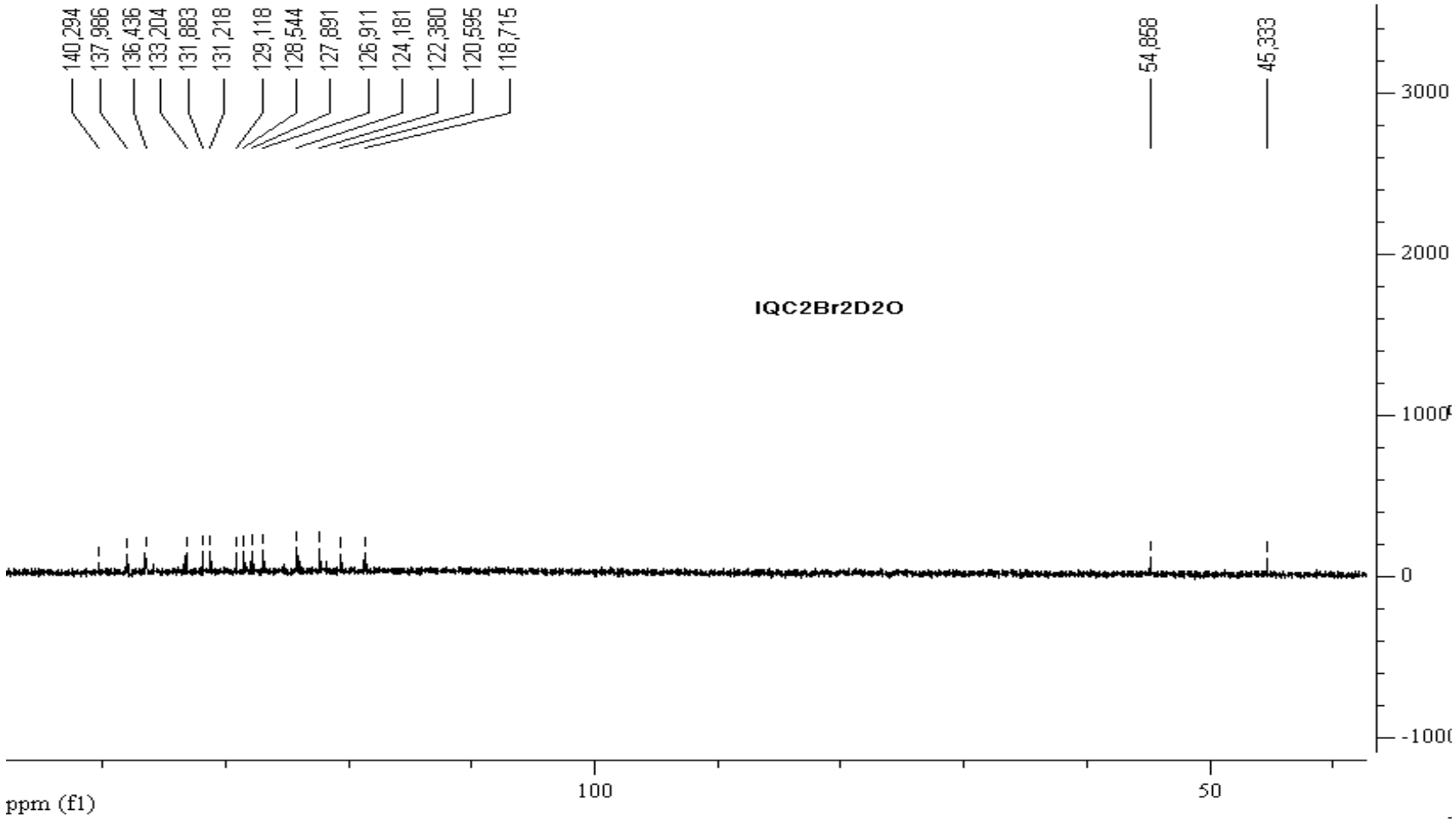

Figure A.20 ^{13}C NMR of $[IQC_2]Br_2$ (400Hz, H_2O)

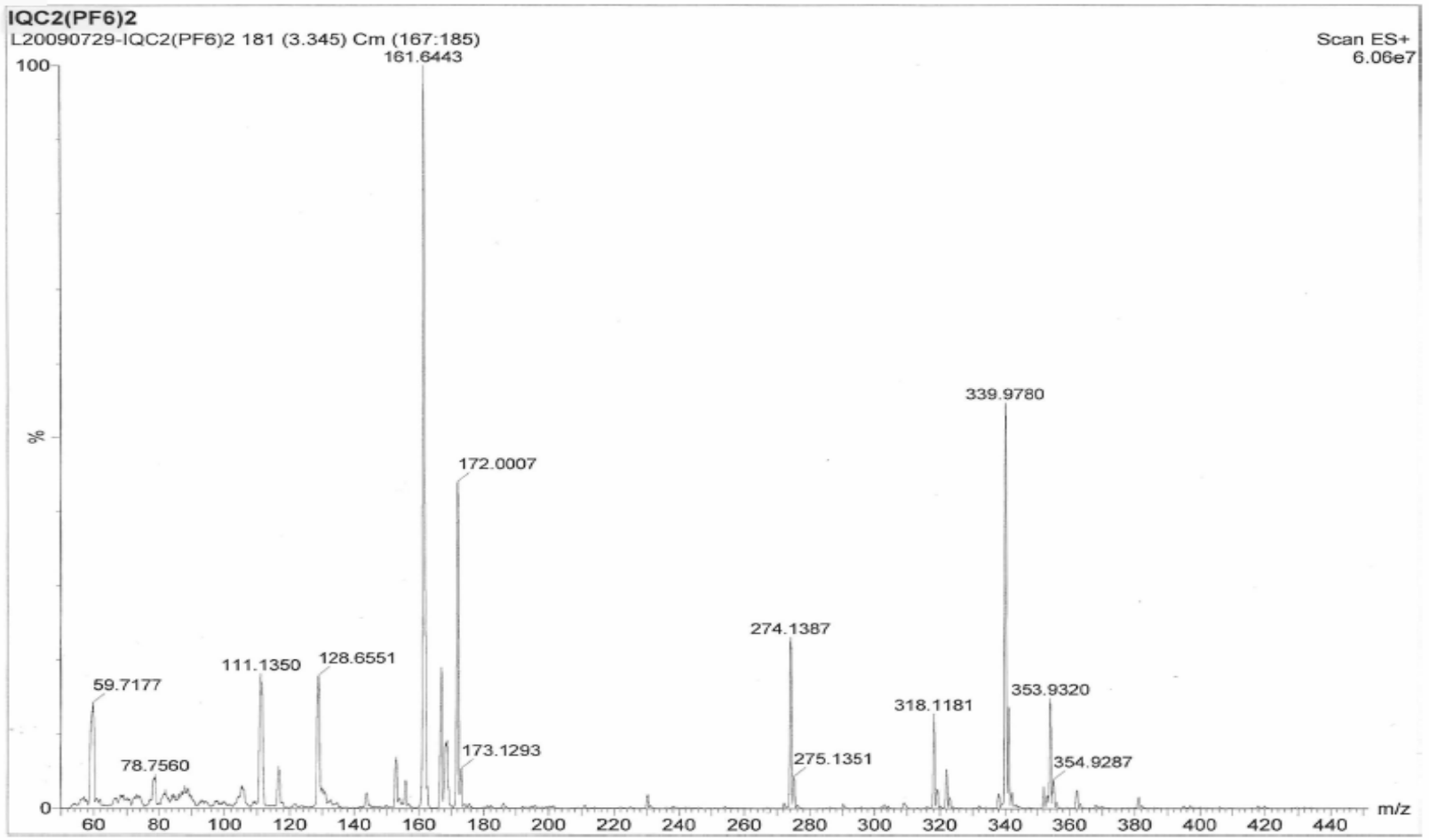

Figure A.21 MS of $[IQC_2](PF6)_2$

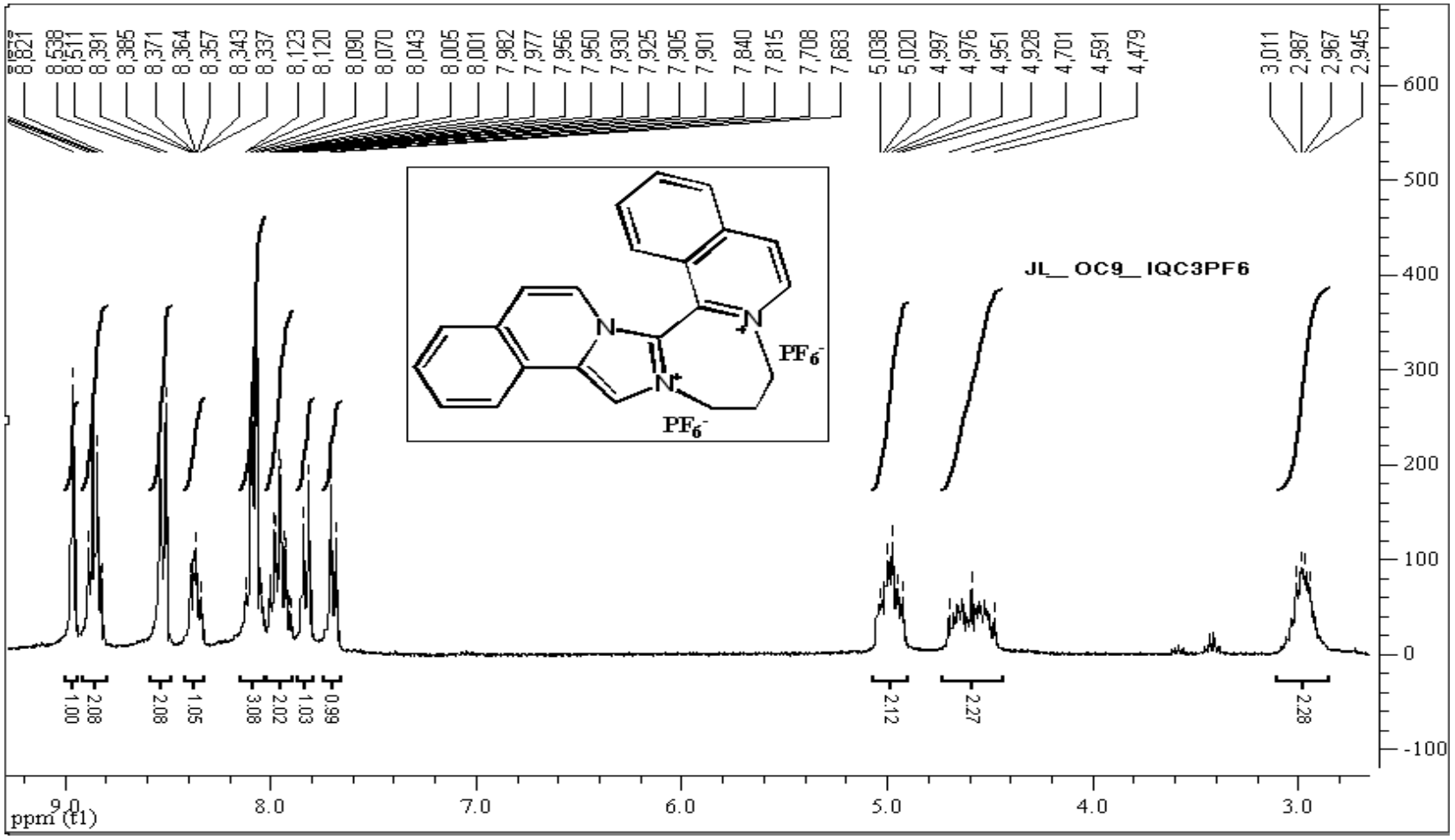

Figure A.22 ^{1}H NMR of $[IQC_3](PF6)_2$ (300Hz, CD3CN)

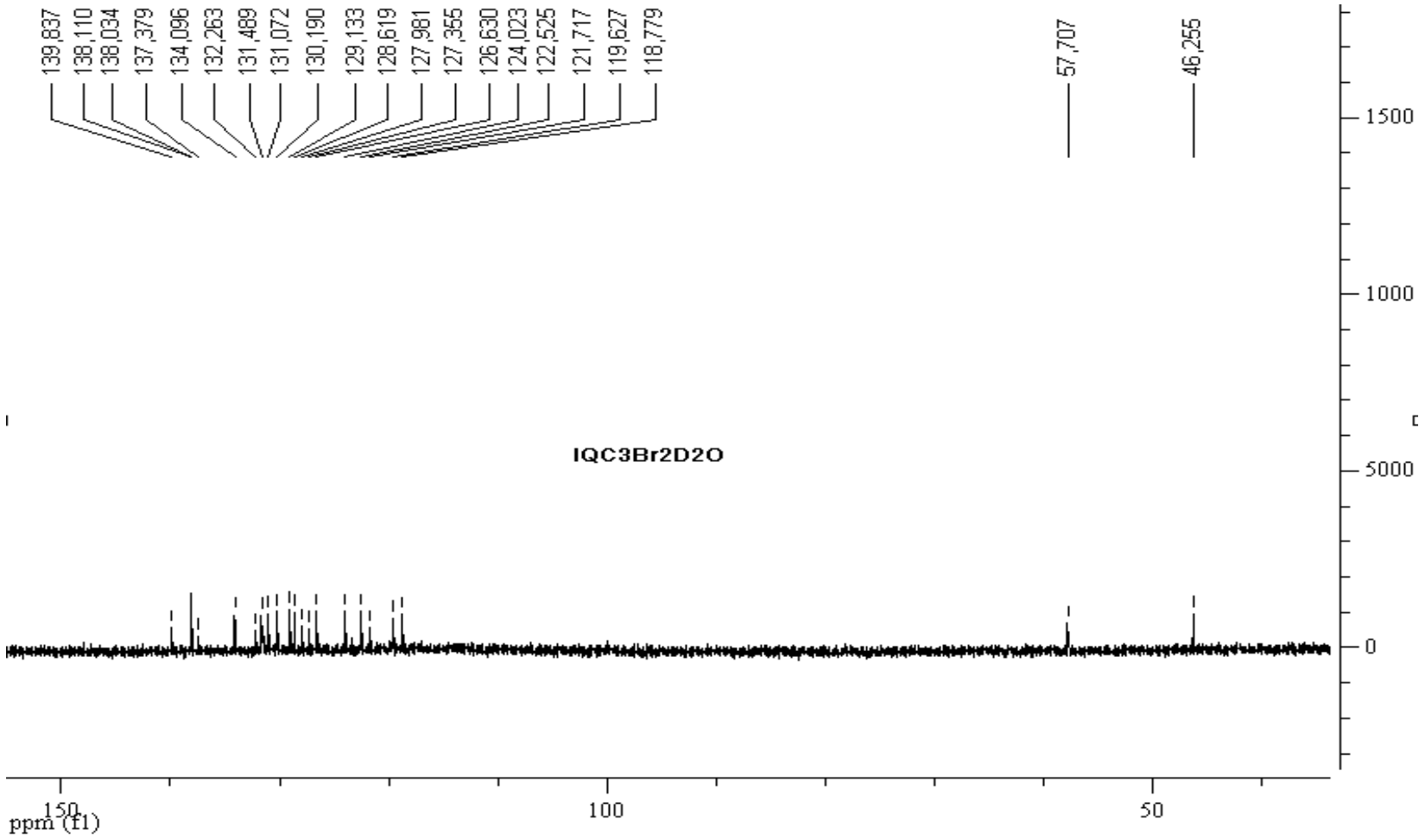

Figure A.23 ^{13}C NMR of $[IQC_3](PF6)_2$ (300Hz, CD3CN)

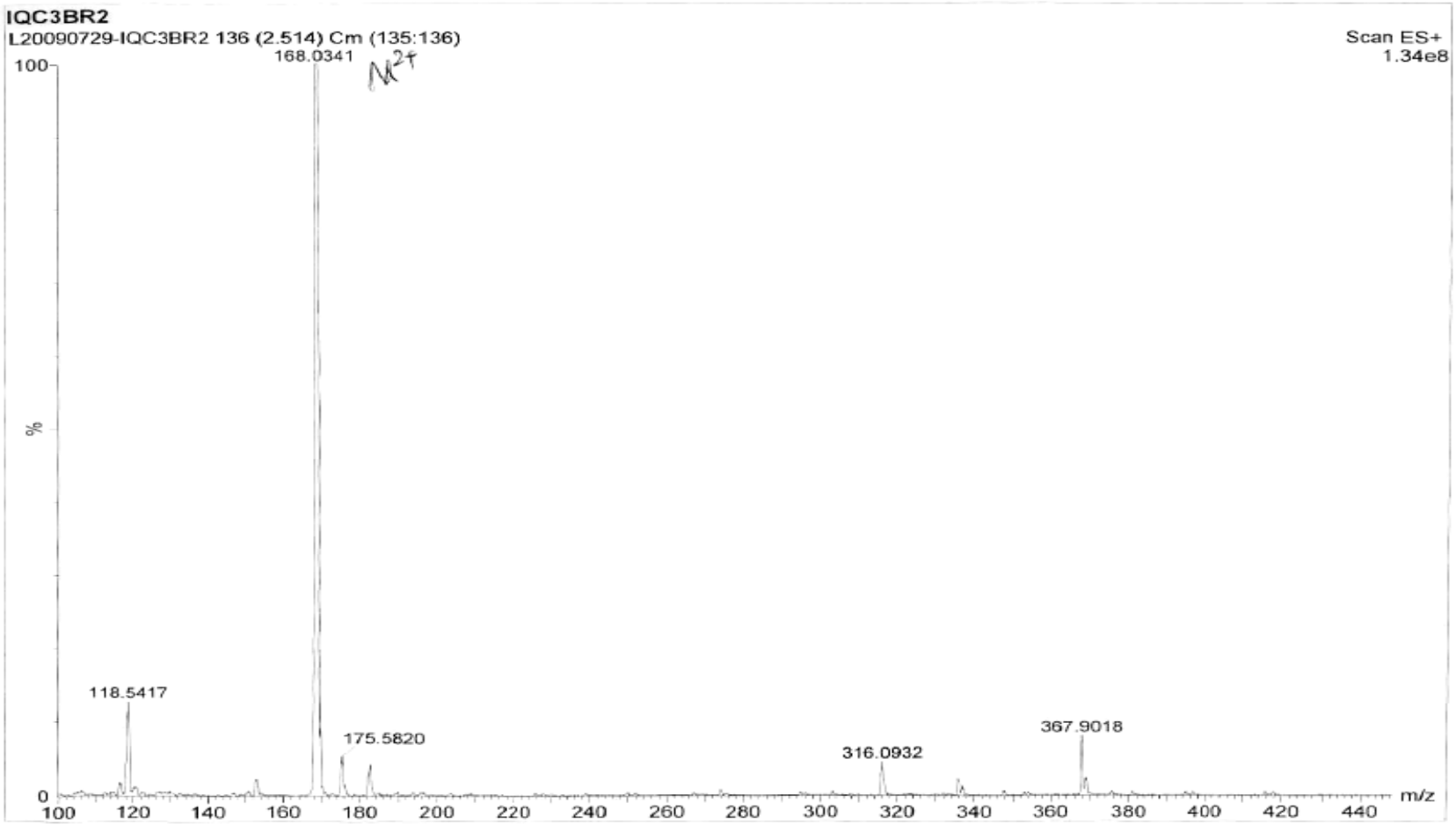

Figure A.24 MS of $[IQC_3]Br_2$

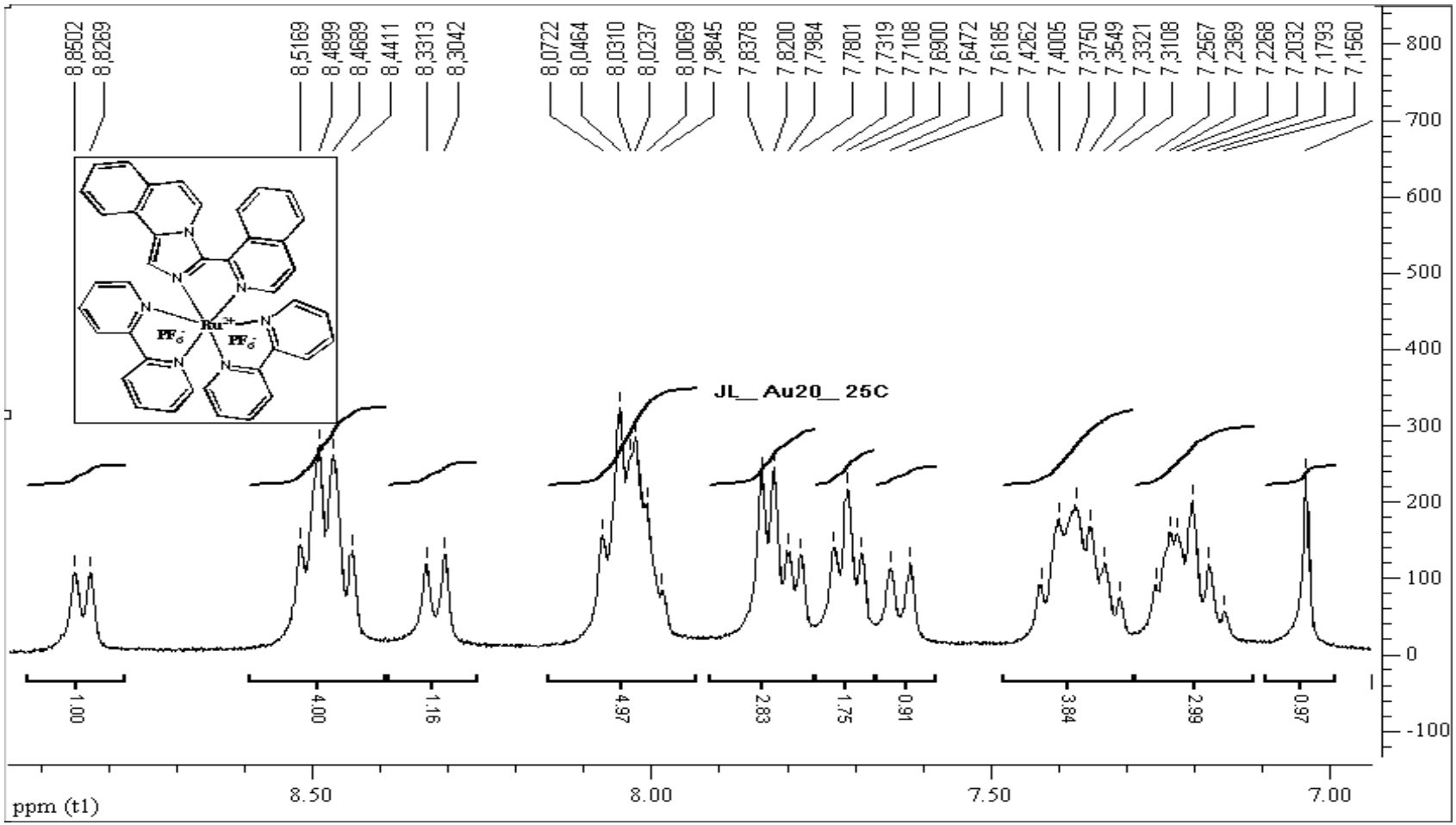

Figure A.25 ^{1}H NMR of $[Ru(bpy)_2IQ](PF_6)_2$ (300Hz, CD_3CN)

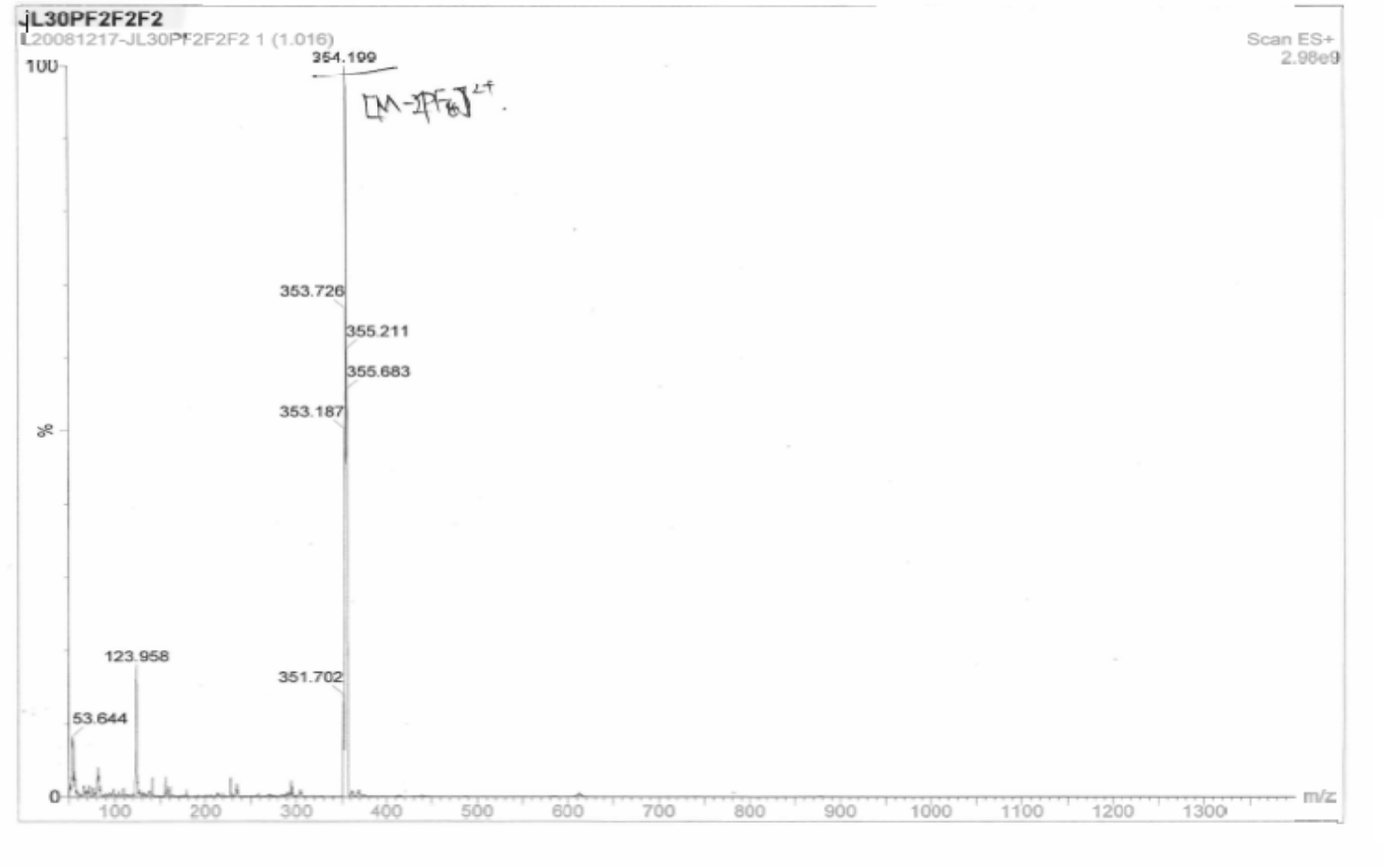

Figure A.26 MS of $[Ru(bpy)_2IQ](PF_6)_2$

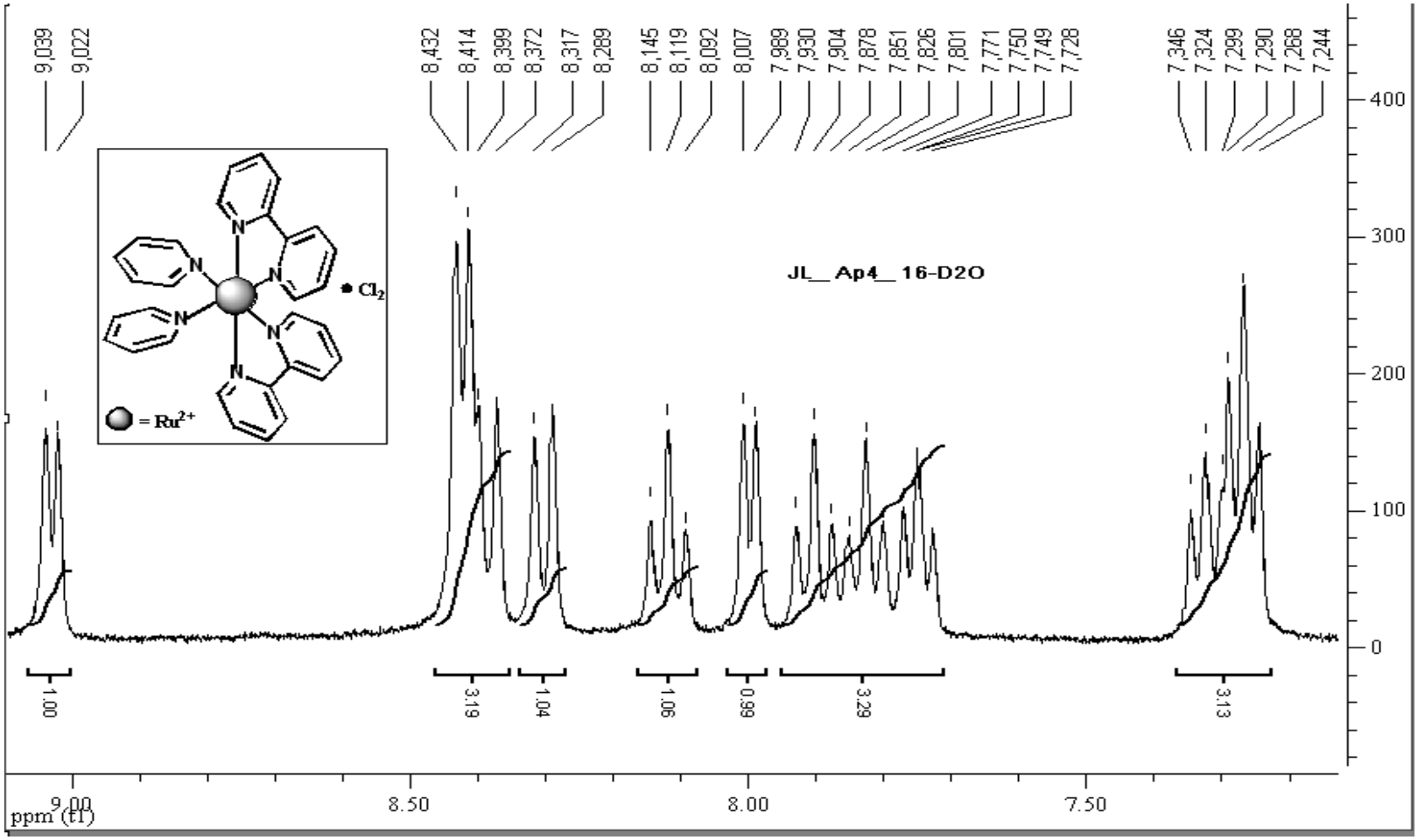

Figure A.27 ^{1}H NMR of [Ru(bpy)$_2$pyridine)$_2$]Cl$_2$ (300Hz, D$_2$O)

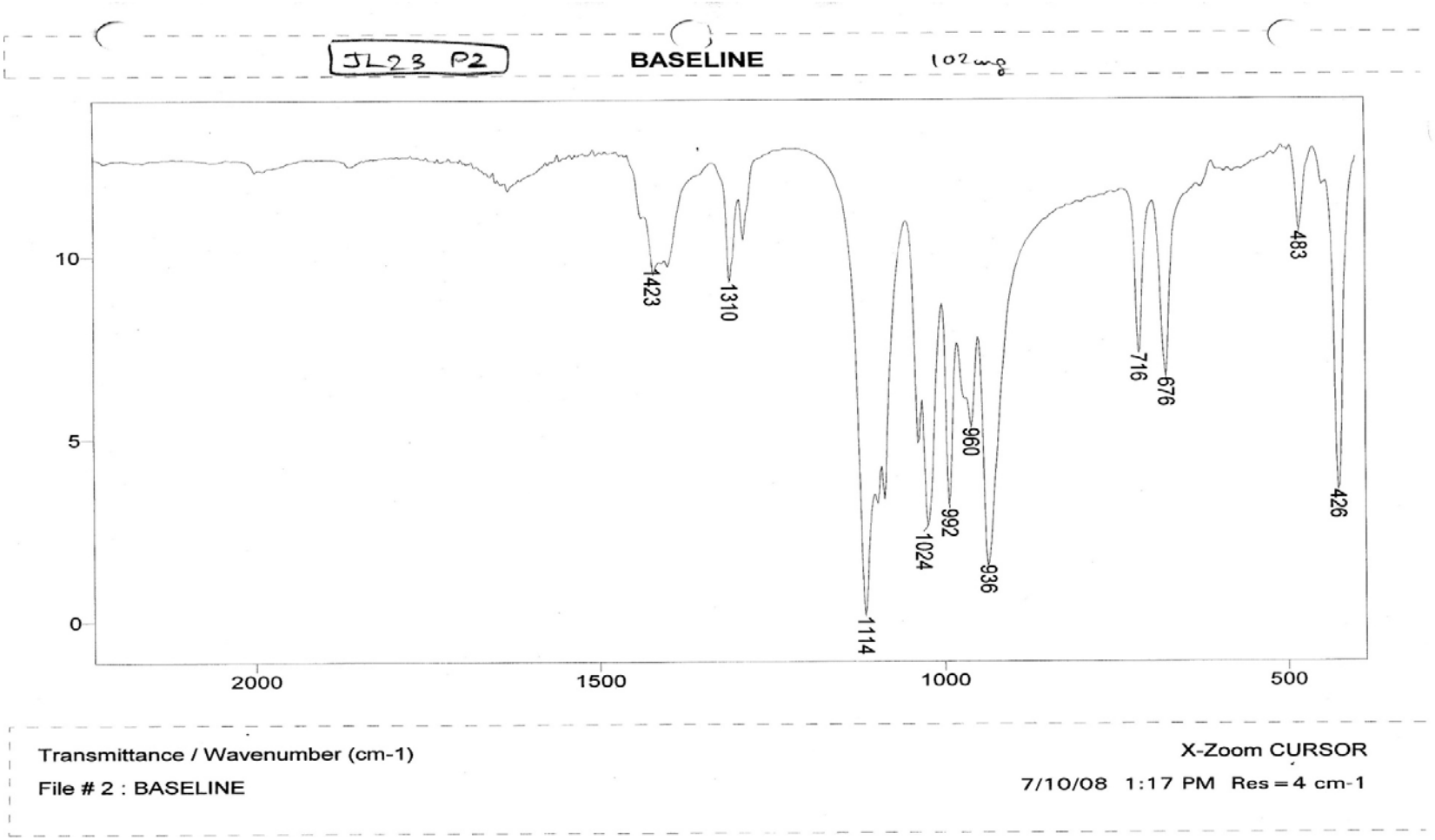

Figure A.28 IR of $Ru(DMSO)_4Cl_2$

The UV absorption spectrum for P ligand is shown below.

P ligand	$C_{UV}=3.8873\times10^{-5}$ mol/L	λ=202	A=0.8438873	ε=21709
M=195.08	$C_{UV}=3.8873\times10^{-5}$ mol/L	λ=226	A=0.7148132	ε =18388
m=1.54mg	$C_{UV}=3.8873\times10^{-5}$ mol/L	λ=246	A=0.6691284	ε =17213
$C_{origenal}=7.8942\times10^{-4}$ mol/L	$C_{UV}=3.8873\times10^{-5}$ mol/L	λ=348	A=0.9467011	ε =24353

Table A.1 UV data for P ligand in Acetonitrile

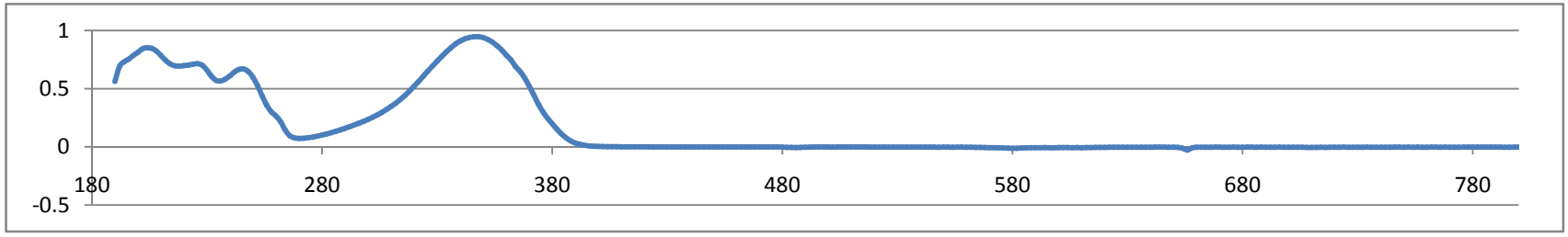

Figure A.29 UV Spectrum for P ligand in Acetonitrile

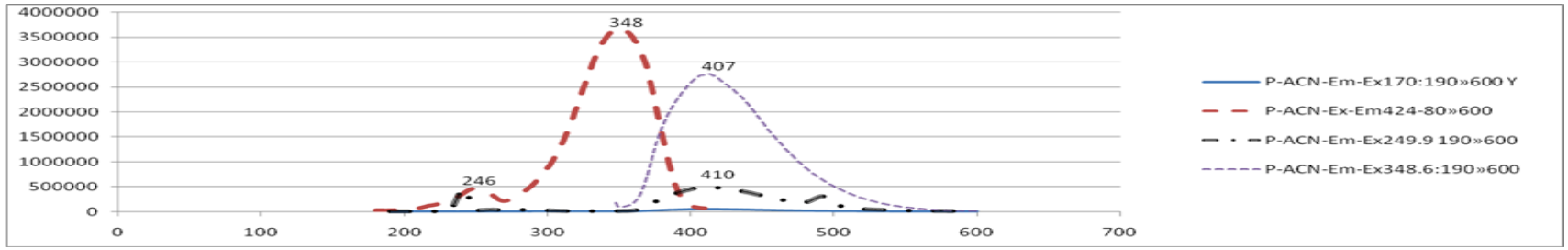

Figure A.30 Fluorescence Spectrum for P ligand in Acetonitrile

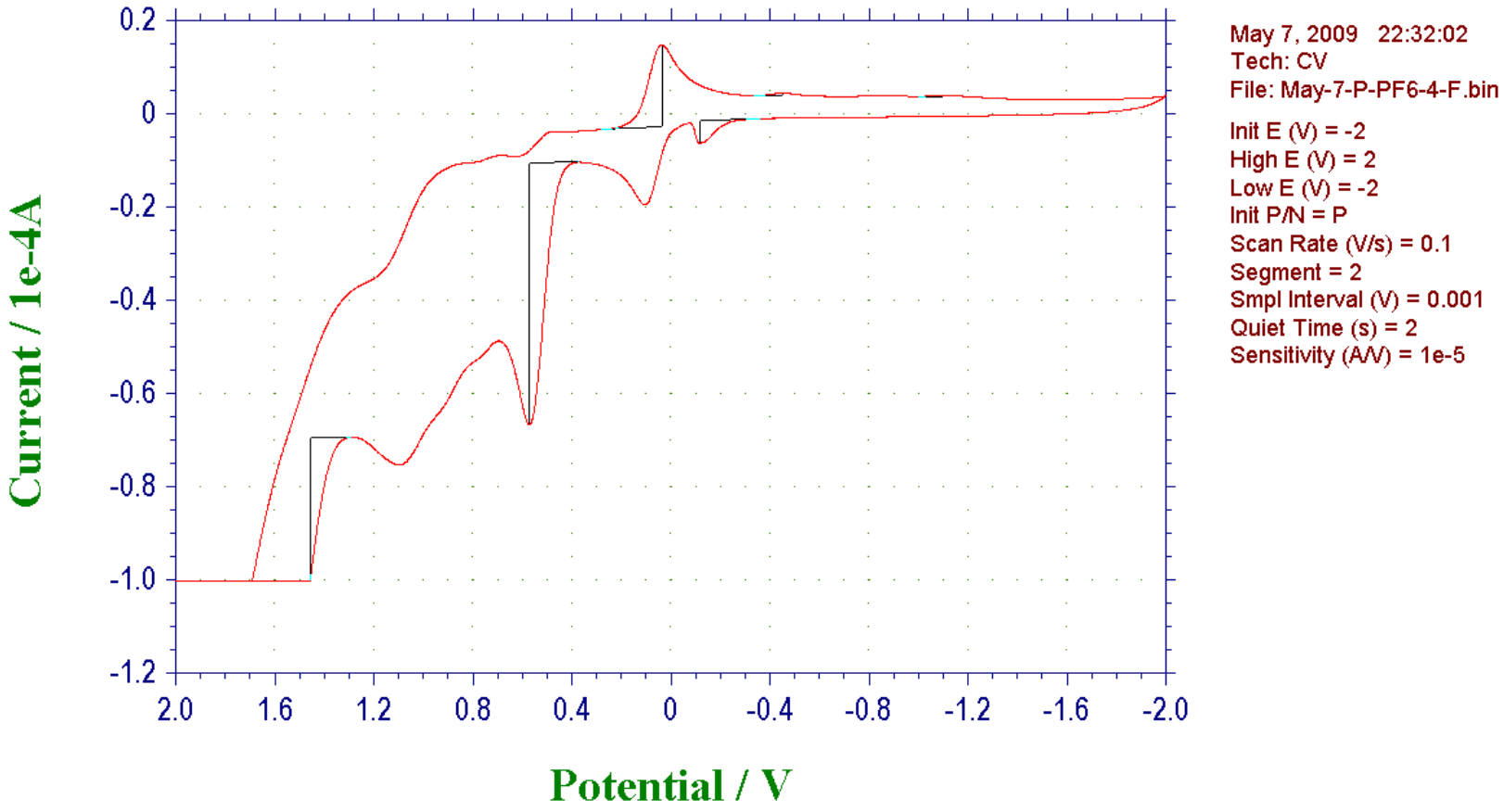

Figure A.31 CV of P

$[PC_2]Cl_2$				
M=294.18	C_{UV}= 2.33870×10^{-4}mol/L	λ=246	A=1.093704	ε =4677
m=3.44mg	C_{UV}= 5.01150×10^{-4}mol/L	λ=310	A=0.887558	ε =1771
$C_{origenal}$ =1.16935×10^{-3}	C_{UV}= 1.16935×10^{-4}mol/L	λ=408	A=0.9576569	ε =8190

Table A.2 UV data for $[PC_2]Cl_2$ in water

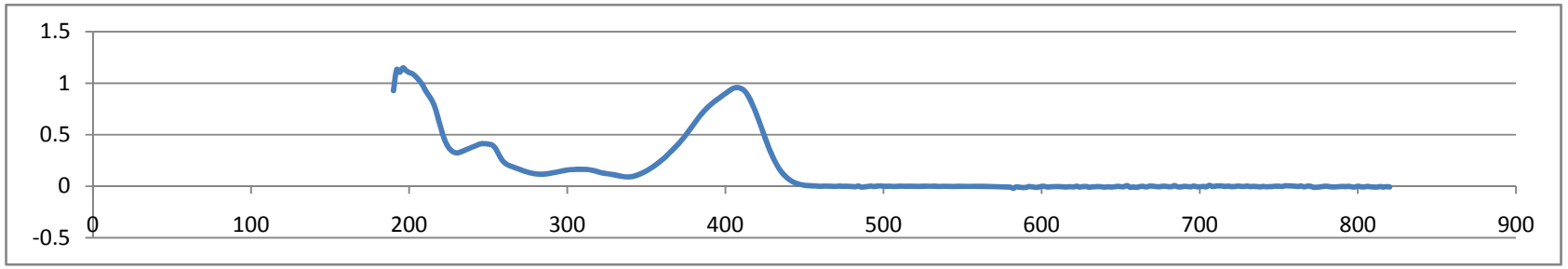

Figure A.32 UV Spectrum for $[PC_2]Cl_2$ in water

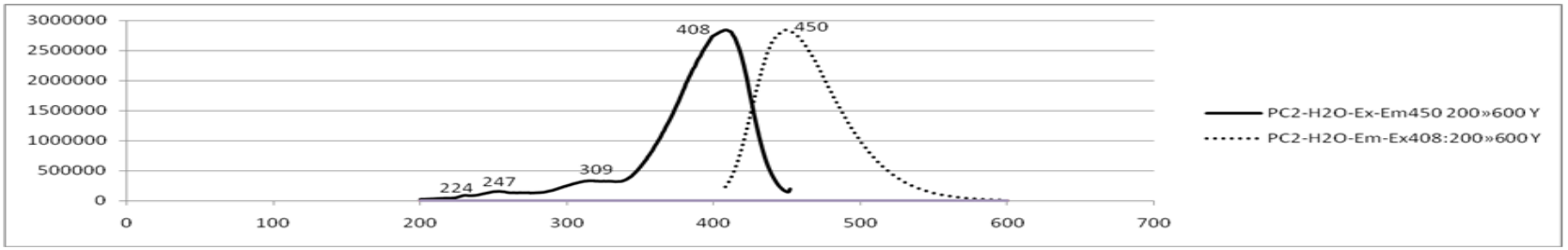

Figure A.33 Fluorescence Spectrum for $[PC_2]Cl_2$ in water

$[PC_2]\ (PF_6)_2$	$C_{UV}=2.4652\times10^{-5}$ mol/L	λ=194	A= 0.6954346	ε=28210
M=515.17	$C_{UV}=6.1630\times10^{-5}$ mol/L	λ=248	A=0.6756744	ε =10963
m=1.27mg	$C_{UV}=1.6435\times10^{-4}$ mol/L	λ=312	A=0.6805725	ε =4141
$C_{origenal}=2.4652\times10^{-4}$ mol/L	$C_{UV}=2.4652\times10^{-5}$ mol/L	λ=406	A=0.6343231	ε =25731

Table A.3 UV data for $[PC_2]\ (PF_6)_2$ in Acetonitrile

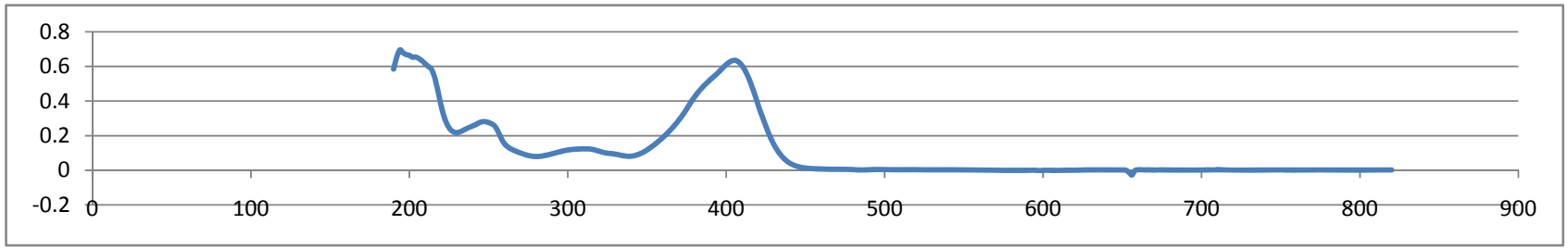

Figure A.34 UV Spectrum for $[PC_2]\ (PF_6)_2$ in Acetonitrile

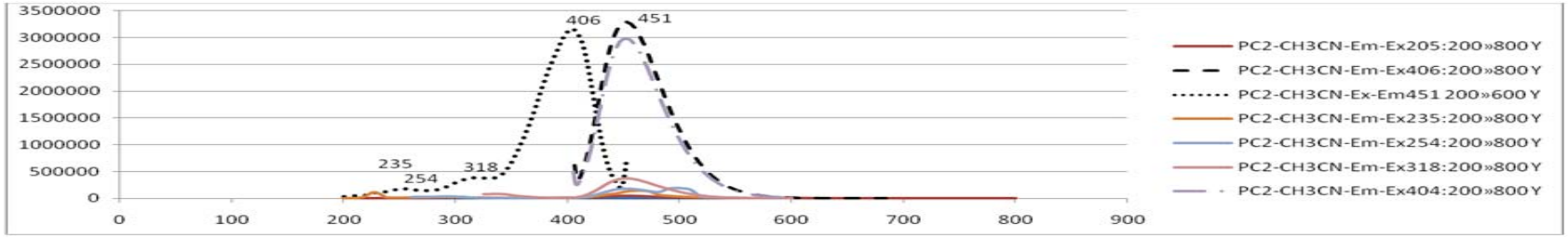

Figure A.35 Fluorescence Spectrum for $[PC_2](PF_6)_2$ in Acetonitrile

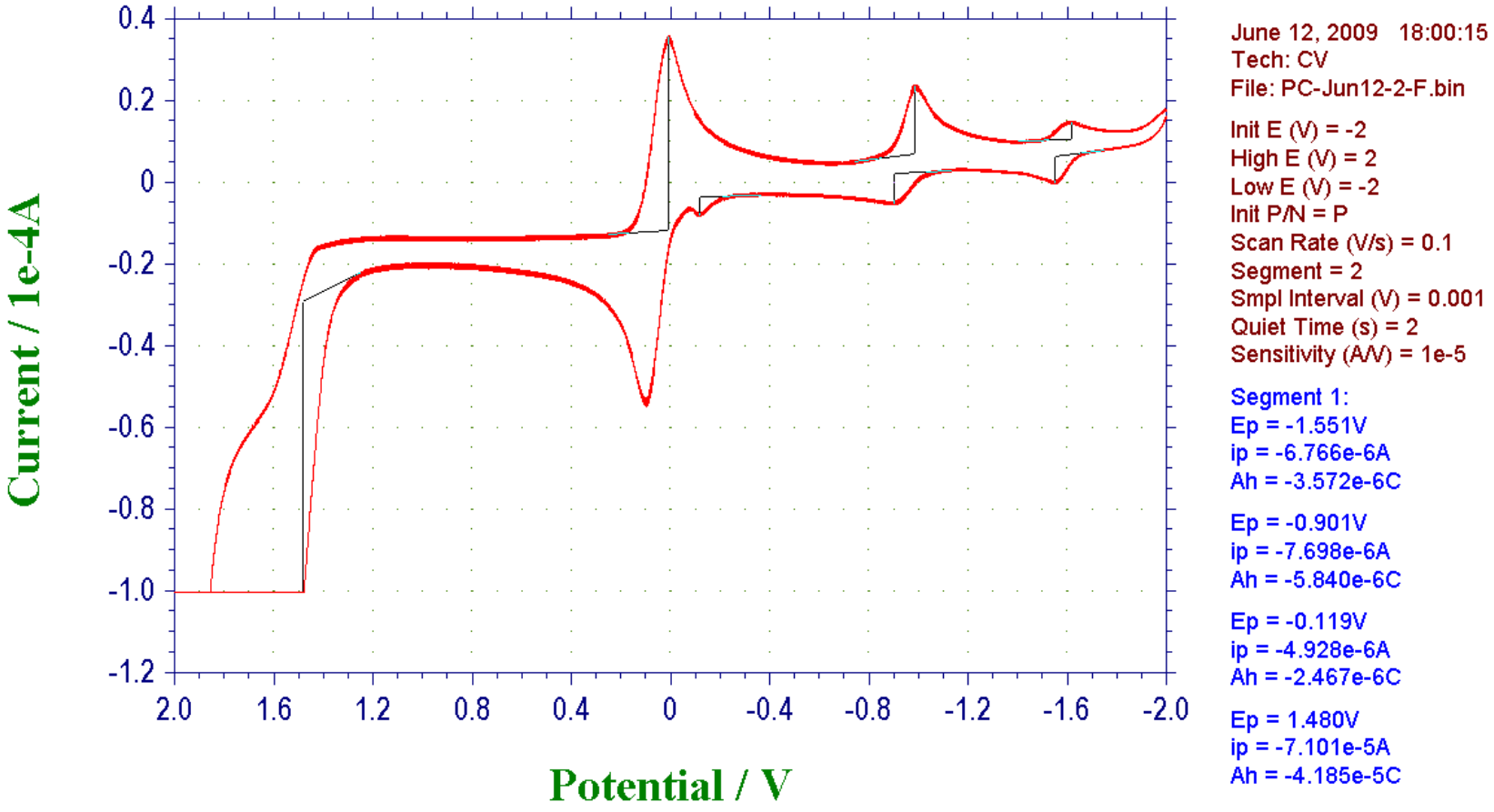

Figure A.36 CV of $[PC_2](PF_6)_2$

$[PC_3]Cl_2$				ε=
M=308.06	$C_{UV}=5.19379\times10^{-5}$ mol/L	λ=254	A=0.5884399	ε =11330
m=1.60mg				
$C_{origenal}=5.19379\times10^{-4}$ mol/L	$C_{UV}=5.19379\times10^{-5}$ mol/L	λ=386	A=0.6430359	ε =12381

Table A.4 UV data for $[PC_3]Cl_2$ in water

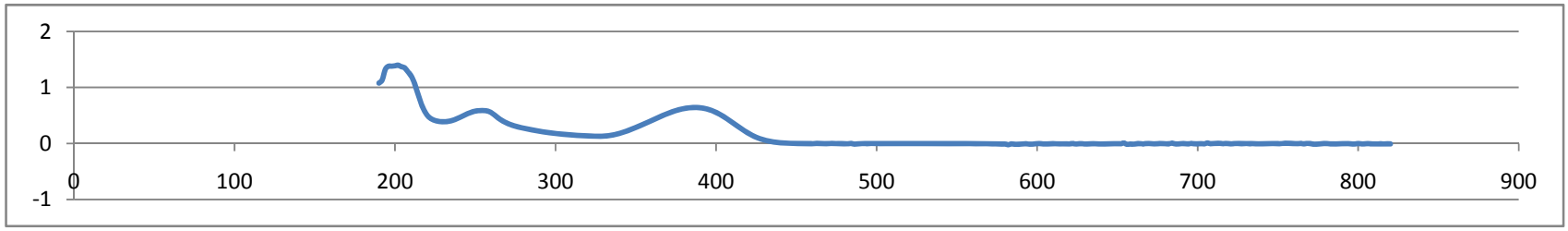

Figure A.37 UV Spectrum for $[PC_3]Cl_2$ in water

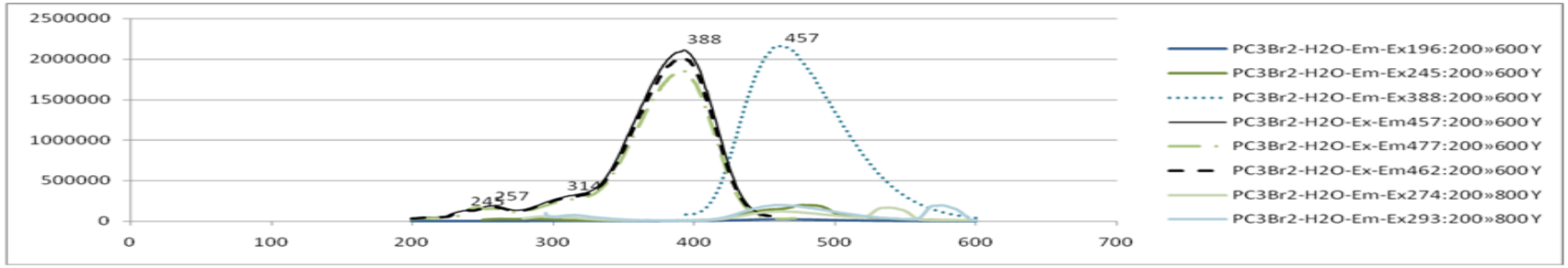

Figure A.38 Fluorescence Spectrum for $[PC_3]Cl_2$ligand in water

$[PC_3](PF_6)_2$	$C_{UV}=3.96940\times10^{-5}$ mol/L	λ=204	A= 0.9658356	ε=24332
M=529.05	$C_{UV}=7.93876\times10^{-5}$ mol/L	λ=250	A=0. 5856323	ε =7377
m=1.26mg				
$C_{origenal}=2.38163\times10^{-4}$ mol/L	$C_{UV}=7.93876\times10^{-5}$ mol/L	λ=384	A=0.9350586	ε =11778

Table A.5 UV data for $[PC_3](PF_6)_2$ in Acetonitrile

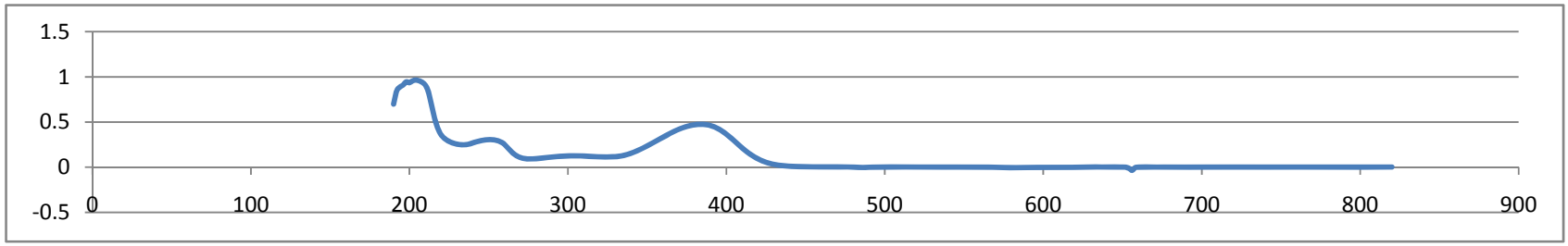

Figure A.39 UV Spectrum for $[PC_3](PF_6)_2$ in Acetonitrile

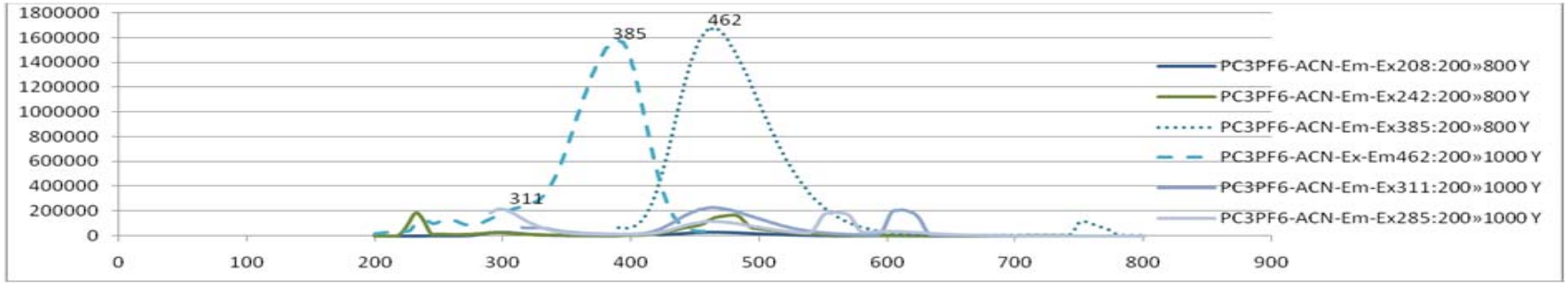

Figure A.40 Fluorescence Spectrum for $[PC_3](PF_6)_2$ in Acetonitrile

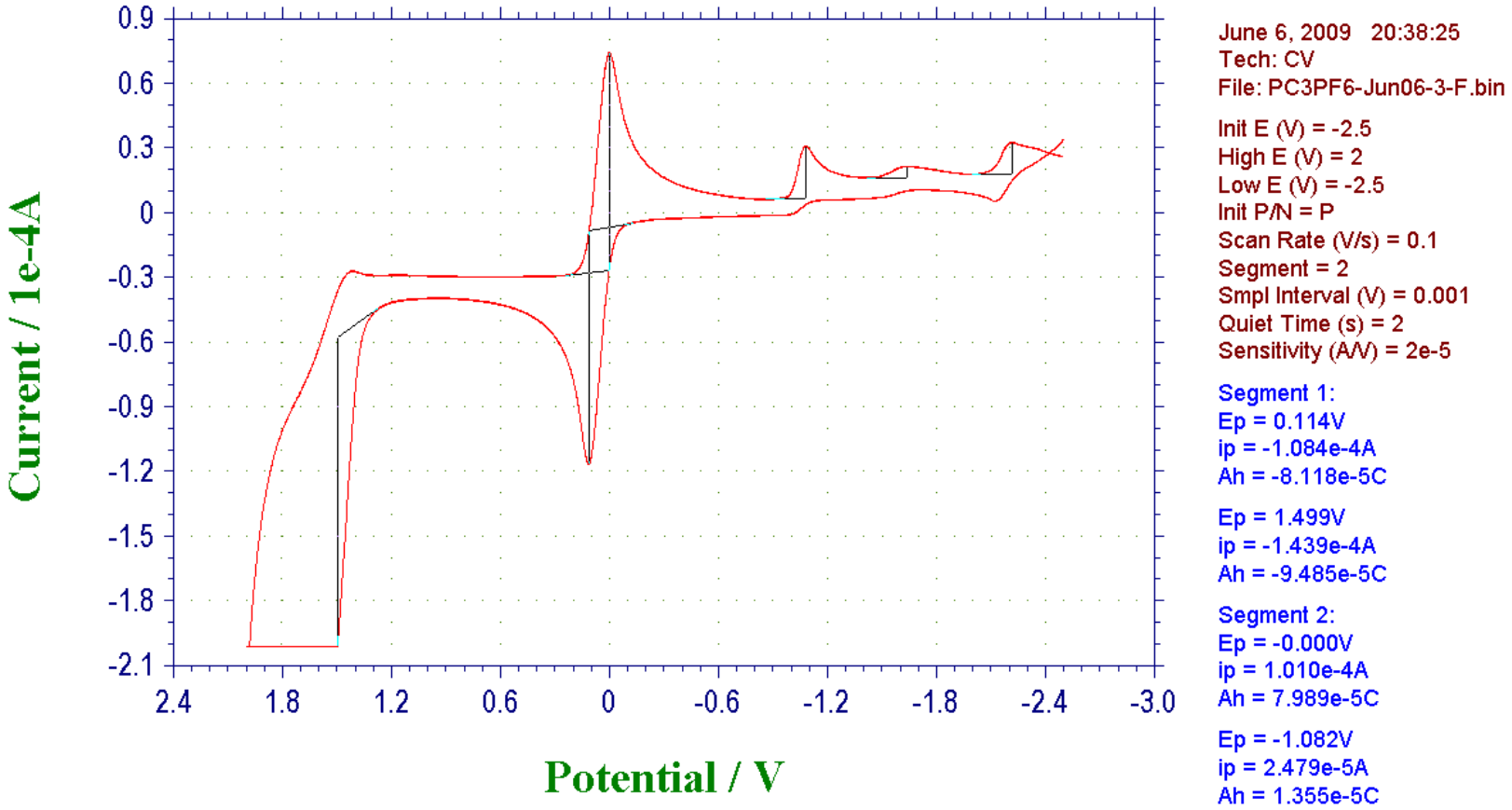

Figure A.41 CV of $[PC_3](PF_6)_2$

$[PC_4]Cl_2$	$C_{UV}=3.85165\times10^{-5}$ mol/L	λ=202	A=0.9216003	ε=23927
M=321.94	$C_{UV}=1.37559\times10^{-4}$ mol/L	λ=258	A= 0.9951019	ε =7234
m=1.55mg				
$C_{origenal}= 4.81456\times10^{-4}$ mol/L	$C_{UV}=1.37559\times10^{-4}$ mol/L	λ=386	A=0.9785919	ε =7114

Table A.6 UV data for $[PC_4]Cl_2$ in water

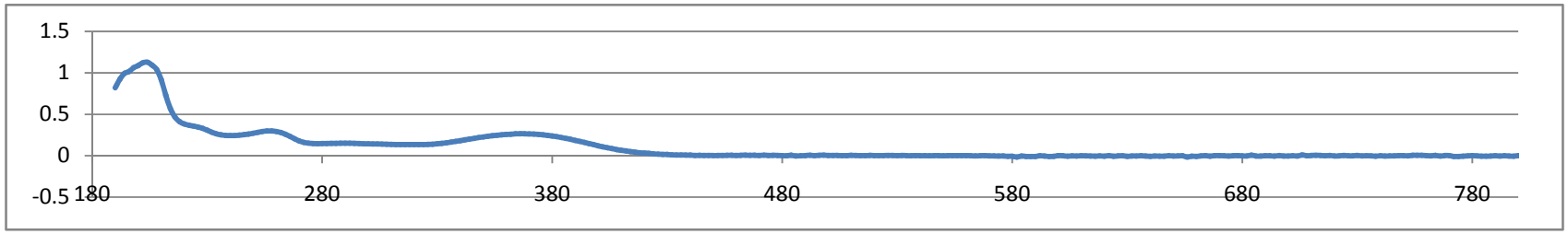

Figure A.42 UV Spectrum for $[PC_4]Cl_2$ in water

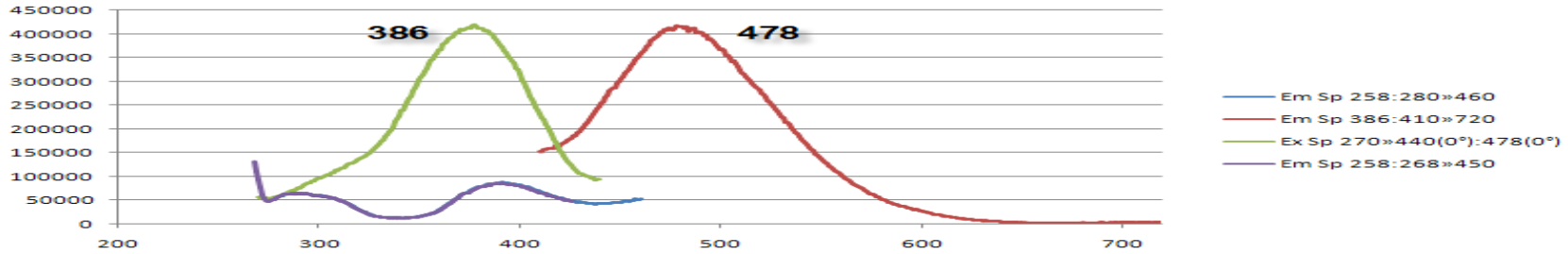

Figure A.43 Fluorescence Spectrum for $[PC_4]Cl_2$ in water

$[PC_4]$ $(PF_6)_2$				ε=
M=542.93	$C_{UV}=7.61301\times10^{-5}$ mol/L	λ=258	A= 0.892273	ε =11720
m=1.24mg				
$C_{origenal}= 2.28390\times10^{-4}$ mol/L	$C_{UV}=7.61301\times10^{-5}$ mol/L	λ=366	A=0.8994598	ε =11815

Table A.7 UV data for $[PC_4]$ $(PF_6)_2$ in Acetonitrile

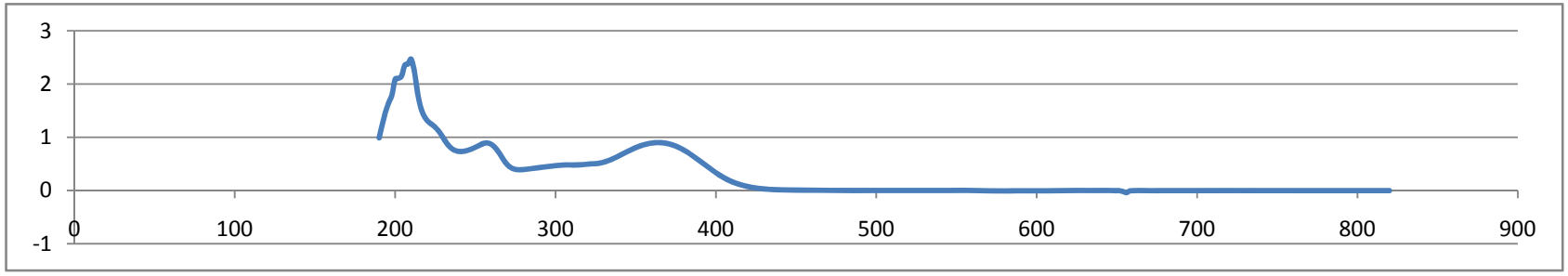

Figure A.44 UV Spectrum for $[PC_4]$ $(PF_6)_2$ in Acetonitrile

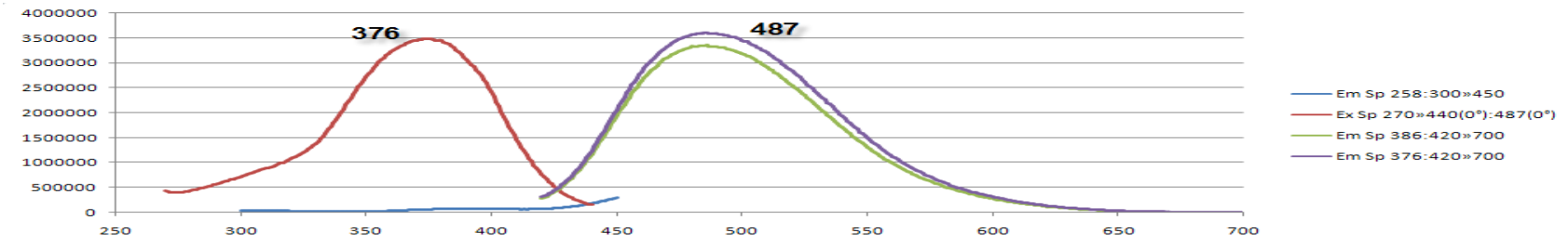

Figure A.45 Fluorescence Spectrum for $[PC_4]$ $(PF_6)_2$ in Acetonitrile

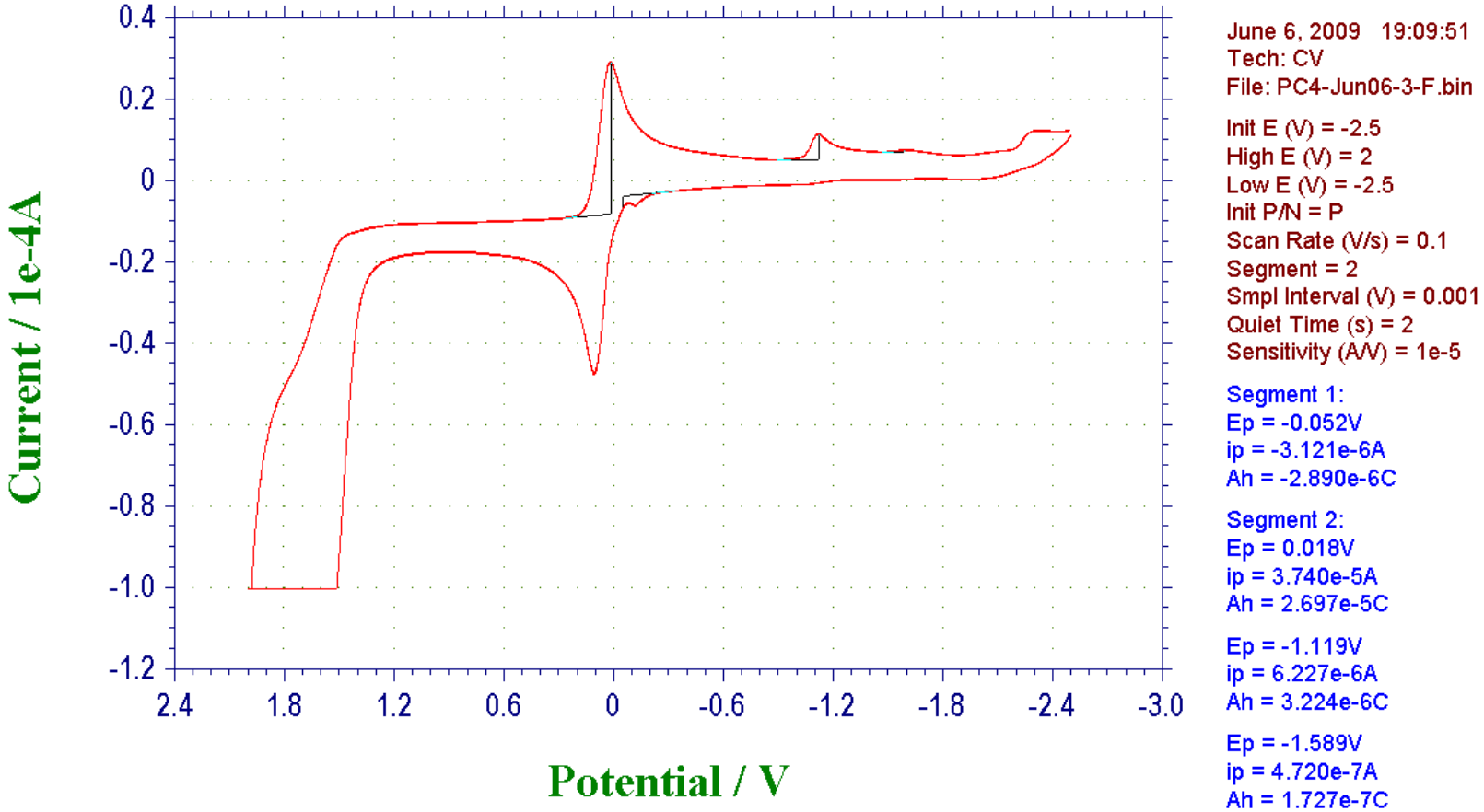

Figure A.46 CV of $[PC_4]$ $(PF_6)_2$

IQ ligand				
M=295.1	C_{UV}=2.0502×10^{-5} mol/L	λ=212	A= 0.9902649	ε =48301
m=2.42mg	C_{UV}=2.0502×10^{-5} mol/L	λ=260	A= 0.8346863	ε =40712
$C_{origenal}$=8.2006×10^{-4} mol/L	C_{UV}=4.1003×10^{-5} mol/L	λ=374	A= 0.8119507	ε =19802

Table A.8 UV data for IQ ligand in Acetonitrile

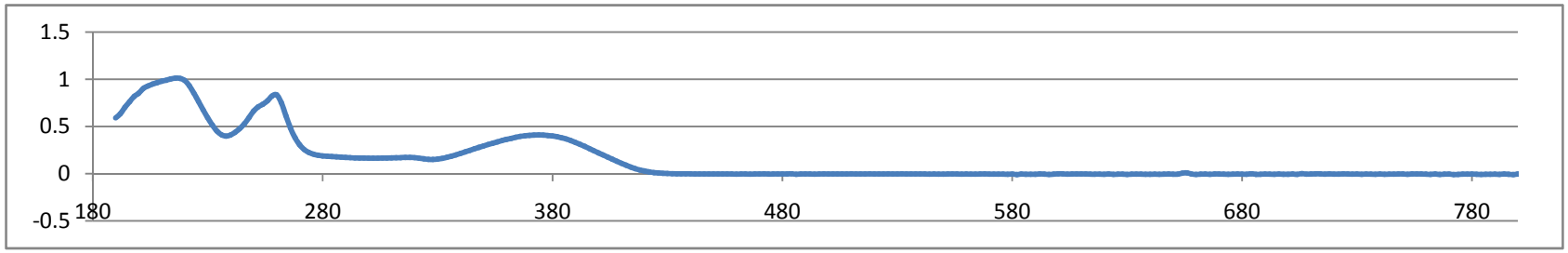

Figure A.47 UV Spectrum for IQ ligand in Acetonitrile

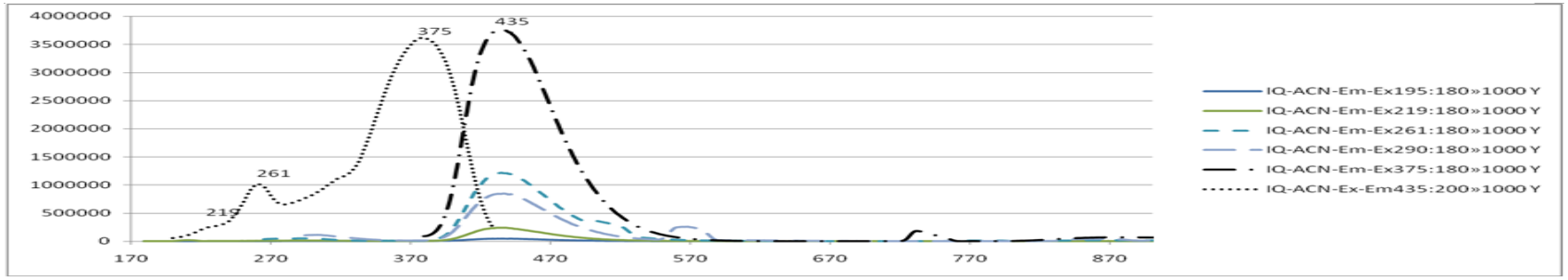

Figure A.48 Fluorescence Spectrum for IQ ligand in Acetonitrile

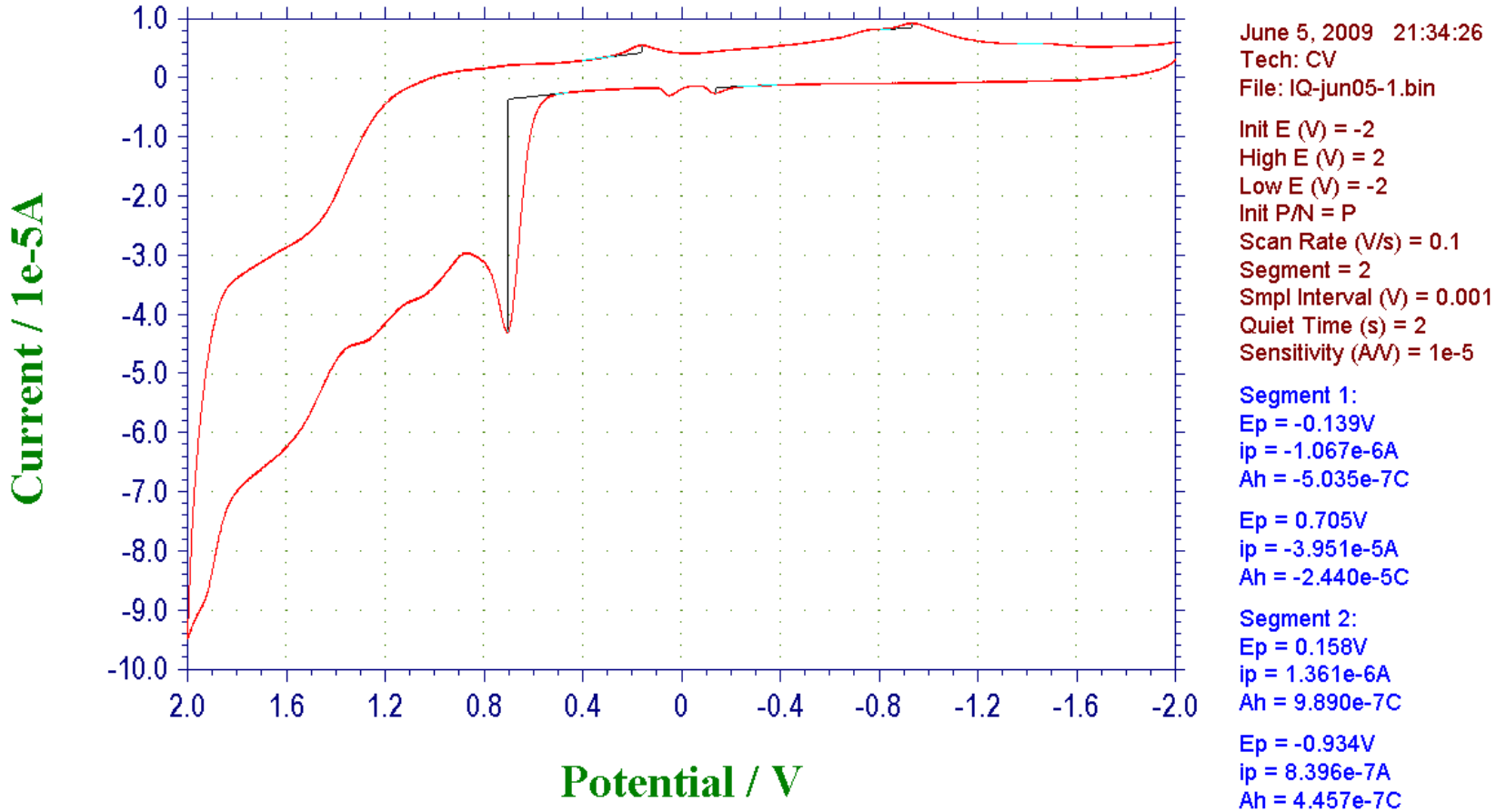

Figure A.49 CV of IQ

$[IQC_2]Cl_2$	$C_{UV}=2.25768\times10^{-5}$ mol/L	λ=206	A=0.9335632	ε=41351
M=394.21				
m=0.89mg	$C_{UV}=1.12884\times10^{-5}$ mol/L	λ=244	A=0.8345947	ε =73934
C= 2.25768×10^{-4}	$C_{UV}=3.22526\times10^{-5}$ mol/L	λ=446	A=0.9270477	ε =28743

Table A.9 UV data for $[IQC_2]Cl_2$ in water

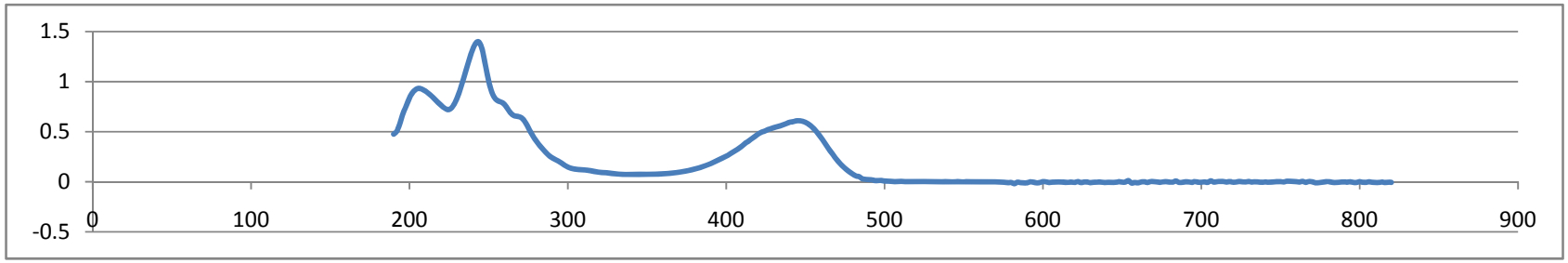

Figure A.50 UV Spectrum for $[IQC_2]Cl_2$ in water

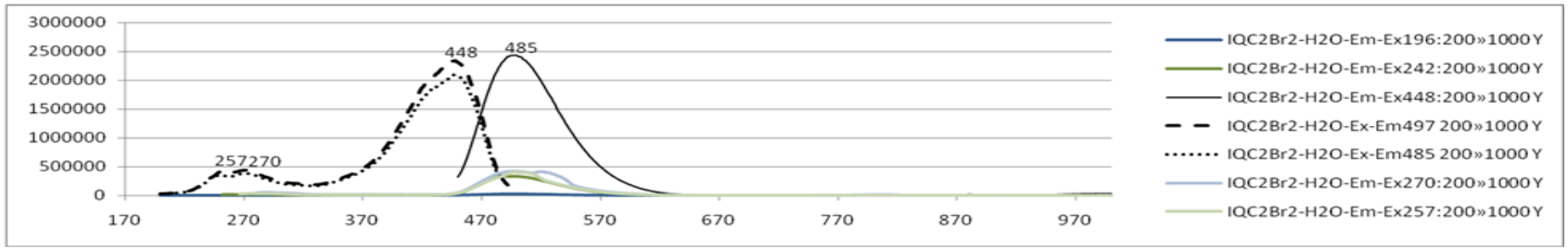

Figure A.51 Fluorescence Spectrum for $[IQC_2]Cl_2$ in water

$IQC_2(PF_6)_2$	$C_{UV}=4.30755\times10^{-5}$ mol/L	λ=206	A=0.7509766	ε=17434
M=615.2				
m=1.06mg	$C_{UV}=4.30755\times10^{-5}$ mol/L	λ=244	A=1.182312	ε =27447
C= 1.72302×10^{-4}	$C_{UV}=4.30755\times10^{-5}$ mol/L	λ=444	A=0.5366669	ε =12459

Table A.10 UV data for $[IQC_2](PF_6)_2$ in Acetonitrile

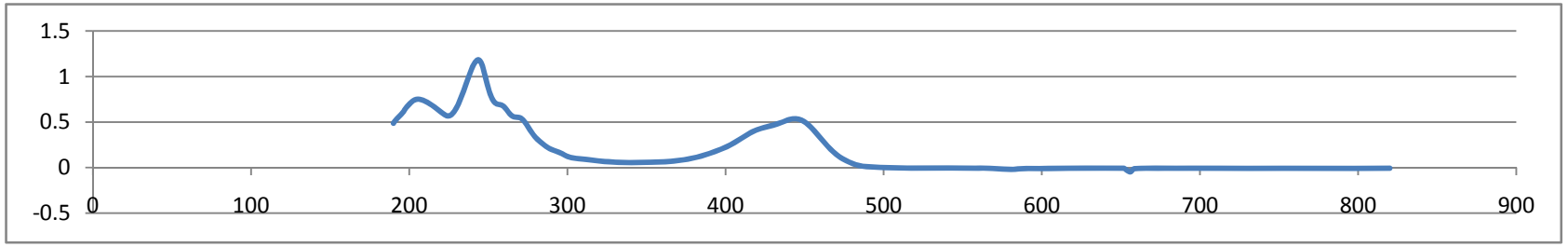

Figure A.50 UV Spectrum for $[IQC_2](PF_6)_2$ in Acetonitrile

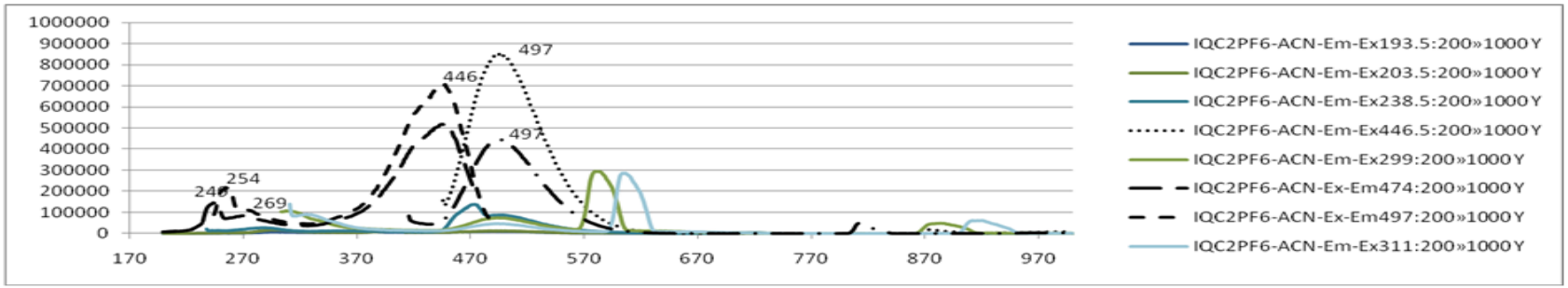

Figure A.51 Fluorescence Spectrum for $[IQC_2](PF_6)_2$ in Acetonitrile

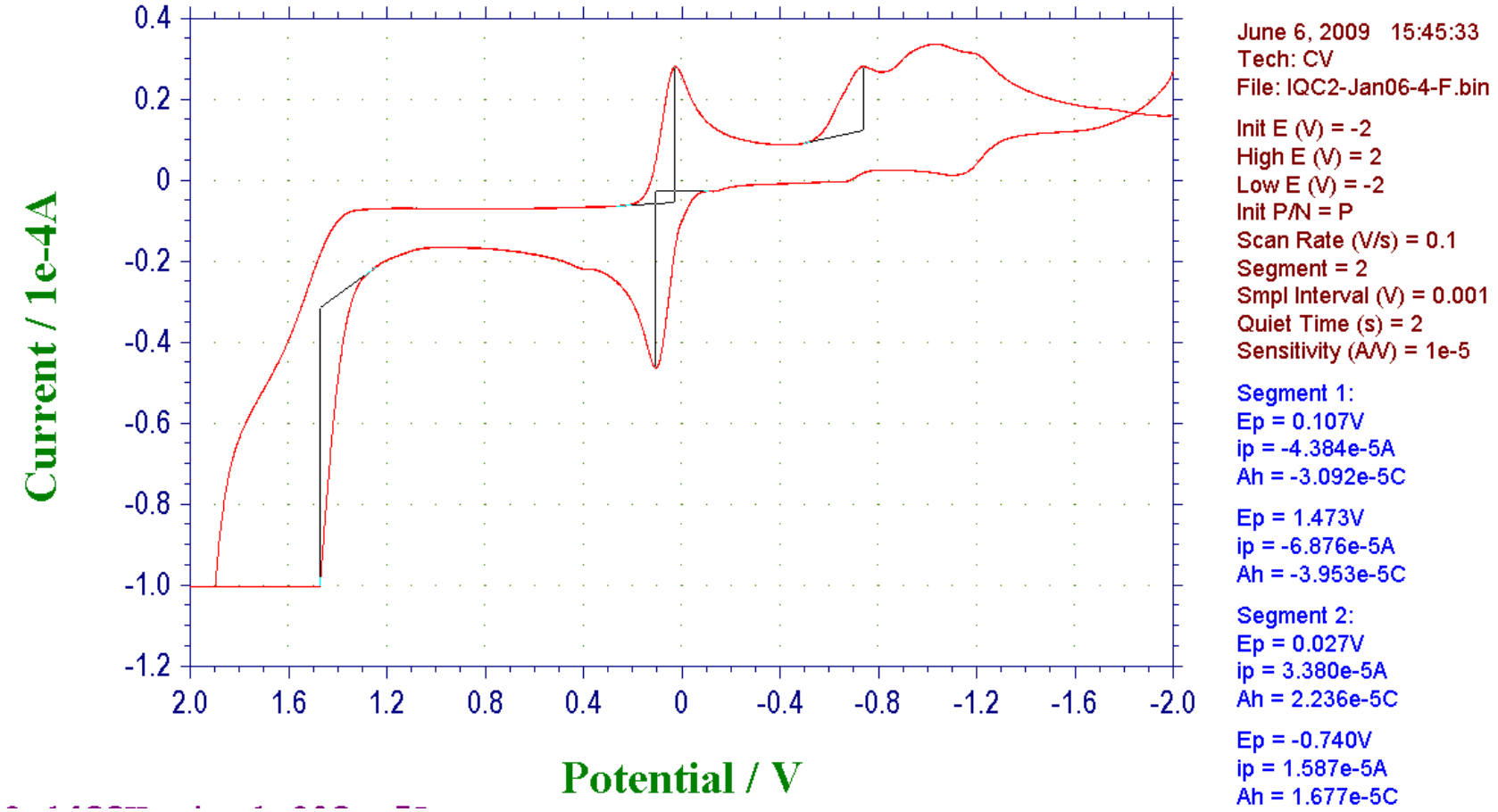

Figure A.52 CV of $[IQC_2](PF_6)_2$

$[IQC_3]Cl_2$	$C_{UV}=3.21008\times10^{-5}$ mol/L	λ=208	A=0.9971161	ε=31062
M=408.09	$C_{UV}=1.60504\times10^{-5}$ mol/L	λ=242	A=0.8023987	ε =49992
m=1.31mg	$C_{UV}=5.35013\times10^{-5}$ mol/L	λ=412	A=0.9083557	ε =16978
$C=3.21008\times10^{-4}$				

Table A.11 UV data for $[IQC_3]Cl_2$ in water

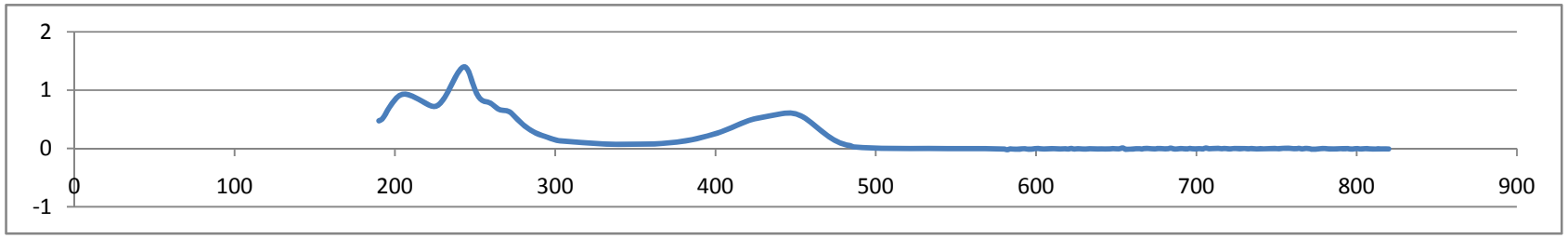

Figure A.53 UV Spectrum for $[IQC_3]Cl_2$ in water

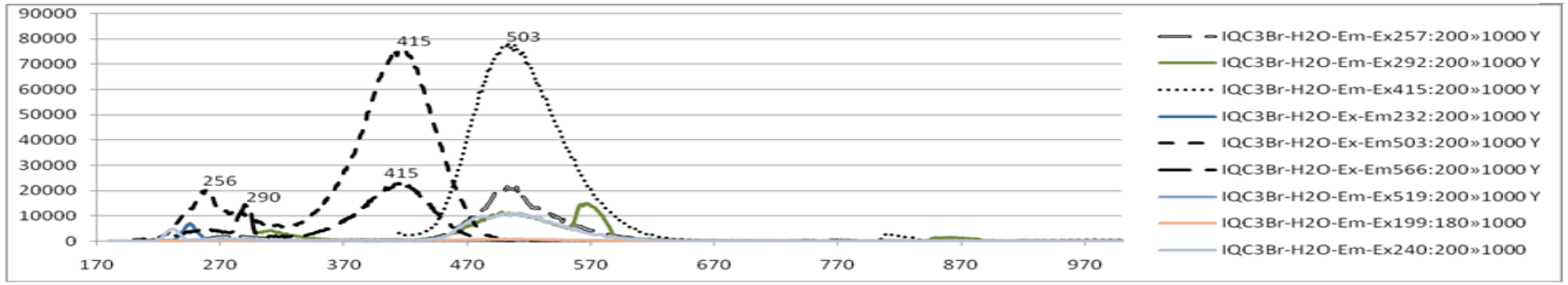

Figure A.546 Fluorescence Spectrum for $[IQC_3]Cl_2$ in water

$[IQC_3](PF_6)_2$	$C_{UV}=2.38443\times10^{-5}$ mol/L	λ=208	A=0.8059387	ε=33800
M=629.08	$C_{UV}=1.19222\times10^{-5}$ mol/L	λ=242	A=0.7852783	ε =65867
m=1.50mg	$C_{UV}=5.961075\times10^{-5}$ mol/L	λ=414	A=0. 9825592	ε =16483
$C=2.38443\times10^{-4}$				

Table A.12 UV data for $[IQC_3](PF_6)_2$ in Acetonitrile

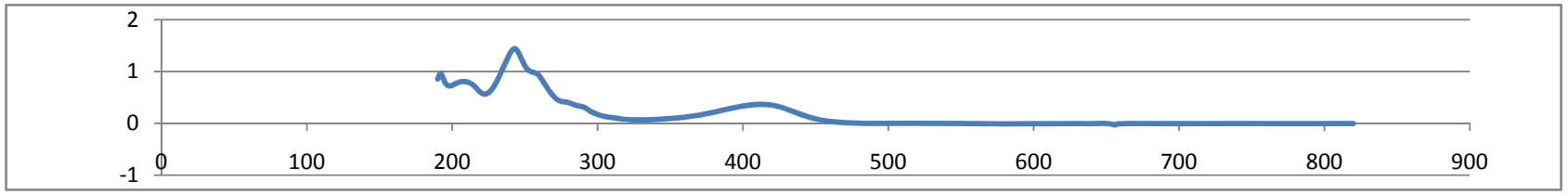

Figure A.557 UV Spectrum for $[IQC_3](PF_6)_2$ in Acetonitrile

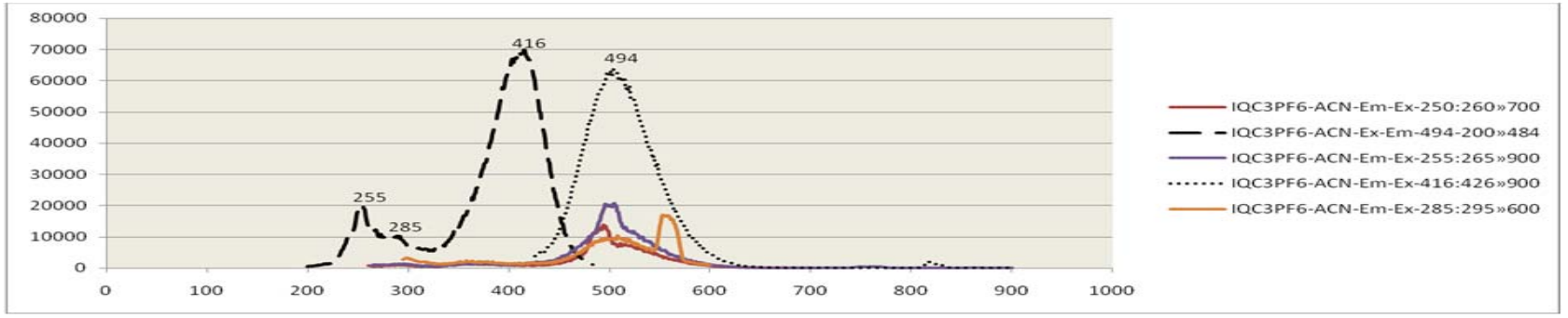

Figure A.58 Fluorescence Spectrum for $[IQC_3](PF_6)_2$ in Acetonitrile

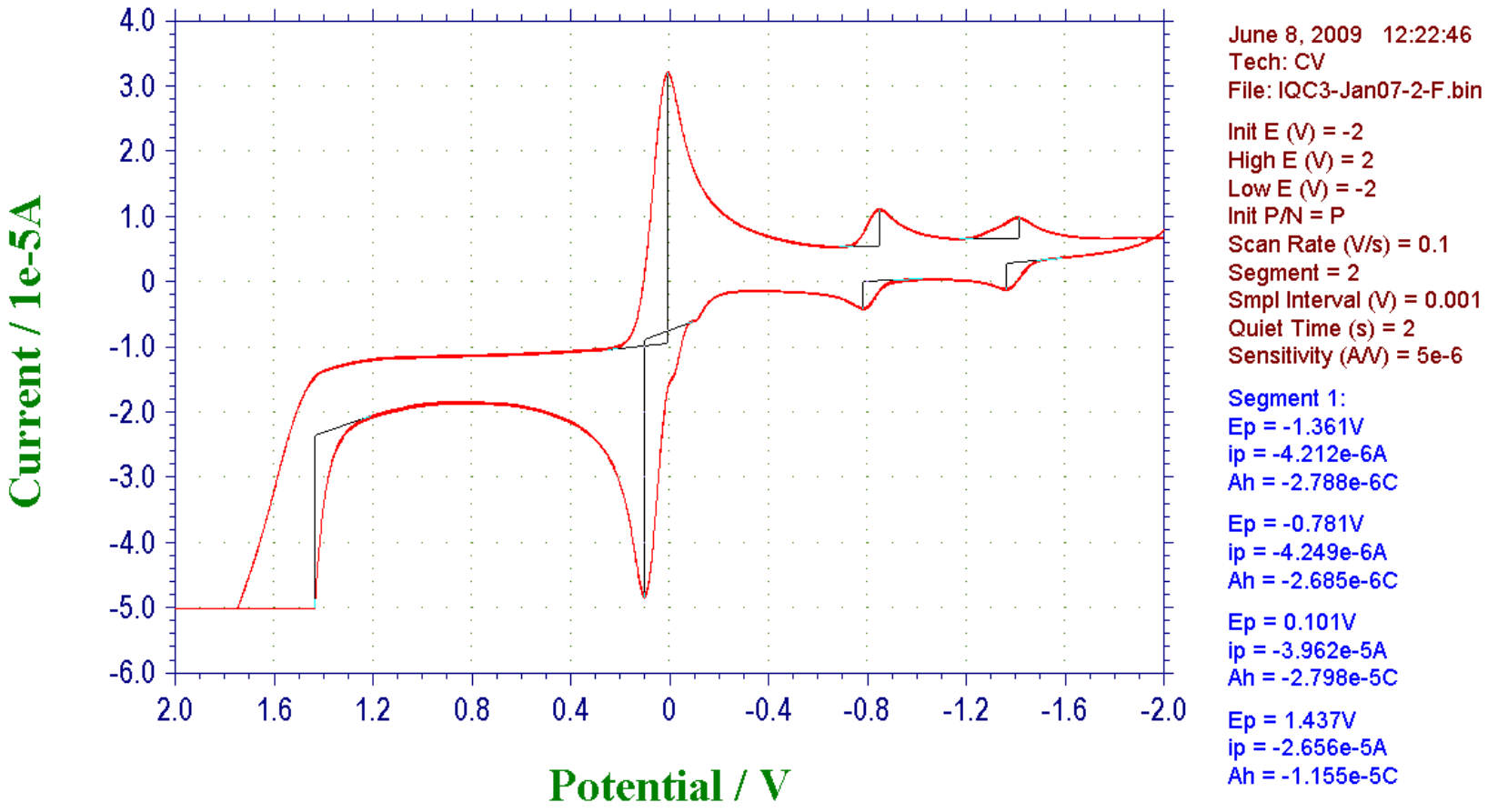

Figure A.59 CV of $[IQC_3](PF_6)_2$

$[RuP_3](PF_6)_2$	$C_{UV}=1.18355\times10^{-5}$ mol/L	λ=202	A=0.9580689	ε=80949
M=997	$C_{UV}=1.77533\times10^{-5}$ mol/L	λ=242	A=0.625351	ε =35224
m=1.77mg	$C_{UV}=1.18355\times10^{-5}$ mol/L	λ=324	A=0.7182159	ε =60683
$C=1.77533\times10^{-4}$	$C_{UV}=5.91777\times10^{-5}$ mol/L	λ=434	A=0.989975	ε =16729

Table A.13 UV data for $[RuP_3](PF_6)_2$ in Acetonitrile

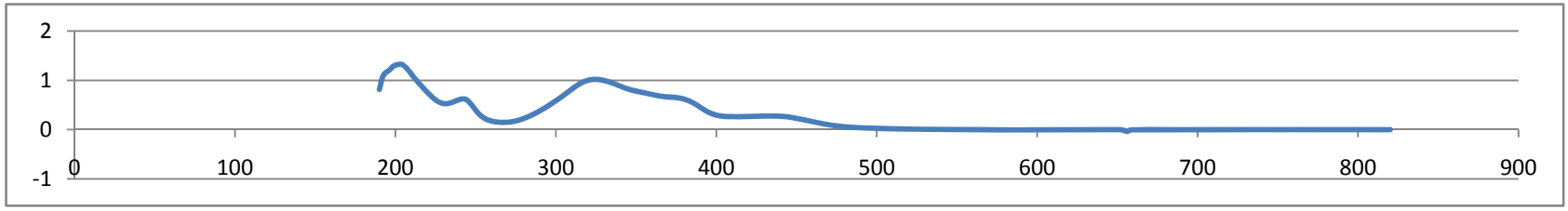

Figure A.60 UV Spectrum for $[RuP_3](PF_6)_2$ in Acetonitrile

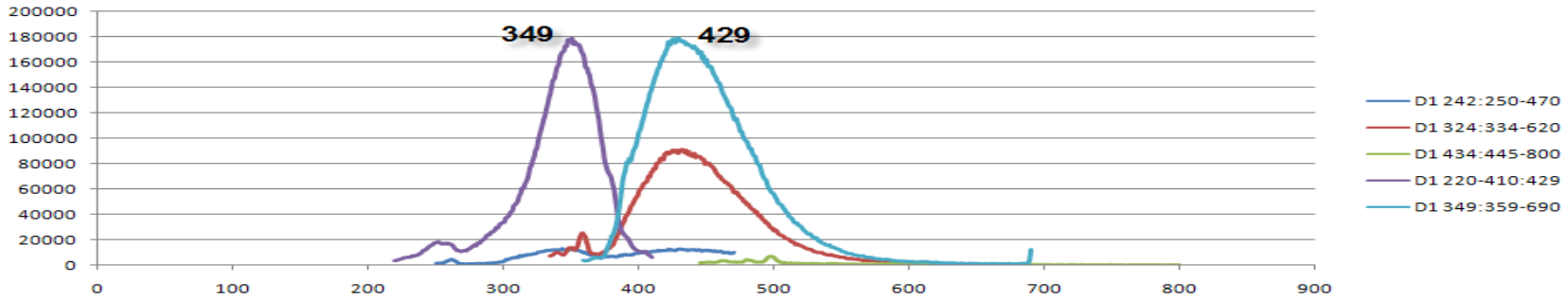

Figure A.56 Fluorescence Spectrum for $[RuP_3](PF_6)_2$ in Acetonitrile

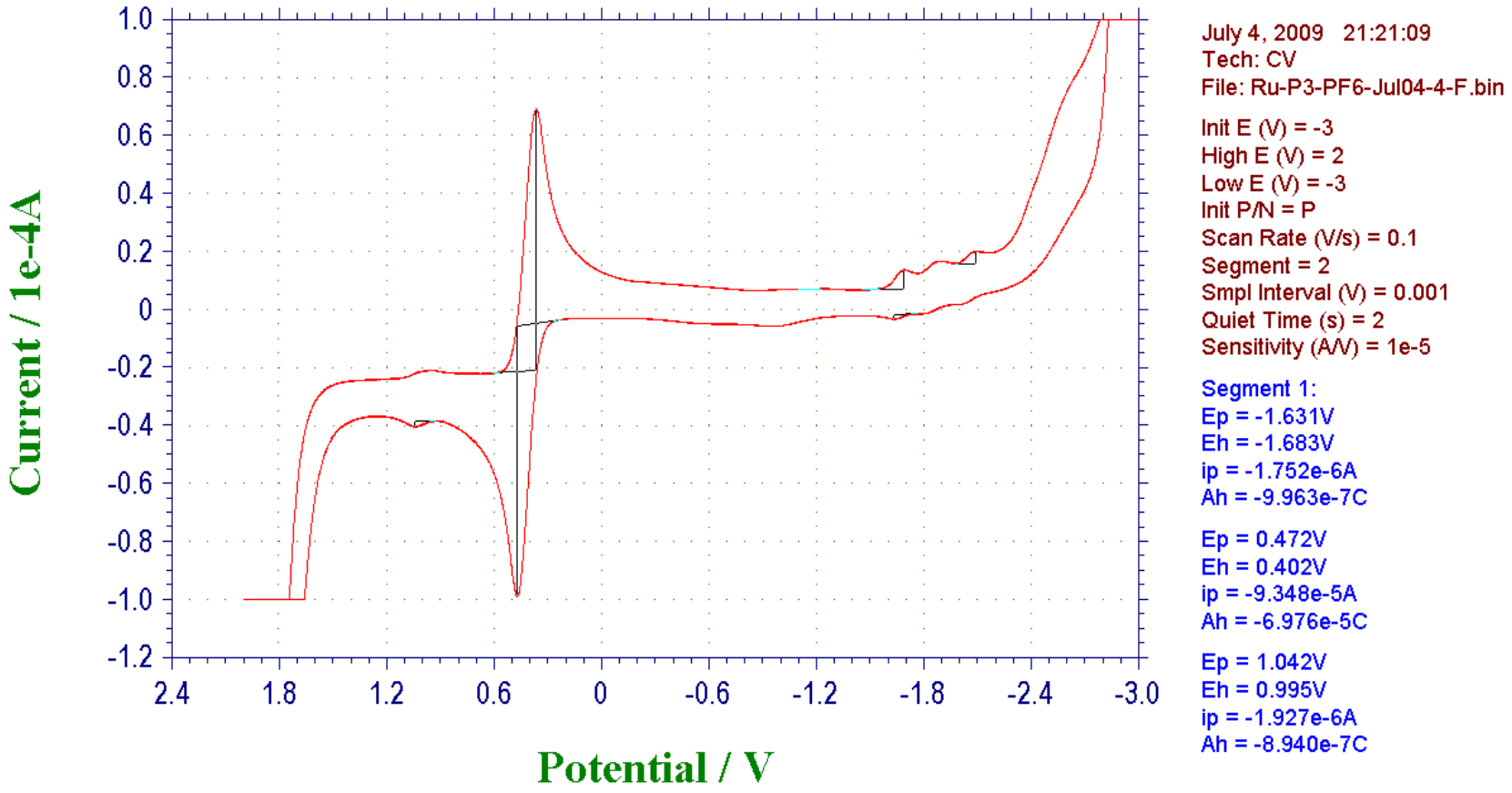

Figure A.57 CV of $[RuP_3](PF_6)_2$

$[RuP_3]Cl_2$	$C_{UV}=1.23207\times10^{-5}$ mol/L	λ=202	A=0.7717743	ε=62640
M=776.01	$C_{UV}=2.46414\times10^{-5}$ mol/L	λ=242	A=0.8639069	ε =35059
m=0.98mg	$C_{UV}=1.23207\times10^{-5}$ mol/L	λ=324	A=0.6515961	ε =52886
$C=1.23207\times10^{-4}$	$C_{UV}=3.080175\times10^{-5}$ mol/L	λ=438	A=0.59375	ε =19277

Table A.14 UV data for $[RuP_3]Cl_2$ in water

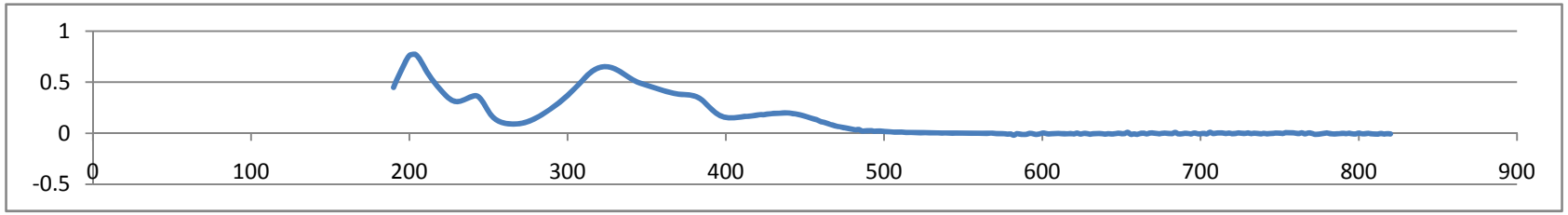

Figure A.58 UV Spectrum for $[RuP_3]Cl_2$ in water

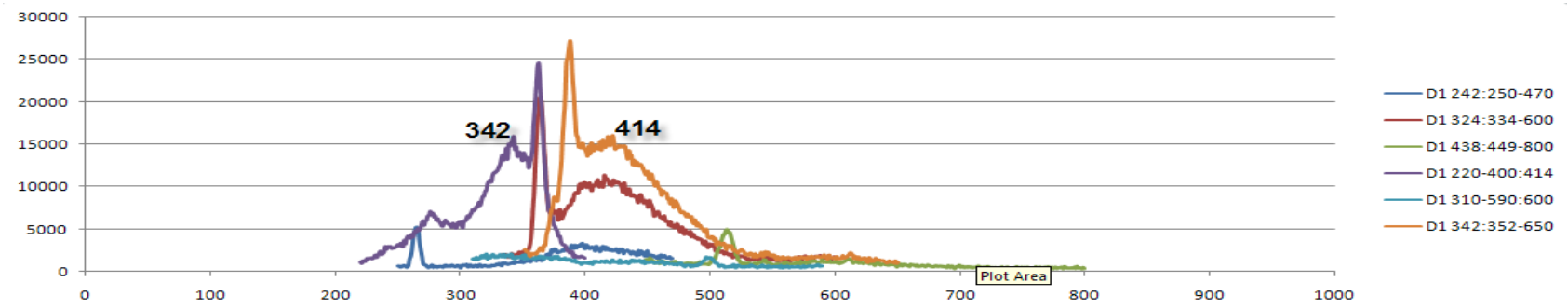

Figure A.64 Fluorescence Spectrum for $[RuP_3]Cl_2$ in water

$[Ru(bpy)_2P](PF_6)_2$	$C_{UV}=1.64550\times10^{-5}$ mol/L	λ=196	A=0.7856903	ε=47748
M=899.42	$C_{UV}=3.55066\times10^{-5}$ mol/L	λ=242	A=0.970398	ε =27330
m=1.48mg	$C_{UV}=1.64550\times10^{-5}$ mol/L	λ=288	A=0.9016266	ε =54793
$C=1.64550\times10^{-4}$	$C_{UV}=3.55066\times10^{-5}$ mol/L	λ=426	A=0.4467163	ε =12581

Table A.15 UV data for $[Ru(bpy)_2P](PF_6)_2$ in Acetonitrile

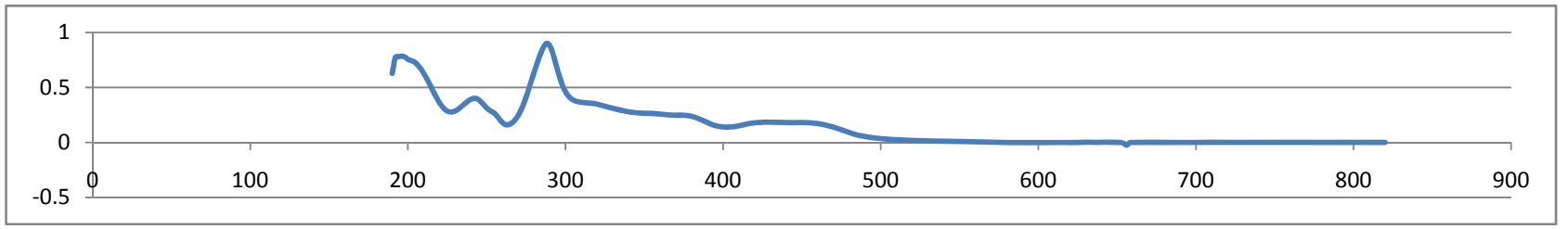

Figure A 59 UV Spectrum for $[Ru(bpy)_2P](PF_6)_2$ in Acetonitrile

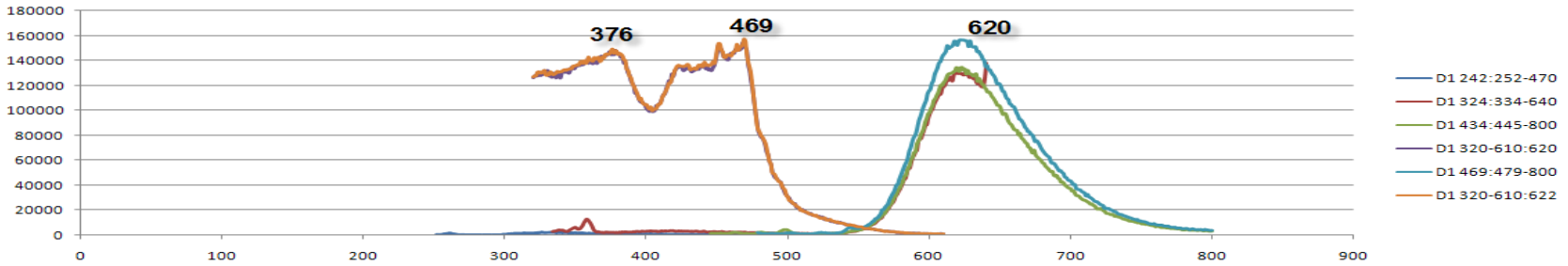

Figure A.60 Fluorescence Spectrum for $[Ru(bpy)_2P](PF_6)_2$ in Acetonitrile

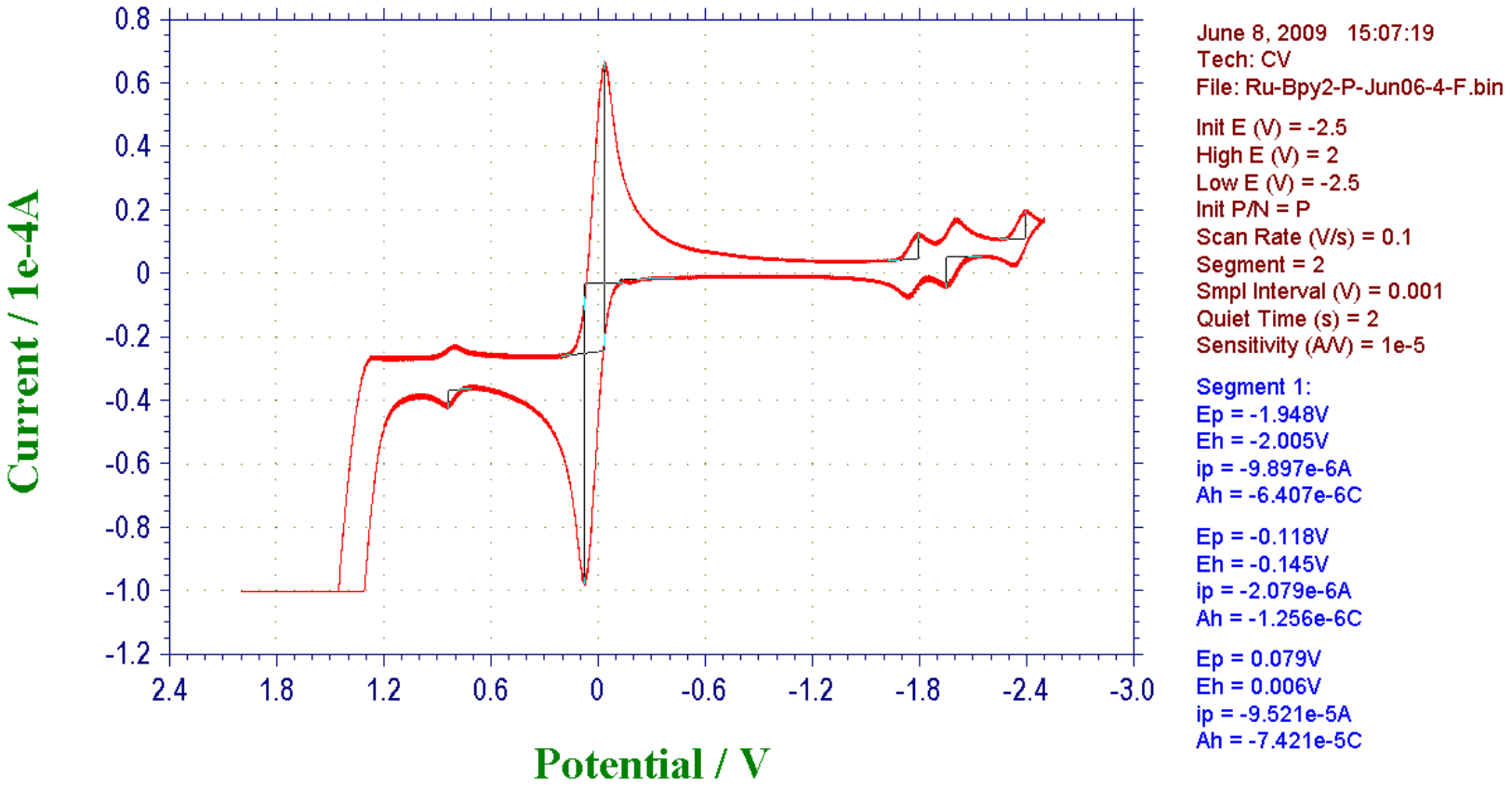

Figure A.61 CV of $[Ru(bpy)_2P](PF_6)_2$

$[Ru(bpy)_2P]Cl_2$	$C_{UV}=1.750363\times10^{-5}$ mol/L	λ=198	A=0.8914185	ε=50928
M=678.43	$C_{UV}=3.500725\times10^{-5}$ mol/L	λ=242	A=0.9291992	ε =26543
m=0.95mg	$C_{UV}=1.40029\times10^{-5}$ mol/L	λ=288	A=0.6762695	ε =48295
$C=1.40029\times10^{-4}$	$C_{UV}=5.60116\times10^{-5}$ mol/L	λ=430	A=0.6863251	ε =12253

Table A.16 UV data for $[Ru(bpy)_2P]Cl_2$ in water

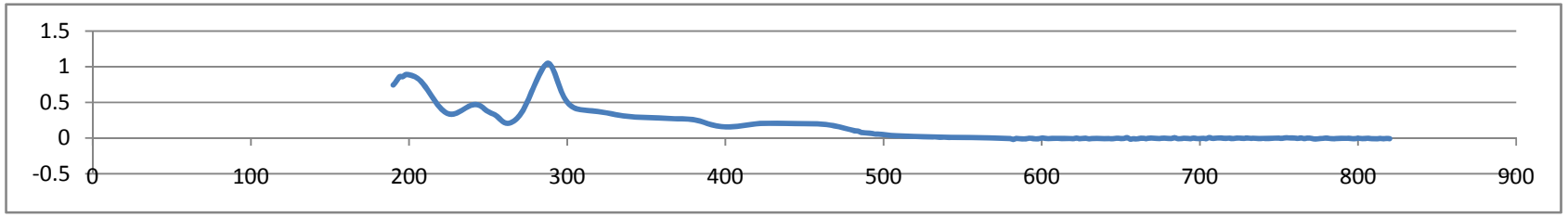

Figure A.68 UV Spectrum for $[Ru(bpy)_2P]Cl_2$ in water

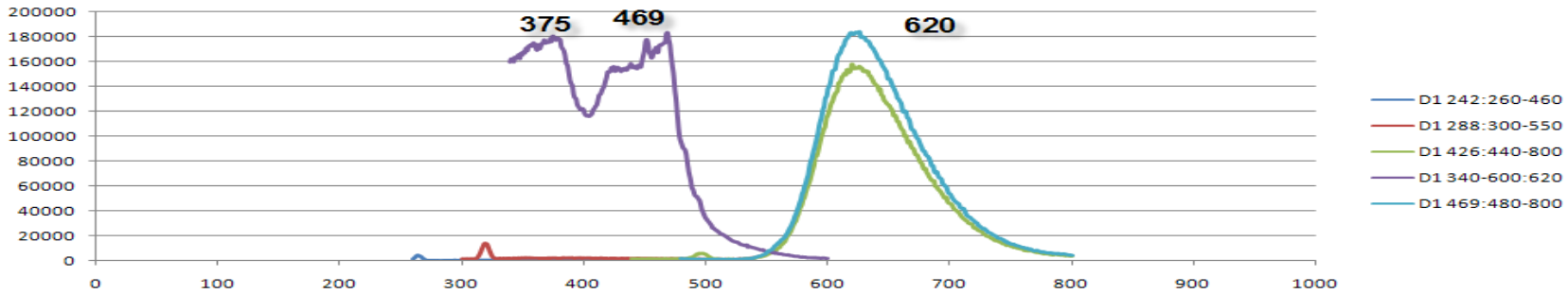

Figure A.69 Fluorescence Spectrum for $[Ru(bpy)_2P]Cl_2$ in water

$[Ru(bpy)_2IQ](PF_6)_2$	$C_{UV}=1.370755\times10^{-5}$ mol/L	λ=196	A=0.7890778	ε=57565
M=999.45	$C_{UV}=1.370755\times10^{-5}$ mol/L	λ=236	A=0.8081207	ε =58954
m=2.74mg	$C_{UV}=1.370755\times10^{-5}$ mol/L	λ=288	A=0.8065949	ε =58843
$C=2.74151\times10^{-4}$	$C_{UV}=3.426888\times10^{-5}$ mol/L	λ=412	A=0.9552612	ε =27875
	$C_{UV}=4.569183\times10^{-5}$ mol/L	λ=468	A=0.8235931	ε =18025

Table A.17 UV data for $[Ru(bpy)_2IQ](PF_6)_2$ in Acetonitrile

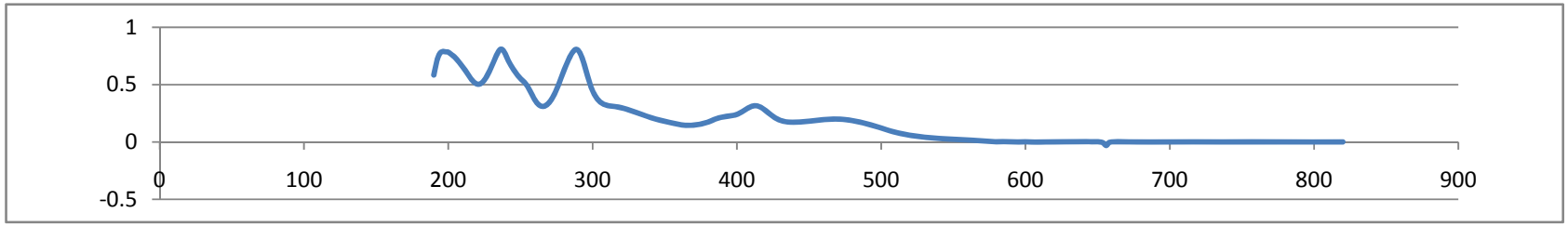

Figure A.62 UV Spectrum for $[Ru(bpy)_2IQ](PF_6)_2$ in Acetonitrile

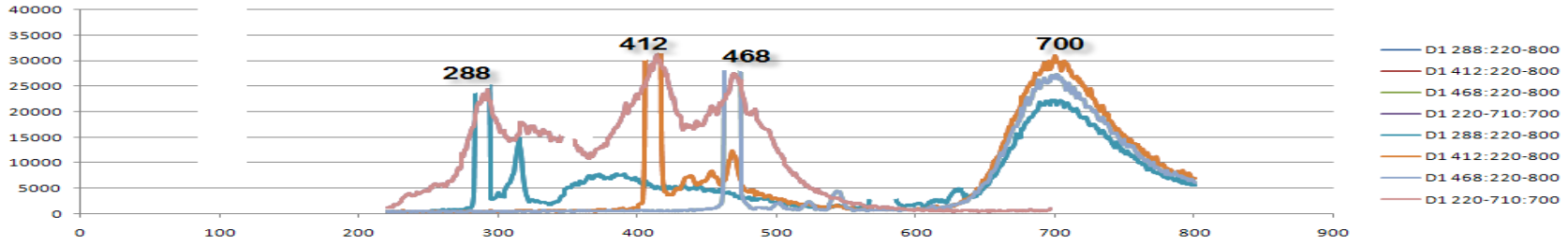

Figure A.63 Fluorescence Spectrum for $[Ru(bpy)_2IQ](PF_6)_2$ in Acetonitrile

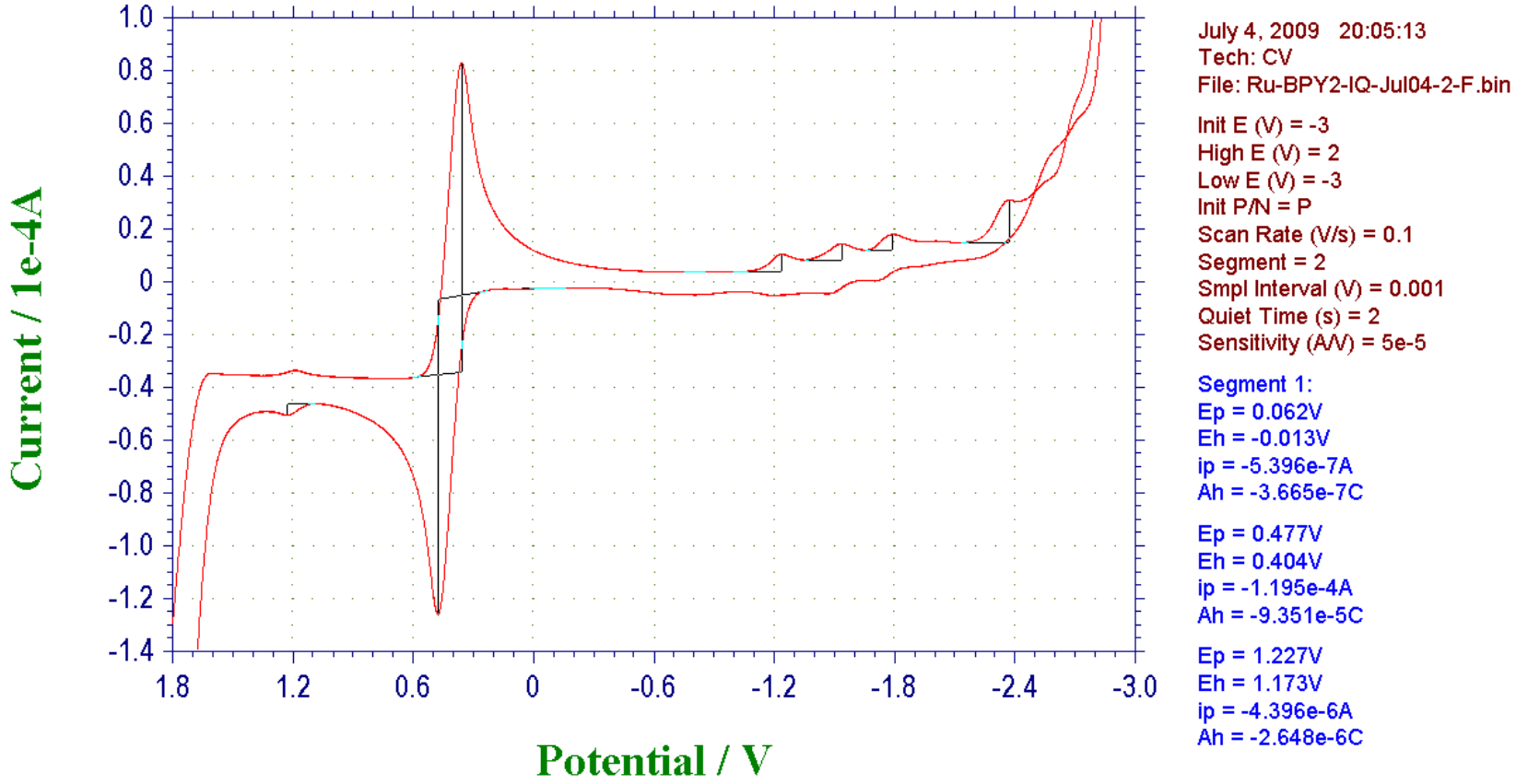

Figure A.64 CV of $[Ru(bpy)_2IQ](PF_6)_2$

$[Ru(bpy)_2IQ]Cl_2$	$C_{UV}=2.8774768\times10^{-5}$ mol/L	λ=198	A=1.035294	ε=35979
M=778.46	$C_{UV}=2.8774768\times10^{-5}$ mol/L	λ=236	A=1.003403	ε =34871
m=1.40mg	$C_{UV}=2.8774768\times10^{-5}$ mol/L	λ=288	A=0.9724579	ε =33796
$C=1.798423\times10^{-4}$	$C_{UV}=5.9947433\times10^{-5}$ mol/L	λ=412	A=0.6988373	ε =11658
	$C_{UV}=8.992115\times10^{-5}$ mol/L	λ=468	A=0.739563	ε =8224

Table A.18 UV data for $[Ru(bpy)_2IQ]Cl_2$ in water

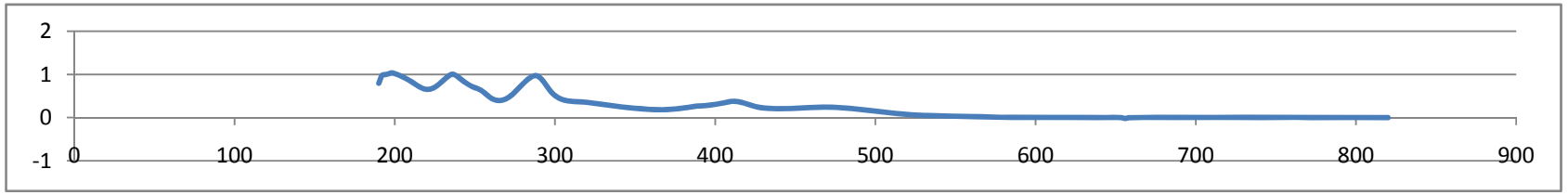

Figure A.65 UV Spectrum for $[Ru(bpy)_2IQ]Cl_2$ in water

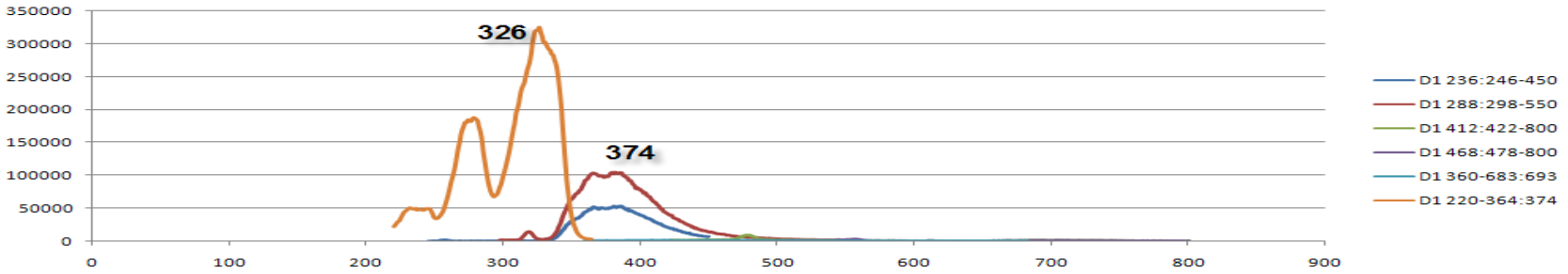

Figure A.66 Fluorescence Spectrum for $[Ru(bpy)_2IQ]Cl_2$ in water

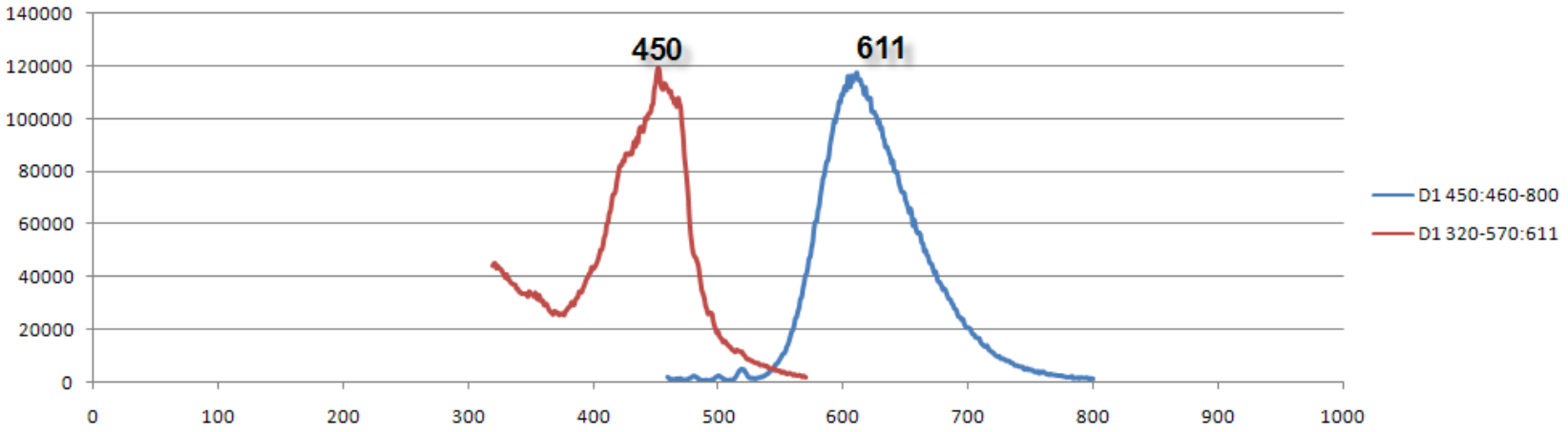

Figure A.67 Fluorescence Spectrum for $[Ru(bpy)_3](PF_6)_2$ in Acetonitrile

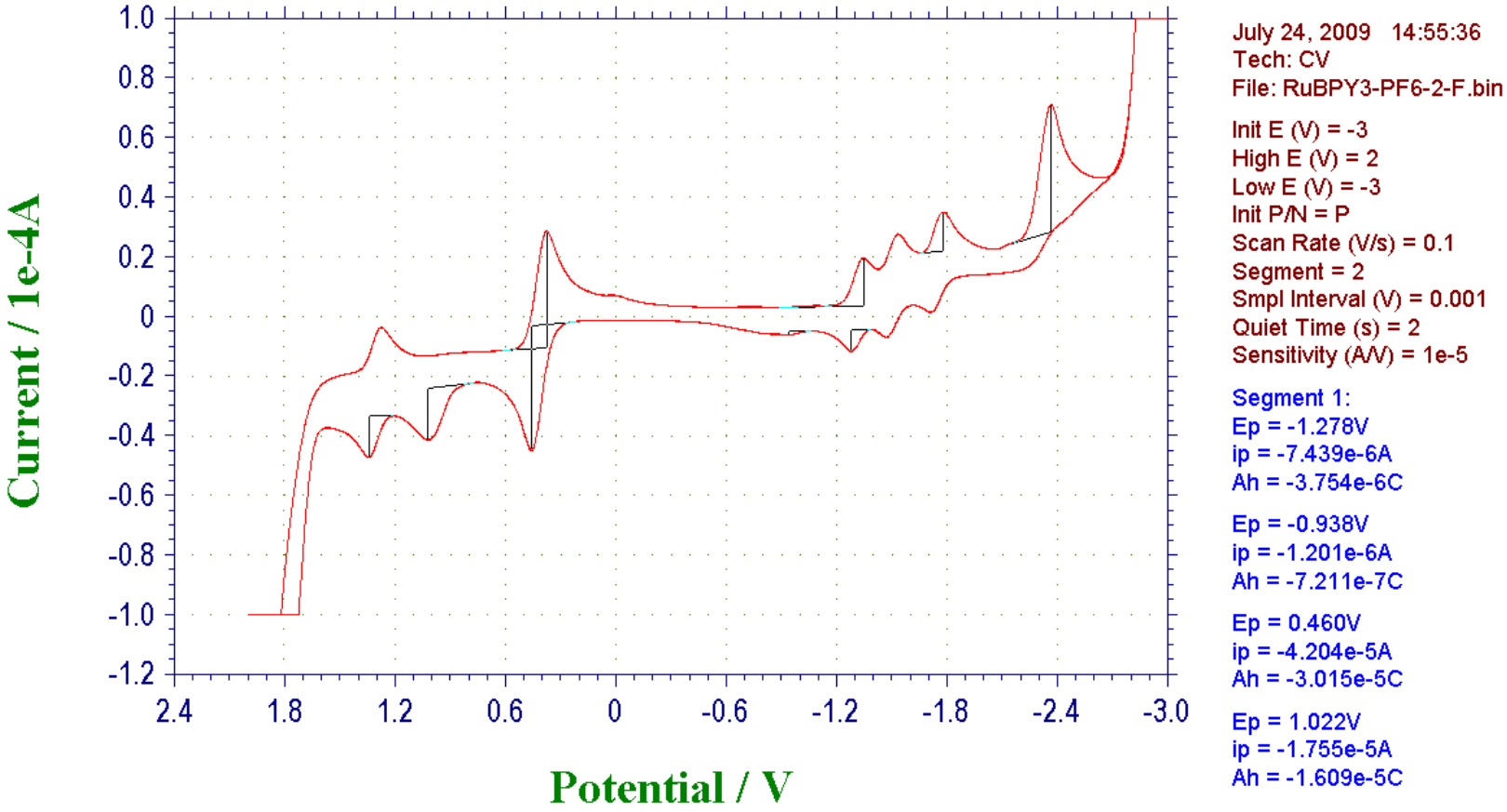

Figure A.68 CV of $[Ru(bpy)_3](PF_6)_2$

Table A.19 Crystal data and structure refinement for $[Ru(bpy)_2P](PF_6)_2$

Identification code	ap08sqz	
Empirical formula	C36 H32 Cl2 F12 N7 O P2 Ru	
Formula weight	1040.6	
Temperature	180(2) K	
Wavelength	0.71073 Å	
Crystal system	Monoclinic	
Space group	P2(1)/c	
Unit cell dimensions	a = 19.1016(8) Å	α= 90°.
	b = 9.4453(5) Å	β= 93.848(4)°.
	c = 23.2390(12) Å	γ = 90°.
Volume	4183.3(4) $Å^3$	
Z	4	
Density (calculated)	1.652 Mg/m^3	
Absorption coefficient	0.673 mm^{-1}	
F(000)	2084	
Crystal size	0.35 x 0.15 x 0.08 mm^3	
Theta range for data collection	2.41 to 26.00°.	
Index ranges	-23<=h<=23, -11<=k<=10, -28<=l<=24	
Reflections collected	18713	
Independent reflections	8200 [R(int) = 0.0578]	
Completeness to theta = 26.00°	99.60%	
Absorption correction	Multi-scan	
Refinement method	Full-matrix least-squares on F^2	
Data / restraints / parameters	8200 / 0 / 514	
Goodness-of-fit on F^2	1.064	
Final R indices [I>2sigma(I)]	R1 = 0.0705, wR2 = 0.1821	
R indices (all data)	R1 = 0.1189, wR2 = 0.1991	
Largest diff. peak and hole	1.010 and -1.081 $e.Å^{-3}$	

Table A.20 Bond lengths [Å] and angles [°] for $[Ru(bpy)_2P](PF_6)_2$.

Ru(1)-N(7)	2.042(5)
Ru(1)-N(2)	2.045(5)
Ru(1)-N(6)	2.047(5)
Ru(1)-N(5)	2.054(5)
Ru(1)-N(4)	2.072(5)
Ru(1)-N(3)	2.082(5)
N(7)-Ru(1)-N(2)	94.0(2)
N(7)-Ru(1)-N(6)	78.6(2)
N(2)-Ru(1)-N(6)	90.98(19)

N(7)-Ru(1)-N(5)	92.96(19)
N(2)-Ru(1)-N(5)	171.0(2)
N(6)-Ru(1)-N(5)	96.07(19)
N(7)-Ru(1)-N(4)	98.3(2)
N(2)-Ru(1)-N(4)	94.6(2)
N(6)-Ru(1)-N(4)	173.83(18)
N(5)-Ru(1)-N(4)	78.7(2)
N(7)-Ru(1)-N(3)	171.16(19)
N(2)-Ru(1)-N(3)	78.3(2)
N(6)-Ru(1)-N(3)	97.0(2)
N(5)-Ru(1)-N(3)	95.2(2)
N(4)-Ru(1)-N(3)	86.7(2)